The

hilosophical Magazine

FIRST PUBLISHED IN 1798

A Journal of Theoretical
Experimental and Applied Physics

UNIVERSITY OF HA
LIBRARY
APR 9 '58

Vol. 3 February 1958 No. 26
Eighth Series

£1 5s. 0d., plus postage
Annual Subscription £13 10s. 0d., payable in advance

ALERE FLAMMAM

Printed and Published by
TAYLOR & FRANCIS LTD
RED LION COURT, FLEET STREET, LONDON, E.C.4

THE PHILOSOPHICAL MAGAZINE

Editor

Professor N. F. Mott, M.A., D.Sc., F.R.S.

Editorial Board

Sir Lawrence Bragg, O.B.E., M.C., M.A., D.Sc., F.R.S.
Sir George Thomson, M.A., D.Sc., F.R.S.
Professor A. M. Tyndall, C.B.E., D.Sc., F.R.S.

Authors wishing to submit papers for publication in the Journal should send manuscripts directly to the Publishers.

Manuscripts should be typed in *double* spacing on one side of quarto (8×10 in.) paper, and authors are urged to aim at absolute clarity of meaning and an attractive presentation of their texts.

References should be listed at the end in alphabetical order of authors and should be cited in the text in terms of author s name and date. Diagrams should normally be in Indian ink on white card, with lettering in soft pencil, the captions being typed on a separate sheet.

A leaflet giving detailed instructions to authors on the preparation of papers is available on request from the Publishers.

Authors are entitled to receive 25 offprints of a paper in the Journal free of charge, and additional offprints can be obtained from the Publishers.

The *Philosophical Magazine* and its companion journal, *Advances in Physics*, will accept papers for publication in experimental and theoretical physics. The *Philosophical Magazine* publishes contributions describing new results, letters to the editor and book reviews. *Advances in Physics* publishes articles surveying the present state of knowledge in any branch of the science in which recent progress has been made. The editors welcome contributions from overseas as well as from the United Kingdom, and papers may be published in English, French and German.

The Interaction Rates of Stopped Negative Muons in Iron and Copper†

By A. M. HILLAS‡, W. B. GILBOY and R. M. TENNENT
Physics Department, University of Leeds

[Received November 11, 1957]

ABSTRACT

An apparatus suitable for measuring the mean lifetimes of negatively-charged muons brought to rest in targets of $Z < 30$ is described. Measurements made on iron and copper yield mean lifetimes of $(204 \pm 14) \times 10^{-9}$ sec and $(157 \pm 20) \times 10^{-9}$ sec respectively.

§ 1. INTRODUCTION

IN the ten years which have elapsed since the crucial experiment of Conversi *et al.* (1947) the interaction rates of negative muons have been investigated by many workers (see Sard and Crouch 1954). Recent work on parity non-conservation has again aroused interest in the muon and it seems likely that the interaction probabilities of negative muons will be of interest in determining the nature of the four fermion interaction and the structure of the nucleus.

The apparatus to be described has been developed with a view to measuring the lifetimes of cosmic-ray muons in elements in the range $Z < 30$, the limit being set by the channel width of the timing apparatus. Using a simple selection scheme it has been possible to determine the mean lives of negative muons in iron and copper by measuring the lifetime distribution of a mixture of positive and negative cosmic-ray muons. The curve obtained is the sum of two exponentials of widely differing decay constants and it is possible to separate the two components with fair accuracy.

§ 2. APPARATUS

2.1. *General*

Figure 1 shows the general arrangement of the apparatus. Incoming cosmic-ray muons enter the target by way of the Geiger counter tray G_1 and the scintillator S_1. The disintegration products produce signals in S_2 while G_2 is in anticoincidence to reduce the background. In the present experiments, the target was 16 in. wide and 3 in. deep and rested on three pieces of angle iron. The iron target was circular in cross section and the copper target square.

---

† Communicated by Professor J. G. Wilson.

‡ Now at Atomic Energy Research Establishment, Harwell.

The various parts of the apparatus were supported on a light framework which was, as far as possible, kept sufficiently far from the counters to render its effect on the counting rate negligible. The apparatus was assembled under a concrete roof, effective thickness 3 in., and no attempt was made at shielding from local radiation.

Fig. 1

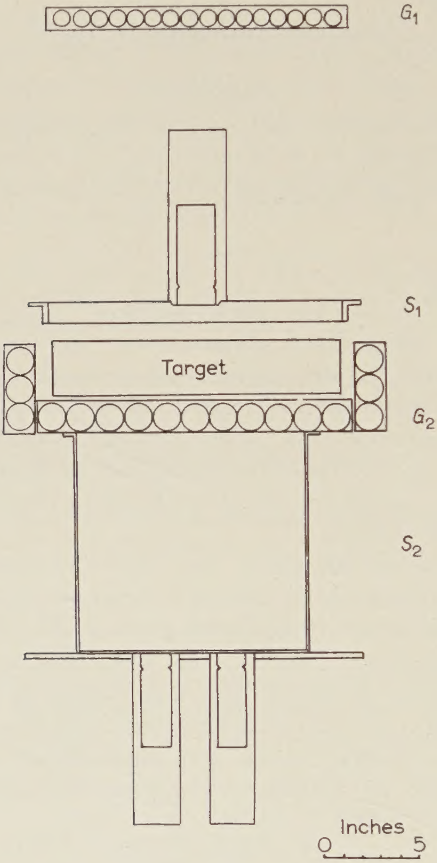

General arrangement of target and detectors.

A negative muon coming to rest in the target, will produce signals in G_1 and S_1 but not in G_2. Neutrons and γ-rays emitted downwards from the capturing nucleus will not produce signals in G_2 but may in S_2. Neutrons can be detected in liquid scintillators by the ionization produced by knock-on protons, and γ-rays by that from 'Compton' electrons. Where the negative meson decays, it is unlikely that the electron will escape from the target, but S_2 can respond to bremsstrahlung from the electron. It is for this reason that the selection scheme does not reject events produced by positive muons coming to rest in the target.

2.2. *The Counters*

The trays G_1 and G_2 were made up of 18 and 17 Geiger counters (20th Century Electronics G60) respectively, the counters being connected in pairs or triplets to quenching units similar to that described by Hodson (1953). The outputs from the quenching units of a particular tray were connected to a mixer circuit which produced a standard pulse when any one, or more, of the counters fired. The counters were protected from daylight by thin aluminium trays and supplied from a source of positive E.H.T. Under these conditions, they were found to be quite reliable and the counting rates of the individual trays remained constant within the expected limits.

The scintillation counter S_1 was originally a liquid scintillator constructed in the following way. Two thin electrolytically polished aluminium sheets were cemented to a polished aluminium ring with Araldite D, cured for three hours at 60°C (see fig. 2). A glass window which allowed the photomultiplier to ' see ' the edges of the scintillator was cemented in at the same time. This container was filled with a solution of terphenyl and POPOP in toluene. It was cheap to make and very efficient and reliable in use. In about a year's service, no evidence of ' poisoning ' of the scintillator was observed. When large plastic scintillators became commercially available, the liquid scintillator was replaced by a disc of Nuclear Enterprises (G.B.) Ltd. plastic scintillator Ne101. The disc, 16 in. diameter by 1 in. deep, was machined to a satin finish and recessed and polished in the centre to take a 2 in. photomultiplier. It was housed in a spun aluminium box and packed around with magnesium oxide.

Fig. 2

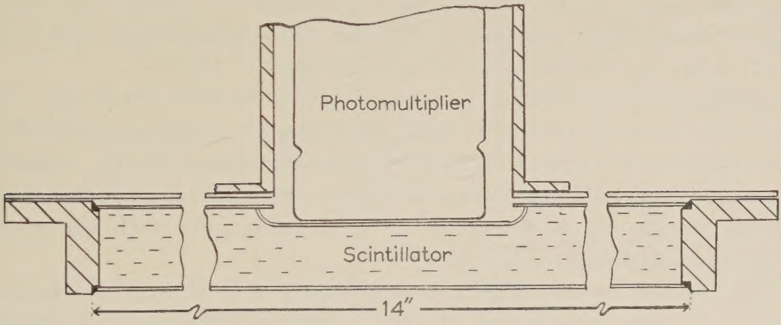

Schematic diagram of liquid scintillator S_1.

It was important that the detector S_1 should be as thin as possible to reduce the numbers of muons stopping in it after being detected, since the lower portion of S_1 is effectively part of the target. Using such thin scintillators and a thin aluminium casing was effective in reducing such events to negligible proportions. The two scintillators described were tested for their detection efficiencies for muons. Using E.M.I. 6262A photomultipliers, each detector was found to be more than 90% efficient for the detection of muons passing through its extreme edge, when the discriminator bias was set to produce a counting rate of 100 counts per second.

The scintillator S_2 was designed with a view to capturing neutrons (see Reines *et al.* 1954) and it is likely that a smaller disc-shaped scintillator would have been more efficient for the experiment described here. It was constructed from stainless steel, and was 12 in. in diameter and 12 in. deep. Before filling it was sand-blasted inside, and painted with a mixture of titanium oxide and water-glass. An electrolytically polished lid of thin aluminium was secured by a retaining ring and a lead washer. The scintillating liquid was viewed by three 6262A photomultipliers through glass windows cemented in with Araldite D. After a year's use, the scintillator was inspected and found to be in excellent condition. The liquid was clean and free from any deposit. During the year, the coincidence counting rate remained sensibly constant. Some slight yellowing of the paint appeared to have occurred, but this evidently did not seriously affect the performance of the scintillator. It should be noted, that while the Araldite joints were resistant to toluene, they were found to soften very rapidly when in contact with benzene or methyl alcohol.

The scintillating solution was prepared by bubbling nitrogen through toluene for several hours and then dissolving the terphenyl and POPOP to concentrations of 3 g per litre and 0·1 g per litre respectively. Small scale tests showed that displacement of oxygen from the scintillator improved its performance by as much as 40% in agreement with the results of Pringle *et al.* (1953).

With 6262A photomultipliers, amplification of the output pulses was found to be unnecessary and, in fact, a crystal diode limiting circuit was incorporated in the photomultipler housings to limit the dynode pulses to 10 volts. These dynode pulses were fed on to the grid of a CV2127 valve acting as a phase inverter and giving pulses of opposite polarity from anode and cathode. The positive pulse was fed directly to one grid of a pair of mixer valves and the negative pulse was fed to the other grid through a delay cable. The output of the mixer circuit was thus a negative pulse of duration equal to the delay introduced by the delay cable. This method of clipping the pulses was found to yield a square pulse free from any after effects.

2.3. *Electronic circuits*

General

A block diagram of the apparatus is shown in fig. 3. Pulses from the anode of the S_1 photomultiplier are fed through an inverting circuit to a fast trigger circuit, using EFP60 valves, similar to that described by Lewis and Wells (1954). The clipped pulses from the dynodes of S_2 are fed to a diode coincidence circuit with a resolving time of 70 mμsec. If a coincidence is obtained, a gate is opened which allows a suitably delayed, common pulse from the three anodes of the S_2 photomultipliers to pass through to a second trigger circuit. The trigger circuits generate negative pulses 15 volts high and rising to maximum height in less than 15 mμsec after the start of the initiating pulse. These pulses generate independently the front and back edges of the counter chronometer gate. As long as the counter chronometer gate is open, pulses generated by a 20 Mc/s crystal-controlled oscillator are fed into a fast binary scaler. The counter chronometer is to be described in a separate paper.

Fig. 3

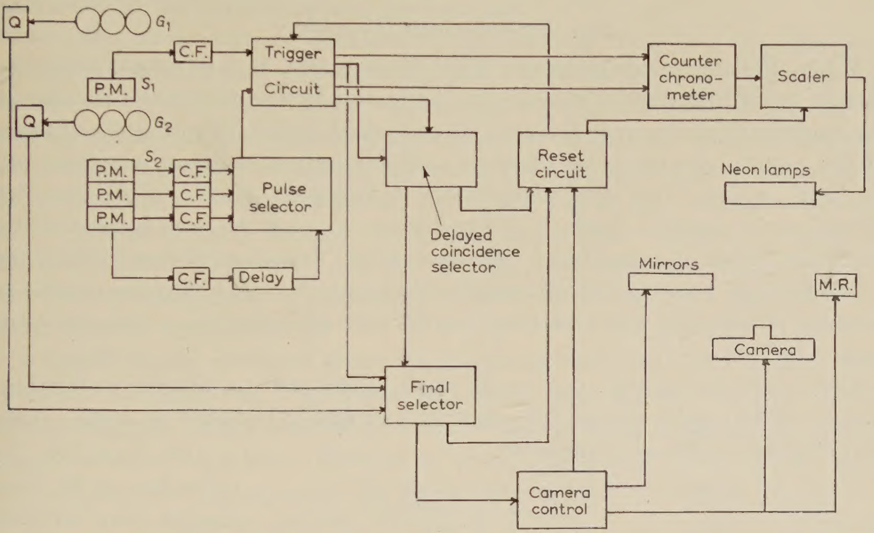

Simplified diagram of electronic circuits.
Q=Quenching circuit. C.F.=Cathode follower. M.R.=Message register.

The delayed coincidence selector and final selector circuit act as event selector circuits so that the camera circuit is only actuated when a $G_1S_1\overline{G}_2$ event is accompanied by a delayed S_2 pulse occurring within the gate length set by the delayed coincidence selector. The Geiger trays were necessary on account of the γ-ray background from the walls of the building which produced a high rate of S_1 delayed S_2 events. Prompt coincidences were avoided by delaying the start of the delayed coincidence selector gate. The display of neon lamps which indicated the scalar count was viewed continuously by the camera (which had no shutter) by reflection in a mirror. When the camera circuit was fired, the mirror was moved slightly by a solenoid so that the image of the lamps was displaced on the film. The neon lamps were reset after two seconds and the camera wound on. In this way, any spurious counts of the scaler, or failures in the resetting circuits could be recognized when the film was read, by images produced on the wrong portion of the film before the mirror had moved.

The arrangement described above allowed the fast timing circuits to operate independently of the slower selection circuits. Thus every S_1 pulse opened the counter chronometer gate and operated a paralysis circuit. The gate remained open for the duration of the trigger pulse unless previously closed by a pulse from S_2. In either case, the information remained stored until the selection circuits decided whether to accept the event. If an event were rejected, the particular selection circuit which rejected the event triggered the resetting circuit which in turn sent resetting pulses to the counter chronometer scalers and also turned off the input paralysis.

2.4. *Experimental Procedure*

When lifetime measurements were in progress, it was found that the rate of recording events was 25 per hour and it was necessary to change the camera film every 16 hours. Every eight hours, the output voltages of the power supplies were checked and the individual counter rates and the G_1S_1 coincidence rate measured. A complete check of the counter chronometer using a pair of ganged pulse generators was made at the start and finish of every film. On one or two occasions it was found that the scaler had become unbalanced during a run. It was, however, always possible to identify the first false record and all subsequent records were neglected.

Operation for about one week was necessary to obtain a lifetime measurement accurate to 10% and it was easily possible to read a film carrying 400 events in one hour.

2.5. *Analysis*

During the run, the gate length of the delayed coincidence selector was set to $2{\cdot}5\,\mu$sec. With this length of gate, the counts in the later channels are made up of positive muon events and chance coincidences, since the short lifetime of the negative muon ensures that they do not contribute significantly to counts in the later channels. The chance background was determined from the $G_1S_1\overline{G}_2$ rate and the known counting rate of S_2, and the positive muon contamination found by subtraction. It was then possible to extrapolate back to the early channels and finally obtain the numbers of counts in each channel caused by negative muons. The uncertainties introduced by this procedure in the final result were found to be small compared with the errors due to limited statistics.

The results were calculated using the method suggested by Peierls (1935). In determining the root mean square error of the result, the signal to noise ratio (λ in Peierls' paper) was derived from the start of the first channel. As the positive muon contamination decreases exponentially, this is likely to be an over-estimate yielding a slightly high value for the error. The signal-to-noise ratio of our apparatus found as above was about five.

Meyer (1954) has considered some sources of systematic errors arising in a similar experimental arrangement and has shown that the soft component of the cosmic radiation yielded spurious counts in the early channels of his detector. In view of this, we used no lead shielding, and also rejected the counts which occurred in the first three counter chronometer channels (i.e. 150 mμsec), as inspection of Meyer's results showed that this eliminated the suspect counts. As the lower parts of S_1 and the upper parts of G_2 are effectively part of our target, it is necessary to consider the effect of their presence on the results we have obtained. Negative muons which stop in the light elements (C, N, H etc.) of the scintillators and counters will have a longer lifetime, in fact nearly 2·2 μsec, than those stopping in the target and will therefore appear to contribute to the positive muon background.

The mass of the targets used was approximately 80 kg and the effective mass of aluminium and glass forming part of the target is estimated to be less than 1 kg. For the copper target, the effect of the iron framework of the apparatus and the target supports must be considered, an approximate calculation shows this to affect the result by less than 1%. We believe that systematic errors introduced by variations in the counter chronometer frequency and channel width are negligible. Observer errors in film reading are likely to be less with the display used than with a display on which measurement is necessary. Some films were read twice but no serious errors were detected.

A check on the positive muon contribution was made in the first iron run when the gate was lengthened to 7·2 μsec and the last 6·4 μsec of the gate analysed. After subtraction of background, an exponential curve was obtained with a mean lifetime of $(2{\cdot}14 \pm 0{\cdot}19)$ μsec. By a rearrangement of the selection system, the mean lifetime of the natural mixture of positive and negative muons coming to rest in S_2 was also measured yielding the result $(2{\cdot}15 \pm 0{\cdot}15)$ μsec.

§ 3. RESULTS

The mean lifetimes of negative muons in iron and copper were found to be (204 ± 14) mμsec and (157 ± 20) mμsec respectively. Figures 4 and 5 show the differential decay curves obtained. The table shows some of the results obtained by workers in this field and also the interaction rates assuming that the decay probability of negative muons is $(2{\cdot}22\,\mu\text{sec})^{-1}$, Bell and Hincks (1951).

It is clearly seen in the table that there are discrepancies in the results from different laboratories, which cannot easily be explained in terms of the quoted errors. A few remarks on this subject may be useful here. Meyer (1954) has objected to some of the results of Keuffel *et al.* (1952) on the grounds that their apparatus was troubled by spurious counts in the early channels of their timing apparatus. This led to a decrease in the measured lifetime and thus to high capture rates. He therefore repeated some of their measurements and for this reason, his result for copper is presumably more reliable than theirs. Meyer did not repeat their measurement on iron, but a similar fault in their apparatus would explain the discrepancy between their result and the last three results in the table.

Fig. 4

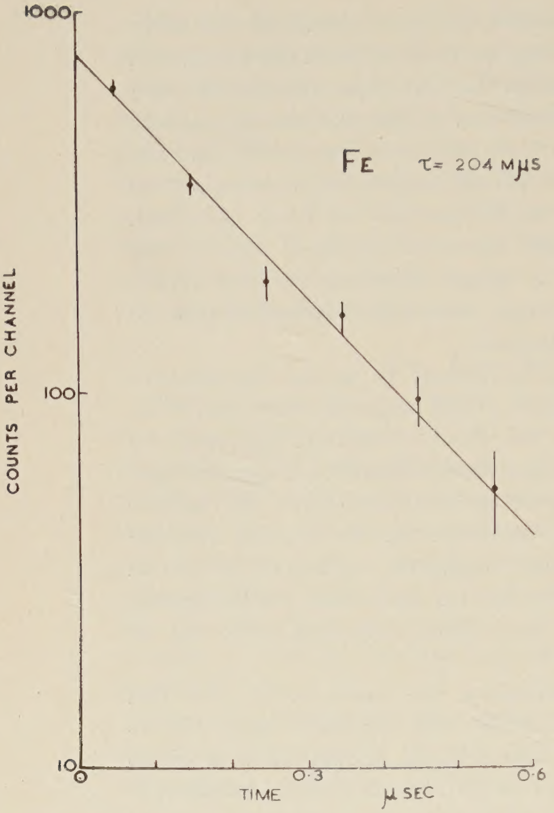

Differential decay curve for iron target.

Fig. 5

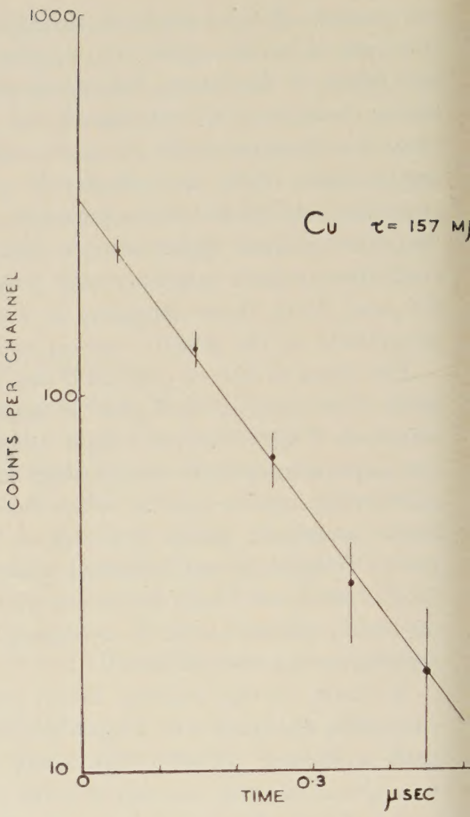

Differential decay curve for copper

The Mean Lifetimes and Interaction Rates of Negative Muons Captured in Iron and Copper

Element	Mean lifetime ($\times 10^9$ sec)	Interaction rate ($\times 10^{-6}$ sec^{-1})	Reference
Fe 26	210 ± 60	$4{\cdot}31 \pm 1{\cdot}4$	Benade (1953).
	163 ± 27	$5{\cdot}68 \pm 1{\cdot}0$	Keuffel *et al.* (1952).
	242 ± 15	$3{\cdot}68 \pm 0{\cdot}23$	Barrett *et al.* (1957)
	†192 ± 20	$4{\cdot}76 \pm 0{\cdot}54$	Lederman and Weinrich (1956)
	‡202 ± 7	$4{\cdot}49 \pm 0{\cdot}15$	Sens *et al.* (1957)
	§204 ± 14	$4{\cdot}45 \pm 0{\cdot}33$	Present work
Cu 29	116 ± 9	$8{\cdot}17 \pm 0{\cdot}67$	Keuffel *et al.* (1952)
	172 ± 8	$5{\cdot}36 \pm 0{\cdot}27$	Meyer (1954)
	†157 ± 12	$5{\cdot}92 \pm 0{\cdot}49$	Lederman and Weinrich (1956)
	‡138 ± 5	$6{\cdot}79 \pm 0{\cdot}22$	Sens *et al.* (1957)
	§157 ± 20	$5{\cdot}92 \pm 0{\cdot}80$	Present work

† Assuming the mean lifetime of negative muons in carbon to be $(1{\cdot}92 \pm 0{\cdot}04)$ μsec.

‡ Assuming the decay probability of negative muons to be $[(2{\cdot}21 \pm 0{\cdot}02) \times 10^{-6}]^{-1}$ sec^{-1}.

§ See note added in proof.

The recent results of Sens *et al.* (1957) are most interesting as representing a series of measurements on a large number of elements. It is noticeable that their measurements on copper yield a decidedly higher result for the interaction probability than other workers (if the Keuffel result is ignored for the reasons stated above). The shortness of the publication by Sens *et al.* makes it difficult to comment on this discrepancy, but it is interesting that in their comparison of their experimental results with a theory by Primakoff the fit is very good throughout the range of measured elements except in the case of copper where the predicted capture rate is $5{\cdot}45\times10^6$ sec^{-1}.

The value of the interaction rate in iron $(4{\cdot}45\pm0{\cdot}26)\times10^6$ sec^{-1} taken in conjunction with that of Weinrich and Lederman for the interaction rate in calcium yields a value for the ratio of the interaction rates in iron and calcium of $1{\cdot}77\pm0{\cdot}177$. A recent paper by Tolhoek and Luyten (1957) suggests that this ratio depends on the nature of the interaction between the four fermions involved in muon capture. Tolhoek and Luyten predict ratios of 1·08 and 1·70 for the scalar–vector interaction and tensor–axial vector interaction respectively using a potential well of radius $1{\cdot}4\times10^{-13}A^{1/3}$ cm. It would therefore seem that experimental results weigh against the pure scalar–vector interaction– a conclusion which is supported by the results of Sens *et al.* in other elements. Further measurements of other elements are in progress.

Note added in proof.—By making use of more channels when calculating the positive muon contribution to the counts, we have been able to reduce the uncertainties in the estimations of the positive muon backgrounds and thus in the final results. As the extra channels used contained counts caused by negative muons, the estimation of the numbers of positive muon events was made by successive approximations. Calculated in this way, the mean lifetimes of negative muons in iron and copper were found to be (201 ± 11) mμsec and (146 ± 17) mμsec respectively.

ACKNOWLEDGMENTS

We should like to thank Professor J. G. Wilson for his advice and encouragement during the course of this work. One of us (A. M. H.) is indebted to the Department of Scientific and Industrial Research for a maintenance grant.

REFERENCES

Barrett, W. A., Holmstrom, F. E., and Keuffel, J. W., 1957, *Bull. Amer.*
Bell, W. E., and Hincks, E. P., 1951, *Phys. Rev.*, **84,** 1243.
phys. Soc., **2,** 319.
Benade, A. H., 1953, *Phys. Rev.*, **91,** 971.
Conversi, M. E., Pancini, E., and Piccioni, O., 1947, *Phys. Rev.*, **71,** 209.
Hodson, A. L., 1953, *Proc. phys. Soc. Lond.* A, **66,** 49.
Keuffel, J. W., Harrison, F. B., Godfrey, T. N. K., and Reynolds, G. T., 1952, *Phys. Rev.*, **87,** 942.
Lederman, L. M., and Weinrich, M., 1956, *CERN Symposium*, **2,** 427 (Geneva).

Lewis, I. A. D., and Wells, F. H., 1954, *Millimicrosecond Pulse Techniques* (London : Pergamon Press), p. 232.

Meyer, A. J., 1954, *Thesis*, Princeton University (unpublished).

Peierls, R., 1935, *Proc. roy. Soc.* A, **149,** 467.

Pringle, R. W., Black, L. D., Funt, B. L., and Sobering, S., 1953, *Phys. Rev.*, **92,** 1582.

Reines, F., Cowan, C. L., Harrison, F. B., and Carter, D. S., 1954, *Rev. sci. Instrum.*, **25,** 1061.

Sard, R. D., and Crouch, M. F., 1954. *Progress in Cosmic Ray Physics*, vol. II, (Amsterdam: North-Holland Publishing Co.).

Sens, J. C., Swanson, R. A., Telegdi, V. L., and Yovanovitch, D. D., 1957, *Phys. Rev.*, **107,** 1464.

Tolhoek, H. A., and Luyten, J. R., 1957, *Nucl. Phys.*, **3,** 679.

A Variational Calculation of the Equilibrium Properties of a Classical Plasma†

By S. F. EDWARDS
Department of Mathematical Physics, University of Birmingham

[Received October 28, 1957]

ABSTRACT

A variational calculation is given for the free energy of a fully ionized classical plasma. The method avoids redundant variables and allows for cross terms between collective and individual modes of oscillation, though these turn out to be small. A relation is given for the shielding distance in terms of the Debye–Hückel radius and the interparticle distance, it being of the order of the former.

§ 1. INTRODUCTION

THE partition function of a classical plasma cannot be calculated in a straightforward way because the infinite range of the coulomb potential will not allow any expansion of the exponent in the formula

$$Z=\sum \exp\left(-H/\kappa T\right).$$

This problem is understood physically in that the gas shows two kinds of behaviour : individual particle motion, and collective, plasma oscillations. It is not easy to consider the collective oscillations as built up from individual particle motion. In many ways the two motions appear almost independent of one another, but of course the gas has only $6N$ degrees of freedom (N electrons, N protons) and one cannot introduce more coordinates than this. However the concept of collective coordinates is only a means to the end of calculating physical quantities, and there is no reason why the same division of the degrees of freedom between collective and individual particle coordinates should be used throughout a calculation. In this paper the coulomb potential will be separated into long and short range potentials using a parameter h which is a variable of the calculation. The short range part can then be treated by expansion into clusters, a particular division between collective and individual coordinates being used for each cluster. The final answer should not depend upon the exact manner in which the separation takes place and so is stationary against a small change in h, which is used to find h. It is found, as is to be expected, of the order of the Debye–Hückel radius. This calculation is much simpler than that of plasma excitation, since the velocities are independent variables in the partition function, and reliable estimates of the various approximations customary in plasma theory can be made. They are all good. The contributions to the free energy from collective and individual motion are comparable. In order that this calculation can be pursued to higher approximation, quantum effects must be invoked to avoid the electrons and protons coalescing. These effects are not treated in this paper as they are negligible in the fully ionized gas discharge, but could be included if required.

---

† Communicated by Professor R. E. Peierls, F.R.S. Work partly performed whilst consultant at A.E.R.E., Harwell.

§ 2. The Evaluation of the Free Energy

The free energy of the system is defined as

$$-F=\kappa T \log Z \quad . \; . \; . \; . \; . \; . \; . \; . \quad (1)$$

where Z is the partition function

$$Z=\int \ldots \int \Pi\, d^3v_i\, d^3x_i \exp -H(1, 2, \ldots, N)/\kappa T. \quad (2)$$

For a system of N protons and N electrons

$$H=\sum \tfrac{1}{2}mv_i^2+\sum_{\alpha} \tfrac{1}{2}Mv_\alpha^2+\sum_{\substack{i\neq j\\ \alpha\neq\beta}} e^2(r_{ij}^{-1}+r_{\alpha\beta}^{-1}-r_{i\alpha}^{-1}) \quad . \; . \quad (3)$$

i, j referring to electrons, α, β to protons. The velocities integrate out straight away and contribute additively to F. Henceforward F will be taken to refer to the remaining potential energy part.

The simplest separation into long and short range forces is to write

$$\frac{1}{r}=\frac{\exp(-r/h)}{r}+\left\{\frac{1}{r}-\frac{\exp(-r/h)}{r}\right\}. \quad . \; . \; . \quad (4)$$

If the latter is fourier analysed in a box of side R, it gives

$$\frac{1}{r}-\frac{\exp(-r/h)}{r}=\frac{1}{\pi R}\sum\sum\sum \exp(2\pi i\mathbf{k}\,.\,\mathbf{r}/R)\{k^{-2}-(k^2+(R/2\pi h)^2\}^{-1} \quad (5)$$

if

$$\left.\begin{aligned}\rho_{\mathbf{k}}&=\sum_{j=1}^{N}\exp(2\pi i\mathbf{k}\,.\,\mathbf{r}_j/R)\\ \sigma_{\mathbf{k}}&=\sum_{\alpha=1}^{N}\exp(2\pi i\mathbf{k}\,.\,\mathbf{r}_\alpha/R\end{aligned}\right\} \quad . \; . \; . \; . \; . \; . \quad (6)$$

and

$$(R/2h)^2k^{-2}(k^2+(R/2h)^2)^{-1}=\Psi \quad . \; . \; . \; . \; . \quad (7)$$

then

$$\sum_{i\neq j}\left\{\frac{1}{r_{ij}}-\frac{\exp(-r_{ij}/h)}{r_{ij}}\right\}=\frac{1}{\pi R}\sum\sum\sum(\rho_{\mathbf{k}}\rho_{\mathbf{k}}^*-N)\Psi(k). \quad . \; . \; . \quad (8)$$

It is convenient to use only N of the ρ's (or subsequently N-6 etc.), so define a potential $\phi(r)$

$$\sum_{i\neq j}\phi(r_{ij})=\frac{1}{\pi R}\sum(\rho_{\mathbf{k}}\rho_{\mathbf{k}}^*-N)\Psi(k) \quad . \; . \; . \; . \; . \; . \; . \quad (9)$$

where the sum now runs over N vectors $\mathbf{k}$, i.e. inside a sphere of radius $(3N/4)^{1/3}$ in k space. The part corresponding to the sum outside this sphere to infinity corresponds roughly to a potential which is significant only inside the interparticle distance, and should be considered as part of the short range potential. Thus now

$$\frac{1}{r}=\phi(r)+\left(\frac{1}{r}-\phi(r)\right)=\phi(r)+\chi(r) \quad . \quad . \quad . \quad (10)$$

is used as separation.

The potential energy now becomes

$$\sum_{\substack{i\neq j\\ \alpha\neq\beta}}(\chi_{ij}+\chi_{\alpha\beta}-2\chi_{i\alpha})+\sum\Psi(k)(\rho_{\mathbf{k}}\rho_{\mathbf{k}}^*-N+\sigma_{\mathbf{k}}\sigma_{\mathbf{k}}^*-N$$
$$-\rho_{\mathbf{k}}\sigma_{\mathbf{k}}^*-\rho_{\mathbf{k}}^*\sigma_{\mathbf{k}}). \quad . \quad . \quad . \quad . \quad . \quad . \quad . \quad . \quad (11)$$

If $\rho_{\mathbf{k}}-\sigma_{\mathbf{k}}=p_{\mathbf{k}}$, the latter becomes

$$\sum\Psi(k)(p_{\mathbf{k}}p_{\mathbf{k}}^*-2N). \quad . \quad . \quad . \quad . \quad . \quad . \quad . \quad (12)$$

Now consider the calculation of the free energy when firstly the latter and then the former terms are neglected. The former can be treated by expansion according to the formula

$$\langle\exp(-H_s/\kappa T)\rangle=\sum(-1/\kappa T)^m\langle H_s^{\,m}\rangle \quad . \quad . \quad . \quad (13)$$

which can be rearranged into

$$\exp\{-H_s/\kappa T+\tfrac{1}{2}(\langle H_s^{\,2}\rangle-\langle H_s\rangle^2)/\kappa^2T^2-\tfrac{1}{6}(\langle H_s^{\,3}\rangle-3\langle H_s\rangle\langle H_s^{\,2}\rangle$$
$$+2\langle H_s\rangle^3)/\kappa^3I^3 \quad (14)$$

so that

$$F=\langle H_s\rangle-\tfrac{1}{2}(\langle H_s^{\,2}\rangle-\langle H_s\rangle^2)/\kappa^2T^2\ldots \quad . \quad . \quad . \quad (15)$$

and for $H_s=e^2\sum(\chi_{ij}+\chi_{\alpha\beta}-2\chi_{i\alpha})$ this series converges well provided that $h\gg r_0$, $\lambda\gg r_0$ where $r_0^{\,3}N=R^3$, $\lambda^2=\kappa Tr_0^{\,3}/4\pi e^2$. It gives

$$\langle H_s\rangle=0$$
$$\langle H_s^{\,2}\rangle=Nr_0^{\,3}h/(8\pi\lambda^4) \quad . \quad . \quad . \quad . \quad . \quad . \quad . \quad . \quad (16)$$
$$\langle H_s^{\,3}\rangle=r_0^{\,3}\lambda^{-2}h^{-1}\langle H^2\rangle\zeta \quad . \quad . \quad . \quad . \quad . \quad . \quad . \quad . \quad (17)$$

where ζ involves the quantal cut-off required to avoid an ultra-violet catastrophe. However assuming the h will be of the order of λ, and physically the value of $r_0\lambda^{-1}\ll 1$ this term is already very small, and the expansion will be pursued no further. The change in separation of long and short range potentials from $\exp(-r/h)r^{-1}$ to $\phi(r)$ makes a change of order $(r_0/h)^2$ in the free energy and confirms that $\exp(-r/h)/r$ can to all intents and purposes be taken as the shielded potential.

If the collective part of the Hamiltonian is now considered, it gives

$$\int\ldots\int_i \Pi\, d^3x_i \exp(-\sum(p_{\mathbf{k}}p_{\mathbf{k}}^*-2N)\Psi(k)/\kappa T). \quad . \quad . \quad (18)$$

If the $p_{\mathbf{k}}$'s are now taken as the basic set of coordinates (with the other combination $\rho_{\mathbf{k}}+\sigma_{\mathbf{k}}$, which does not enter the Hamiltonian) a Jacobian is required from the x's to the p's. Although this is well known to be $\exp-\{p^*p/2N\}$ (e.g. Bohm and Pines 1952), a derivation is given in an Appendix which also estimates the errors involved. Strictly the $|p_{\mathbf{k}}|$ cannot exceed $2N$, but the integral (18) is strongly convergent and can be taken to be

$$\int \dots \int_{k \text{ in sphere}} \Pi\, dp_{\mathbf{k}} \exp\{-p_{\mathbf{k}}p_{\mathbf{k}}^*(\Psi/\kappa T+(2N)^{-1})+2N\Psi/\kappa T\}$$
$$=\exp\{N\textstyle\sum\Psi/\kappa T\}\pi(\Psi/\kappa T+(2N)^{-1})(\kappa T)^N\pi^{N/2}. \quad . \quad . \quad . \quad (19)$$

The contribution to the free energy is then, omitting additive constants

$$-F_{\text{long}}=N\textstyle\sum\Psi(k)+\kappa T\sum\log(\Psi/\kappa T+(2N)^{-1}). \quad . \quad . \quad . \quad (20)$$

Now consider the whole problem. The series expansion cannot now be simply applied with the above evaluation of the collective contribution except in the first term, which is just the collective contribution alone. In the term $\langle H_s{}^2\rangle$ integrals are in the form

$$\int\phi^2(ij)\, d^3x_i\, d^3x_j$$

collective term, and one is using all the coordinates already in the collective term. This is easily overcome by separating out the $i.j$ coordinates, say electrons 1 and 2 without loss of generality and redefining

$$p_{\mathbf{k}}'=\sum_7^N \exp(2\pi i\mathbf{k}\,.\,\mathbf{r}_l/R)-\sum_1^N \exp(2\pi i\mathbf{k}\,.\,\mathbf{r}_\alpha/R) \quad . \quad . \quad (21)$$

Then

$$\textstyle\sum(p_{\mathbf{k}}p_{\mathbf{k}}^*-2N)\psi(k)\rightarrow$$
$$\textstyle\sum\{p_{\mathbf{k}}'p_{\mathbf{k}}'^*-p_{\mathbf{k}}'(\exp(-2\pi i\mathbf{k}\,.\,\mathbf{r}_1/R)+\exp(-2\pi i\mathbf{k}\,.\,\mathbf{r}_2/R))+\text{c.c.}$$
$$+\exp\{2\pi i\mathbf{k}\,.\,(\mathbf{r}_1-\mathbf{r}_2)/R\}+\text{c.c.}-2N+2\} \quad . \quad . \quad (22)$$

The $p_{\mathbf{k}}'$ can now be integrated away, and the only final change lies in the $2N-2$ rather than $2N$ is the exponential, and that the k sphere now should have a radius of order $(N-1)^{1/3}$ rather than $N^{1/3}$. Both of these are order N^{-1} down from the principal terms, and in effect the two independent calculations can just be added together:

$$-F=N\textstyle\sum\Psi+\kappa T\sum\log(\Psi/\kappa T+(2N)^{-1})+(Nr_0{}^2h)/(8\pi\lambda^4\kappa I) \quad . \quad . \quad (23)$$

§ 3. THE DETERMINATION OF THE SHIELDING RADIUS

The free energy mainly comes from short range encounters of the particles and from long wavelength fluctuations of the charge density. Between them lies a region which roughly speaking can be treated in either way and somewhere in this region the diversion is made which involves the radius h. If h is increased by δh, this amounts to removing some part of the short range potential and including its effect in the long range potential. It is reasonable that there is a range of values of h for which it makes no difference whether this part of the potential is treated in one way or the other. It has been checked that the actual $F(h)$ has a broad minimum and the value of h giving this minimum represents the best value of h, i.e. that which makes the calculation most accurate. It has been assumed that taking more terms into the calculation will not materially alter this position, and this certainly appears to be the case. As it stands, however, the method does not have the power of a minimal principle.

After algebraic manipulation the equation $\partial F/\partial h=0$ becomes

$$r_0^3\lambda^{-2}h^{-1}=16\pi\sum(k^2[2\pi h/R]^2+1)^{-2}\{N+4\pi^2\lambda^2Rr_0^{-3}k^2[k^2(2\pi h/R)^2+1]^{-1}\}. \quad . \quad . \quad . \quad (24)$$

The sum over k can be replaced by the integral inside the sphere $(4/3)\pi k^3{}_{\max}=N$, and putting $k=k'(4/3)^{1/3}(2\pi)^{-1}$, (24) becomes

$$1=\frac{8\lambda^2h}{r_0^3\pi}\int_0^{2\pi(3\pi/4)^{1/3}}(k^2h^2r_0^{-2}+1)^{-1}(1+k^2\lambda^2r_0^{-2}[k^2h^2r_0^{-2}+1])^{-1}k^2\,dk. \quad (25)$$

Provided that $\lambda\gg r_0$, which is the case under consideration, the upper limit of this integral can be extended to infinity and finally the result is

$$\left(\frac{h}{\lambda}\right)^2=\frac{8}{\pi}\int_0^{\infty}(j^2+1)^{-2}(1+j^2\lambda^{-2}h^{-2}[k^2+1])^{-1}j^2\,dj \quad . \quad . \quad (26)$$

which gives $2h^2\sim\lambda^2$, i.e. the shielding distance is of the order of the Debye–Hückel radius, and the free energy is now given by (23) using h from (26).

It is interesting to note that the contribution to the free energy from both types of contribution is of the same order: $(V/\lambda^3)kT$ (V the total volume).

§ 4. CONCLUSION

It appears from this calculation that the usual approximations of plasma theory are justified in thermal equilibrium, and that the method given here gives a reliable calculation of the thermodynamic quantities of a fully ionized gas, in the region where quantal effects play no part. The problem of the correlation energy can be approached in a very similar manner except that since the free energy is a number, so also is h, whereas the correlation energy, being a function of r requires an $h(r)$. It is hoped to publish a treatment of this in due course. The other problem remaining in thermal equilibrium is that of the correlations in space and time of the charge density in an equilibrium state, and the frequency of oscillations associated. It is hoped to treat this also.

APPENDIX

It is required to find the Jacobian of the transform $x\rightarrow\rho$. For simplicity consider the one dimensional transformation

$$\rho_k=\sum_{-N/2}^{N/2}\exp(2\pi ik\,.\,x_i/R).$$

The Jacobian is the ratio of the elements of volume $dx_1\,.\,.\,.\,.\,.\,dx_N$ to $d\rho_{-N/2}\,.\,.\,.\,.\,.\,d\rho_{N/2}$. Now this can be regarded as the probability of finding $\rho_{-N/2} \cdot \cdot \cdot \cdot \cdot \rho_{N/2}$ when the $x_1 \cdot \cdot \cdot \cdot \cdot x_N$ is random since if P is the probability of a distribution

$$P(x_1 \ldots x_N)\, dx_1 \ldots dx_N = d\rho_{-N/2} \ldots d\rho_{N/2} P(\rho_{-N/2} \cdots \rho_{N/2})$$

and if the x's are random $P(x_1 \ldots x_N)$ is unity. This probability is the coefficient of $\xi_{-N/2}^{\rho_{-N/2}} \ldots \xi_{N/2}^{\rho_{N/2}}$ in

$$\left\{ \int_{-R/2}^{R/2} \xi_{-N/2}^{\exp(-\pi i N x/R)} \xi_{N/2+1}^{\exp(-\pi i (N-2) x/R)} \ldots \xi_{N/2}^{\exp(\pi i N x/R)}\, dx \right\}^N \quad . \quad . \quad (27)$$

which is, putting $\xi_j = \exp i\zeta_j$

$$P(\rho_{-N/2} \cdots \rho_{N/2}) = \Pi(2\pi)^{-1} \int_{-\infty}^{\infty} \ldots (2\pi)^{-1} \int_{-\infty}^{\infty}$$

$$\times \left\{ \int_{-R/2}^{R/2} \exp i \left[\sum_j \zeta_j \exp^{(2\pi i j x/R)} \right] dx \right\} \Pi d\zeta_k \quad (28)$$

The value of this integral lies almost all near $x=0$ and the x integration can be performed by expansion and recombination in the exponential. This is essentially the method of stationary phase. Then the first integral is

$$\Pi(2\pi)^{-1} \int_{-\infty}^{\infty} \ldots (2\pi)^{-1} \int_{-\infty}^{\infty} \exp \Big[-\sum \zeta_j \rho_j - \frac{N}{2} \sum \zeta_j \zeta_j$$

$$- \frac{N}{24} \sum \zeta_a \zeta_b \zeta_c \zeta_d \delta(a+b+c+d) \Big] = \Pi \exp\left(-\rho_k \rho_k^*/N\right) \left(\frac{\Pi}{N}\right)$$

$$\times \exp \left[-\frac{1}{24 N^3} \sum \zeta_a \zeta_b \zeta_c \zeta_d \delta(a+b+c+d) \right] \quad . \quad . \quad . \quad . \quad . \quad . \quad . \quad (29)$$

when N is large this becomes

$$(\pi/N)^N \exp\left(-\sum \rho_k \rho_k^*/N\right) \quad . \quad . \quad . \quad . \quad . \quad . \quad . \quad . \quad (30)$$

Note that the form (27) will vanish when the x's lie outside the interval $(-\frac{1}{2}R, \frac{1}{2}R)$ and so $P(\rho)$ vanishes over a certain part of the ρ space. This is represented by the terms in the expansion, which are so small that effectively the integral can go to infinity.

ACKNOWLEDGMENTS

The author would like to thank Professor Peierls, and Drs. W. B. Thompson and J. Hubbard of A.E.R.E., Harwell for their helpful comments upon this work.

REFERENCE

BOHM, D., and PINES, D., 1952, *Phys. Rev.*, **85**, 338.

On the Origin of Dislocations†

By Doris Kuhlmann-Wilsdorf
School of Metallurgical Engineering, University of Pennsylvania

[Received September 21, 1957]

Abstract

In the face-centred cubic lattice a stacking fault, caused by the condensation of vacancies on a {111} plane, is converted into a dislocation source of Frank–Read type if it is swept by a half-dislocation of a kind that restores lattice order. Dislocation sources will also arise in other major lattice types through the condensation of vacancies on close-packed lattice planes. It is proposed that these are the dislocation sources which release a major proportion, if not all, of the dislocations formed during plastic deformation. Besides several minor advantages, the introduction of this kind of dislocation source can account for all the important glide systems found in crystals of the most common lattice types.

§ 1. Introduction

For a number of years now the theory that the dislocations formed during plastic deformation are released from a random network of dislocations (Mott 1952) in which the links act as Frank–Read sources of dislocations (Frank and Read 1950) has been accepted almost universally. This is not surprising since this theory is at the same time simple and theoretically convincing. Not only are there theoretical reasons to account for dislocation networks, even in the most carefully prepared specimens (Frank 1950), but moreover Hedges and Mitchell (1953) found evidence of dislocation networks in silver bromide crystals. It seems quite certain that, given suitable stresses, such a network can release dislocations by the Frank-Read mechanism. An important question, however, still remains to be answered, namely whether in actual fact all, or at least most of, the dislocations produced during plastic deformation are formed in this way.

Since the above theory of three-dimensional dislocation networks was proposed the number of published experimental observations which appear to be in more or less severe disagreement with it has increased. In the following five such observations are listed.

(i) At small strains, before slip bands appear, face-centred cubic pure metals show surface striations, usually not fully resolved even in the best electron micrographs. These have been named 'fine slip'

---

† Communicated by the Author.

(Brown and Honeycombe 1951) or 'elementary structure' (Wilsdorf and Kuhlmann-Wilsdorf 1951). Measurements of this structure on super-purity aluminium crystals suggest—for every one of the twelve possible glide systems—the presence of about 10^7 sources/cm^2, which are capable of acting at stresses below 1 kg/mm^2 (Wilsdorf and Kuhlmann-Wilsdorf 1952, Kuhlmann-Wilsdorf and Wilsdorf 1953). Such a source density is rather too high to be easily credible.

(ii) Recently Toaka and Sakata (1957) observed that strained specimens of Cu_3Au alloy exhibit the elementary structure when deformed while in the ordered state, but show the long sharp lines first described for α-brass (Kuhlmann-Wilsdorf and Wilsdorf 1953) when disordered. The latter type of surface structure would indicate a very much smaller number of active Frank–Read sources than the former, and it is difficult to see how a simple heat treatment could have such a profound effect on the structure of a dislocation network.

(iii) A similar unexpected effect of heat treatment on surface structure is observed on pure aluminium and copper. These metals show elementary structure and slip bands when well annealed (Kuhlmann-Wilsdorf and Wilsdorf 1953) but produce a slip line structure resembling that of α-brass when deformed after rapid quenching from a high temperature and subsequent ageing (Maddin and Cottrell 1955, Maddin 1957 (private communication)).

(iv) In a random network of dislocations a considerable fraction of the links, acting as Frank–Read sources, would give rise to the so-called 'homogeneous slip' (Suzuki and Fujita 1954, Suzuki 1954, Bilby 1955), but a thorough study of the surface structure on α-brass (Wilsdorf and Fourie 1956) failed to reveal any homogeneous slip.

(v) Gilman and Johnston (1956, 1957) Gilman (1957), in a series of ingenious and careful experiments, found no evidence of pre-existing dislocations at the centre of newly-formed dislocation loops, and concluded that, in crystals of LiF, dislocations are not released from (network) Frank–Read sources.

§ 2. STACKING FAULTS AS DISLOCATION SOURCES

A dislocation represents a very strong concentration of elastic energy. This fact makes it unlikely that dislocations can arise through the action of stresses comparable to the typical yield stresses of pure face-centred cubic metal crystals, and, because a dislocation in order to be stable at such stresses has to be about 10^{-4} cm long, thermal fluctuations cannot materially assist in their formation. Further, since the most carefully prepared specimens usually have the lowest yield points, local stress concentrations, such as might exist in the vicinity of sub-boundaries, impurities and other lattice defects, cannot be responsible for the formation of dislocations in metal crystals at low stresses.

The obvious remaining way, then, to explain the profuse generation of dislocations taking place at low stresses in metals is to seek their origin in some kind of lattice defect which can be assumed to be present in large numbers in every real crystal. This was done most successfully by Frank and Read in that mechanism which carries their name, after a previously-developed model of dislocation multiplication by reflection (Frank 1948) had for some time been widely accepted as the correct explanation for the origin of dislocations.

Dislocation reflection may well take place under certain conditions, but it is not now believed to be the normal process of dislocation production in ductile crystals, mainly because calculations showed the required stresses to be too high (see Cottrell 1953 b). Further, the predicted rapid formation of slip lines, and the corresponding sudden strain increments could not be verified experimentally (Leibfried 1950). Another possible model for the generation of dislocations, explored by Frank and Stroh (1952), is the formation of dislocations at the ends of kink bands; but this requires kink bands of a strength which cannot possibly be expected in pure, undeformed crystals.

Since Seitz (1952) studied the interactions between vacancies and dislocations much evidence has become available to indicate the profound influence which vacancies—singly, in groups or condensed into stacking faults—can have on the plastic properties of metals (see the review article by Cottrell 1957). Therefore it seemed promising to search for a process by which vacancies would be responsible for the creation of dislocations. The simplest way for this to happen in the face-centred cubic system would be by the condensation of vacancies into two adjacent, continuous and similar layers in the $\{110\}$ plane, bounded at one end by a $\langle 110\rangle$ direction. This would yield a normal edge dislocation (Barnes 1954) or, more accurately, an edge dislocation forming part of a prismatic dislocation (Seitz 1952). However, there is no apparent reason for vacancies to condense in this peculiar fashion, but instead it is highly likely that they will condense in $\{111\}$ planes, thereby forming stacking faults bordered by Frank sessile dislocations (Read 1953).

Seitz (1952) believes such vacancy condensation to be possibly 'a very important means by which dislocation rings are generated in practice, for example, during cooling of a melt in which there is a high density of vacancies. . .'. Again, this idea of dislocation formation through the condensation of vacancies has been employed to account for the origin of sub-grain boundaries (Teghtsoonian and Chalmers 1951, 1952, Frank 1956). Moreover, the same kind of stacking faults could, and probably do, arise through growth accidents during crystallization from the melt or during recrystallization. Hence it is reasonable to assume that significant proportions of stacking faults are formed in every real crystal, although probably not enough to be detectable by x-rays (Smallman and Westmacott 1957). Further it appears to be most likely that the stacking faults in face-centred cubic crystals will tend to be bounded by $\langle 110\rangle$ directions, these being the close-packed lattice directions.

It is a property of the stacking faults under discussion that order is restored if the area of the fault is swept by a half-dislocation having any of three possible slip vectors in $\langle 211\rangle$ directions. (The other three, of the total of six slip directions—counting forward and reverse motion separately—which lie in any {111} plane are excluded because they would cause the atoms in the two adjacent layers to face each other.) Any such half-dislocation will combine with the Frank sessile dislocation according to $\frac{1}{6}[211]+\frac{1}{3}[111]=\frac{1}{2}[011]$, thus forming a total dislocation of normal type (Read 1953). Depending on the slip direction of the half-dislocation, the resultant dislocation may have any of the three slip directions of $\langle 011\rangle$ type which do not lie in the plane of the fault (figure). From now on a dislocation formed in the manner described, and encircling the site of an eliminated stacking fault, will be called an R-dislocation—for ‘resultant’ dislocation.

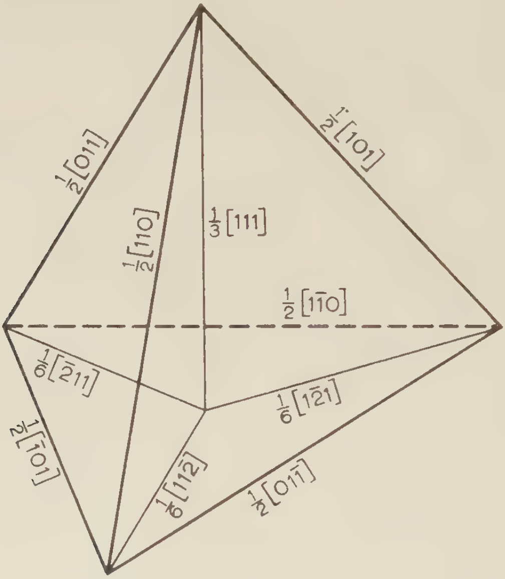

The geometry of slip planes, and slip directions of complete and of half dislocations in the face-centred cubic lattice.

As was argued before, stacking faults in face-centred cubic lattices will tend to be bounded by $\langle 110\rangle$ directions, and hence the R-dislocations will mostly consist of straight segments parallel to the three $\langle 110\rangle$ directions which lie in the plane of the original stacking faults. These directions, together with the slip direction of the R-dislocation, define the possible slip planes on which the R-dislocation could glide. From the figure it can be seen that only two of the three $\langle 110\rangle$ directions in the plane of any particular fault share a {111} plane with the slip direction, i.e. share that plane which experimentally is known to act as slip plane. Consequently R-dislocations can act as Frank–Read sources, such that those parts which lie in a favourably oriented {111} plane can form expanding loops. Those parts which are parallel to the third, unfavourable $\langle 110\rangle$ direction or which lie in a little-stressed {111} plane provide the immobile or dragging dislocation nodes,

§ 3. SOME NUMERICAL ESTIMATES ON R-DISLOCATIONS

In the preceding section we saw that R-dislocations will arise wherever half-dislocations are formed in a stacking fault, and it should now be investigated under what conditions they can be expected to form. Obviously the creation of half-dislocations in stacking faults is a much easier process than the formation of glide dislocations in an undisturbed lattice. This is so because a half-dislocation has a considerably smaller energy and because it is strongly attracted towards the still-faulted regions, so that it moves as if under the influence of a strong shear stress tending to increase the diameter of a newly-created loop. The resolved shear stress corresponding to this attractive force depends on γ, the stacking fault energy. In face-centred cubic metals its magnitude is estimated between about 20 ergs/cm² and 200 ergs/cm², whereby the lower figure would be applicable to copper, the higher to aluminium (Seeger and Schöck 1953, Smallman and Westmacott 1957). The equivalent shear stress of a stacking fault is easily calculated as follows.

If a 1 cm dislocation line with slip vector b moves under the action of a shear stress τ through the distance s the mechanical work done thereby equals τsb. The energy released if the same dislocation moves over a stacking fault, leaving order in its path, is given by γs. Equating the two expressions, the equivalent shear stress becomes $\tau_e = \gamma/b$. With $b = 2 \times 10^{-8}$ cm and $\gamma = 20$ ergs/cm² this yields $\tau_e = 10^9$ dynes/cm² $= 10$ kg/mm², and with $\gamma = 200$ ergs/cm² the equivalent stress is $\tau_e = 100$ kg/mm². The typical yield stress for pure face-centred cubic metals is about 0·1 kg/mm². According to a calculation and curves given by Frank (1950) it appears that a stacking fault energy of 200 ergs/cm² will lead to the spontaneous nucleation of half dislocations, but not a fault energy of 20 ergs/cm².

An additional factor which may have to be taken into consideration is a possible interaction between the sessile dislocations and the half dislocations. Since the resulting undissociated dislocation has about as much energy as the two single dislocations together before the reaction, there is no first-order effect. A second-order effect may exist, though, as the resulting dislocation—where it lies in a $\{111\}$ plane—will dissociate into half-dislocations of type $\frac{1}{6}\langle 211\rangle$, thereby reducing its energy; and also because of changes in the core energy. Superficially one might think that this interaction could assist in the formation and initial growth of a half-dislocation if it were nucleated at such a small distance from the sessile dislocation that parts of them could combine while the half-dislocation was still very small.

Considering all these points together it seems probable that in those cases in which half-dislocations are not formed spontaneously great numbers will be formed through thermal activation during the unavoidable periods of heat treatment.

For specimens still containing a majority of unconverted stacking faults it is to be expected that half-dislocations will be formed through the action of the stress fields of dislocations which either pass through the faults or move past them at close distances. From the first few dislocations a chain reaction will result since the newly-formed R-dislocations can release loops which in turn will trigger more R-dislocations and so on.

The process outlined is possible because the stresses near the centre of a dislocation reach values, sufficient for the formation of half dislocations in stacking faults, within distances of 10 atomic diameters or more from the dislocation axis, and because the critical radius of a half-dislocation in a fault is quite small. It remains to be seen what types of dislocations are likely to result in this way.

As was found earlier the slip direction of an R-dislocation cannot lie in the plane of the original fault. Therefore, if a dislocation approaches a stacking fault in its own slip plane or cross slip plane the resulting R-dislocation cannot have the slip vector of that triggering dislocation. Since normally an R-dislocation can release dislocations in both planes which contain its Burgers vector we see that, at the very minimum, sources on four different glide systems must be produced. Moreover, remembering that the active stresses strongly depend on the relative position of fault and triggering dislocation, on its type—whether edge, screw or mixed—and possibly on its speed (which may determine whether the nucleation of the half-dislocation takes place ahead of the approaching dislocation or behind it), one comes to the conclusion that the passage of just one dislocation loop through a random array of stacking faults can lead to R-dislocations on all possible slip systems.

Another problem to be considered concerns the probable size and number of stacking faults in a crystal. An estimate of the total faulted area can be made from the concentration of vacancies at the melting point. This is approximately given by $c \simeq \exp(-U/kT)$ with U the energy of formation of a vacancy. If all the vacancies which are present in a crystal at its melting point would condense into stacking faults the total fault area per cubic centimetre could be found as

$$A \cong (1/d)[\exp(-U/kT)]$$

where d is the distance between closely-packed lattice planes. This formula will give a somewhat too high value because a fraction of the vacancies will not find their way to stacking faults but will be absorbed by other types of sinks for vacancies. On the other hand there will be an additional—and so far unknown—contribution due to faults arising from growth accidents. Thus the above formula seems to be adequate, particularly since there exists some uncertainty about the value of U for most crystals, which probably introduces a larger error than that due to vacancies not captured by stacking faults.

To make an estimate as to the average size of the stacking faults is a difficult task. It is dependent on a number of parameters, as for instance, the thermal history of the specimen under consideration, the stacking fault energy, the activation energy for the nucleation of a stacking fault, the binding energy between vacancies to form groups, and the diffusion constant of single vacancies and aggregates of vacancies. However, it is still possible to give limits and probable trends: the diameters of stacking faults probably range from several microns to less than 50 Å. An upper limit of stacking fault diameter is to be expected because the faults will hardly become larger than the cross section of the sub-grains in their parent crystal. A lower limit is necessary because below a critical size the energy of all contributing vacancies together becomes smaller than the energy of the stacking fault plus the energy of the dislocation surrounding it.

In order to estimate the lower limit of stacking fault diameter we compare the surface energy of a disc-shaped hole—the potential stacking fault before its sides have collapsed—with the energy of the fault plus surrounding dislocation. The energy of a dislocation loop of very small diameter, D, is about equal to Gb^2D (Frank 1950), with G the modulus of rigidity, and the energy of the stacking fault is equal to $\frac{1}{4}\pi D^2\gamma$. The sum of these two energies must be equal to, or smaller than, $\frac{1}{2}\pi D^2\sigma$ where σ is the surface energy of the metal considered. From this we get $(D/b) \gtrsim 4Gb\,[\pi(2\sigma-\gamma)]$. For aluminium this formula gives $D \cong 10$ Å.

The wide variations in size and number of R-dislocations, which, according to the preceding argument, are obviously possible, can account for the observed great differences in the plastic properties of specimens of different metals, or of specimens of the same material but with a different history. For instance one will expect that in order to generate large stacking faults long periods of heat treatment will be necessary, and that specimens rapidly cooled from the melt will tend to have many small faults. So qualitatively one sees why single crystals should have low yield points (slow cooling leads to small supersaturations, fewer but larger stacking faults, yielding R-dislocations able to act at low stresses) while rapidly solidified specimens should be much harder.

As was argued above, the longest segments of R-dislocations should be comparable in length to the diameter of the subgrains. Approximately, then, the yield stress τ_y should be connected with the average diameter of the subgrains, L, as $\tau_y = Gb/L$, where G is the modulus of rigidity and b the Burgers vector. This formula was previously derived by Bragg (1942) in a quite different way and found to be in satisfactory agreement with experimental data.

§ 4. Fine Slip, Slip Bands, α-Brass Structure and Cross Slip

Qualitatively the interpretation of the phenomena of elementary structure and slip bands will hardly be affected by the introduction of a new type of dislocation source. A theory developed earlier (Kuhlmann-Wilsdorf *et al.* 1952) seems to be adequate. There it was argued that at stresses near the yield point a multitude of dislocation sources start to act almost simultaneously, and that the dislocation loops emitted by them spread out fairly slowly until they are stopped through the interaction with loop sequences from neighbouring sources. Because of the high density of active sources the mean free path of the dislocations remains so small that only comparatively few loops, say up to 30, can be emitted from any one source, leading to the observed shallow, closely-spaced elementary lines.

In the same paper the formation of slip bands was explained as follows : the first few dislocation loops from any elementary lines which, accidentally, have become particularly strong can first encircle, and then force back into their respective sources those dislocation loops which block their path. The annihilation of the blocking loops aids the action of other, suitably situated dislocation sources which in turn allows their loop sequences to grow strong enough to repeat the process, and so on.

The interpretation of the α-brass structure, which we believe appears on alloys with a short range order, has already been given in a recent lecture (Kuhlmann-Wilsdorf *et al.* 1957). The significant difference between metals with an elementary structure and metals with an α-brass structure apparently does not lie in the number, quality or distribution of the dislocation sources, but in the changes caused on a slip plane by the passage of a dislocation. In an alloy containing a short range order the yield stress is higher than the stress which would be necessary to activate the available dislocation sources in a disordered lattice. This is so because, by their motion, dislocations disturb the order along their slip planes, and thus the external stress has to provide this ordering energy in addition to that needed to move the dislocations through a disordered lattice (Fisher 1953, Cottrell 1953 a, Logie 1957). Once slip has started on any lattice plane the disordering proceeds at a decreasing rate, and complete disorder is reached after the slip on a plane is about equal in magnitude to the diameter of the average domains. Consequently the stress necessary to move a dislocation along a slip plane is highest for the first one to cross that plane and then diminishes until the stress corresponds to complete disorder. Therefore, although an alloy exhibiting the α-brass structure probably contains stacking faults of similar sizes and numbers as a pure metal—which may or may not have already been converted into R-dislocations—slip will only start at the threshold stress which is necessary to destroy the short range order ; but once slip has started from a source it will be propagated at a high speed over comparatively large areas of the slip plane, thus causing the long and sharply defined slip lines typical of α-brass.

'Clear' cross slip, i.e. sharp slip lines abruptly changing from one slip plane to the corresponding cross slip plane, is prominent wherever the α-brass structure is observed, but, according to electron micrographs, it is exceedingly rare in pure metals (Wilsdorf and Kuhlmann-Wilsdorf 1952, Noggle and Koehler 1957). This can be easily understood on the basis of our argument that sequences of dislocations in pure metals are obstructed by slip from neighbouring sources even at low stresses, whereas in α-brass and similar alloys the sources which act at small strains are unimpeded by other sources.

The straight segments of the R-dislocations which act as Frank Read sources are, in face-centred cubic metals, mostly linked to one segment on the corresponding cross slip plane. Where there is little freedom of movement for the dislocations, as in pure metals, this will be of little consequence, but wherever the R-dislocations emit loops, unhindered by neighbouring dislocations, there will be a probability that the dislocation loops spreading out on the active slip system will, at the same time, drag out loops on the cross slip system. In this way cross slip arises although the dislocations never change their slip planes.

This does not mean that cross slip does not also come about through dislocations moving from one slip plane into another—indeed this process seems to have been directly observed by Hirsch *et al.* (1956). If significant numbers of dislocations do change their slip planes, then, in a metal with short range order, there is a high probability that several dislocations will follow the same path, a process which will lead to clear cross slip. However, in the case of pure metals no noticeable difference exists between slip planes on which dislocations have moved already and those which are still undisturbed (except possibly after severe straining and near surfaces). Therefore in them dislocations changing their planes will do so more or less at random, and no sharp cross slip traces can be expected as a result of this process. Sharp cross slip can be produced in pure metals only under unusual conditions, such as, for instance, in the strongly inhomogeneous stress field near an etch pit, where the two-fold action of R-dislocations, discussed above, takes place.

In agreement with this idea, the expected distinct difference between the diffuse cross slip linking slip bands, and sharp cross slip lines near etch pits has been often observed in aluminium. Several examples of this can be found in the micrographs published by Wilsdorf and Kuhlmann-Wilsdorf (1952) and by Noggle and Koehler (1957).

§ 5. Some Particular Advantages of the Proposed Theory

At the beginning of this paper five sets of experimental results have been listed which appear to be in disagreement with the concept of the emission of dislocations from a random dislocation network. We shall now see that part of these problems can be solved with the theory proposed in this paper.

(i) In order to make a quantitative comparison between the number of dislocation sources apparently active during the formation of an elementary structure, and the number of sources which can be expected through the condensation of vacancies, use will be made of measurements made on super-purity aluminium by Wilsdorf and Kuhlmann-Wilsdorf (1952). The measurements had been done with great care but were published with the warning that " not too much reliance must be put on such measurements" because the lines were not clearly resolved, their average height being below the resolving power of the preparation techniques available.

Using the formula $A=(1/d)[\exp(-U/kT)]$ derived in § 3, and assuming that on the average the stacking faults are hexagonal with sides L we find n, the number of stacking faults per cubic centimetre of material, as $n=(2\cdot 6L^2d)^{-1}[\exp(-U/kT)]$. Each of the hexagonal R-dislocations represents four possible dislocation sources, so that on each of the twelve glide systems $n'=n/3$ sources per cm^3 can be expected. Taking, for example, a resolved shear stress of 1 kg/mm^2, corresponding to a source length of about 10^{-4} cm, and using $U=0\cdot 76$ ev, due to Bradshaw and Pearson (1957), which is quoted by Cottrell (1957) as the latest measurement of U in aluminium, we obtain $n'=4\cdot 5\times 10^{10}/\mathrm{cm}^3$. This value must be compared with the following measurements which represent the mean obtained from two different crystals stressed to 1 kg/mm^2: mean distance between the elementary lines $s=400$ Å, average length of lines $D=17\cdot 5\ \mu$. The density of active sources can be found as

$$1/V=(\tfrac{1}{4}\pi D^2 s)^{-1}=9\cdot 7\times 10^{10}/\mathrm{cm}^3.$$

In view of the several simplifications and uncertainties involved this agreement is most satisfactory.

(ii), (iii) No complete answer to these points can be given in the present paper. It is believed that the strong dependence of surface structure and plastic properties on heat treatment often is based on the same phenomenon that was discussed above in connection with the α-brass structure, i.e. the changes which may occur on a slip plane as a result of the passage of the first dislocation or the first few dislocations, to move along that plane. It would appear that in many cases the changes in surface structure and plastic behaviour are not primarily due to any variations in the source density or their properties. A theory on this basis was outlined in the lecture mentioned before (Kuhlmann-Wilsdorf *et al.* 1957.) and it is hoped to deal with it more fully soon in a separate paper.

(iv) All possible types of R-dislocations represent dislocation sources of the non-homogeneous type which cannot give rise to 'homogeneous' slip. This follows from a principle first given by Seitz (1952) that the area circumscribed by the projection in slip direction of a general dislocation ring—of which R-dislocations are examples—cannot be changed through slip of the dislocation ring or any parts of it.

(v) The most important argument in favour of the present theory would seem to be the results obtained by Gilman and Johnston. Not only do they represent the most serious challenge to the theory of the three-dimensional dislocation network, but moreover they seem to be in excellent agreement with the generation of dislocations from sheets of condensed vacancies—stacking faults in the case of face-centred cubic metals. In fact Gilman and Johnston (1957) give as one of three possible explanations for their results that "small unseen dislocation loops might be present which grow to form Frank–Read sources when a stress is applied.

Although small loops on the glide planes would be expected to be unstable and hence not present, prismatic loops, which could not disappear by gliding might form by vacancy condensation (J. C. Fisher and F. C. Frank private communication) ". However, the authors then proceed to discount this possibility for the reasons that such prismatic dislocations ought to be eliminated through slow cooling and that they should be easily seen.

While the first of these two reasons appears to be unsound the second is more difficult to judge by anyone not very familiar with the experimental technique used. It should be noted, however, that the necessary R-dislocations would have dimensions in the order of 1 micron only, and that they would hardly be distinguishable from the dislocation loops grown from them. Hence both reasons are probably not convincing enough to discredit the idea of R-dislocations as the origin of dislocations.

§ 6. THE CHOICE OF GLIDE SYSTEMS IN VARIOUS CRYSTAL LATTICES

Except for the satisfactory explanation of the fact that the active slip direction is always the most densely packed lattice direction, advanced by Nabarro (1952), no general and detailed theory on the choice of slip systems has so far been developed. In the idea of dislocation formation through condensed sheets of vacancies, presented here, the glide systems operating in any type of lattice are determined through the slip direction of the R-dislocations and through the orientations which the axes of the R-dislocations will tend to assume. If these parameters can be predicted then a theory of slip systems is obtained.

At present our knowledge of vacancy condensation is scant, and no experimental data are available from which we could definitely deduce on what crystallographic planes it takes place, whether condensation layers are single or multiple, and what are the intermediate steps which lead to the nucleation of a fault. However, primarily vacancies are tiny holes in the material, and, with this idea in mind, we may make the following assumption. Vacancies, which accidentally meet during their thermal motion, form loosely bound groups of a few—say up to seven. The energy of such groups will be lowest if they take the shape of discs parallel to the most densely packed planes. If in the course of their thermally activated motion two or more such groups meet on the same plane they combine to form a disc-shaped hole large enough to allow its collapse, thereby creating an R-dislocation. Or it might even be that already the largest of the primary groups collapse.

Hence we assume vacancies to condense preferentially on the most densely packed atomic planes, and the faults thus created to be bounded by the most densely packed directions in that plane. These, then, will be the directions of the axes of the R-dislocations, and, at the same time, will be the lines of intersection between the slip planes and the plane of the fault. The slip direction is found by considering what type of fault will arise when the two sides of a sheet of vacancies collapse, and what movement will restore the correct lattice order. The imaginary path which any atom of one side of the sheet of vacancies will traverse with respect to the other side of the sheet, from the start of the collapse to the re-establishment of order, is the slip vector. In this way both, slip plane and slip vector, can be predicted, but it should be added that the slip planes thus found are not necessarily those which offer least resistance to the movement of dislocations. Therefore the predicted slip planes could be supplemented by planes into which the dislocations move through cross slip motion. Good reviews of glide systems found experimentally in a number of different lattices are contained in the book by Schmid and Boas (1950) and in a more recent review article by Maddin and Chen (1954).

(i) The face-centred cubic lattice has been partly examined already. The vacancies condense in {111} planes forming stacking faults bounded by ⟨110⟩ directions. The movement due to the collapse of the sheets of vacancies, or in other words, the Burgers vector of the resulting sessile dislocation is $\frac{1}{3}\langle 111\rangle$. The movement which restores order, i.e. the Burgers vector of the half-dislocation, is $\frac{1}{6}\langle 112\rangle$, and the slip vector is the sum of the two movements, namely $\frac{1}{3}[111]+\frac{1}{6}[11\bar{2}]=\frac{1}{2}[110]$.

Slip planes are all planes which contain the slip direction of the R-dislocation and a ⟨110⟩ direction lying in the plane of the fault. We saw (see figure) that two of the three slip planes defined in this way are {111} planes. The third plane, so far neglected, is a {100} plane, a slip plane which is reported on aluminium at elevated temperatures.

(ii) The geometry in the hexagonal lattice is rather complicated, and it ought to be investigated more closely than is done here. It is unique in that removal of one {0001} plane yields a stacking fault which cannot be removed by slip (Read 1953), and the same holds true for the removal of one $\{10\bar{1}0\}$ plane. Consequently no slip dislocation can be formed by the condensation of single layers of vacancies on either the basal plane or the prism face. The Burgers vector which results in both cases is $\langle\bar{1}013\rangle$. This vector lies in the $\{11\bar{2}2\}$ plane, recently identified a as slip plane in zinc by Bell and Cahn (1957), and includes a small angle only with $\langle 11\bar{2}3\rangle$, the slip vector found by the same scientists. However it is extremely improbable that a dislocation with $\langle\bar{1}013\rangle$ as Burgers vector could move because of the severe lattice disturbance which would thereby be created.

The slip vector $\langle 11\bar{2}0\rangle$, commonly observed as slip direction in all hexagonal metals, could arise through vacancy condensation on either $\{11\bar{2}0\}$ or $\{11\bar{2}2\}$. The most probable slip planes associated with these planes are {0001}, the basal plane, and $\{10\bar{1}0\}$, the prism plane.

(iii) In the NaCl structure, which is also the structure of lithium fluoride, vacancies would be expected to condense in {100} planes, and the resultant faults to be bounded by ⟨100⟩ directions. The removal of one {100} plane must be accompanied by an offset of $\frac{1}{2}\langle 100\rangle$ because otherwise like ions would face each other. The slip vector thus becomes

$$\tfrac{1}{2}[100]+\tfrac{1}{2}[010]=\tfrac{1}{2}[110],$$

in agreement with experimental fact. The planes which intersect {100} planes in ⟨100⟩ directions and contain the ⟨110⟩ slip direction are {110} and {100}, representing possible slip planes. {100} is the slip plane actually observed in this lattice type.

(iv) The body-centred cubic lattice, which is geometrically identical with the caesium chloride structure, was recently investigated by Rachinger and Cottrell (1956) because of its interesting property that the slip direction found experimentally is ⟨111⟩ when the atomic bonds in it have metallic character, but is ⟨100⟩ is they are ionic. Rachinger and Cottrell succeeded in interpreting this dependence of slip direction in terms of partial dislocations. Another simple explanation follows from the present theory.

The most densely packed lattice plane is {110}. Removing one {110} plane leaves a fault which will be rectified by an offset of either $\frac{1}{2}\langle 100\rangle$ or $\frac{1}{2}\langle 110\rangle$. The former of the two possibilities represents the smaller lateral motion and, therefore, must be strongly favoured in the body-centred cubic lattice. In ionic crystals with the same structure, on the other hand, an offset of $\frac{1}{2}\langle 100\rangle$ would cause like ions to face each other, which obviously is energetically impossible, and hence, the offset in that lattice will be $\frac{1}{2}\langle 110\rangle$. The resultant slip vectors become $\frac{1}{2}[110]+\frac{1}{2}[001]=\frac{1}{2}[111]$ for the case of metallic bonds, and $\frac{1}{2}[110]+\frac{1}{2}[\bar{1}10]=[010]$ for ionic bonds, in agreement with experimental evidence.

As before, the slip planes are found as the planes which are common to the slip vector and the most densely packed lattice directions in the plane of the fault. In this case the ⟨111⟩ directions are the most closely packed, and two of these lie in any {110} plane, which, as we saw, is the plane of the R-dislocations in the body-centred cubic lattice as well as in the caesium chloride structure. In metals with ⟨111⟩ as slip direction both ⟨111⟩ directions in the plane of the fault define {110} as the slip plane, and this is in fact the dominant slip plane found experimentally. Also if ⟨100⟩ should serve as bounding direction {110} results as slip plane, while with ⟨101⟩ as boundary—the third densest lattice direction in body-centred cubic lattices—{121} becomes a possible slip plane. The third slip plane reported for body-centred cubic metals, {123}, cannot be explained in an obvious way.

The failure to account for {123} as slip plane, and the rather remote probability that {121} would result through vacancy condensation might lend support to the contention of Maddin and Chen (1954) that the wavy slip lines of body-centred cubic metals, usually attributed to the simultaneous action of the three types of slip planes mentioned, could be the result of intimate cross slip on {110} planes only. It is also possible, though not very probable, that in the body-centred cubic lattice a plane other than {110} offers the least resistance to the motion of dislocations, and that, therefore, many dislocations change to that slip plane by means of cross slip—{110} being the only plane on which dislocations can be formed.

For ionic crystals with ⟨100⟩ as slip direction again {110} is the slip plane defined by both ⟨111⟩ directions in the plane of any R-dislocations, The two next densest directions, ⟨100⟩ and ⟨110⟩, would yield {100} as possible slip plane. Experimentally {110} is found as slip plane in the caesium chloride structure.

The above theory of slip systems rests on the assumption that vacancies condense in single layers parallel to the most densely packed planes. If, on the other hand, we were to assume that the vacancies do not condense in this way, but such that they yield R-dislocations with the smallest possible energy the resultant agreement between theory and experimental fact would be much poorer. In all cases double layers normal to the shortest lattice vector give the smallest possible energy, so that the slip directions would be accounted for. However, probable slip planes are found in the order given: body-centred cubic . . . {112} and {101}; CsCl . . . {100} and {110}; NaCl . . . {110} and {100}; hexagonal lattice . . . {0001}. Thus with the exception of the hexagonal lattice. the dominant slip planes always appear as second choice.

ACKNOWLEDGMENTS

To Professor R. Maddin and to my husband, Dr. H. Wilsdorf, sincere thanks are due for many helpful discussions and constant encouragement.

REFERENCES

BARNES, R. S., 1954, *Acta Metall.*, **2,** 380.
BELL, R. L., and CAHN, R. W., 1957, *Proc. roy. Soc.* A, **239,** 494.
BILBY, B. A., 1955, *Report of the Conference on Defects in Crystalline Solids, Bristol,* 1954 (London: Physical Society), p. 124.
BRADSHAW, F. J., and Pearson, S., 1957, *Phil. Mag.*, **2,** 570.
BRAGG, L., 1942, *Nature, Lond.*, **149,** 511.
BROWN, A. F., and HONEYCOMBE, R. W. K., 1951, *Phil. Mag.*, **42,** 1146.
COTTRELL, A. H., 1953 a, *Seminar on the Relation of Properties to Microstructure* (New York: American Society Metals), p. 151; 1953 b, *Dislocations and Plastic Flow in Crystals* (Cambridge: University Press), p. 82; 1957, Symposium on "Vacancies and Other Point Defects in Metals and Alloys", *Institute of Metals, Monograph* no. 23.
FISHER, J. C., 1953, *Phys. Rev.*, **91,** 232.
FRANK, F. C., 1948, *Report on the Strength of Solids* (London: Physical Society), p. 46; 1950, *Report of Pittsburgh Conference on Plastic Deformation of Crystals* (Washington: Carnegie Institute of Technology and Office of Naval Research), p. 89; 1956, *Deformation and Flow of Solids* (Berlin: Springer), p. 73.
FRANK, F. C., and READ, W. T., 1950, *Phys. Rev.*, **79,** 722.
FRANK, F. C., and STROH, A. N., 1952, *Proc. phys. Soc. Lond.* B, **65,** 811.
GILMAN, J. J., 1957, *J. Metals, N.Y.*, **9,** 449.
GILMAN, J. J., and JOHNSTON, W. G., 1956, *J. appl. Phys.*, **27,** 1018; 1957, *General Electric Res. Lab. Report,* no. 57–RL–1662.
HEDGES, J. M., and MITCHELL, J. W., 1953, *Phil. Mag.*, **44,** 223.
HIRSCH, P. B., HORNE, R. W., and WHEELAN, M. J., 1956, *Phil. Mag.*, **1,** 677.
KUHLMANN-WILSDORF, D., MADDIN, R., and WILSDORF, H., 1957, *Meeting American Physical Society* (Philadelphia), March.
KUHLMANN-WILSDORF, D., VAN DER MERWE, J. H., and WILSDORF, H., 1952, *Phil. Mag.*, **43,** 632.

Kuhlmann-Wilsdorf, D., and Wilsdorf, H., 1953, *Acta Metall.*, **1,** 394.
Leibfried, G., 1950, *Z. Phys.*, **127,** 580.
Logie, H. J., 1957, *Acta Metall.*, **5,** 106.
Mott, N. F., 1952, *Phil. Mag.*, **43,** 1151.
Maddin, R., and Chen, N. K., 1954, *Progr. Metal Phys.*, **5,** 53.
Maddin, R., and Cottrell, A. H., 1955, *Phil. Mag.*, **46,** 735.
Nabarro, F. R. N., 1952, *Advanc. Phys.*, **1,** 269.
Noggle, T. S., and Koehler, J. S., 1957, *J. appl. Phys.*, **28,** 53.
Read, W. T., 1953, *Dislocations in Crystals* (New York: McGraw-Hill).
Rachinger, W. A., and Cottrell, A. H., 1956, *Acta Metall.*, **4,** 109.
Schmid, E., Boas, W., 1950, *Plasticity of Crystals* (London: F. A. Hughes and Co., Ltd.), p. 85.
Seeger, A., and Schöck, G., 1953, *Acta Metall.*, **1,** 519.
Seitz, F., 1952, *Advanc. Phys.*, **1,** 43.
Smallman, R. E., and Westmacott, K. H., 1957, *Phil. Mag.*, **2,** 669.
Suzuki, H., 1954, *J. phys. Soc. Japan*, **9,** 531.
Suzuki, H., and Fujita, F. E., 1954, *J. phys. Soc. Japan*, **9,** 428.
Taoka, T., and Sakata, S., 1957, *Acta Metall.*, **5,** 61.
Teghtsoonian, E., and Chalmers, B., 1951, *Canad. J. Phys.*, **29,** 370; 1952, *Ibid.*, **30,** 388.
Wilsdorf, H., and Fourie, J. T., 1956, *Acta Metall.*, **4,** 271.
Wilsdorf, H., and Kuhlmann-Wilsdorf, D., 1951, *Naturwissenschaften*, **38,** 502; 1952, *Z. angew. Phys.*, **4,** 361, 409 and 418.

The Calculation of the Drag in Problems Solved by the Hodograph Method†

By A. G. Mackie
St. Salvator's College, St. Andrews

[Received November 8, 1957]

Abstract

Explicit formulae are found for the total drag on a class of obstacles placed in a uniform stream of an inviscid fluid when the stream function is given in terms of the velocity variables. The formulae are given for incompressible flow and for the exact equation of compressible flow.

There are a number of problems in fluid dynamics for which an exact solution for the stream function Ψ can only be found in terms of the velocity variables. Such problems are said to be solved in the hodograph plane. It is one of the disadvantages of the hodograph method that the transition to the physical plane can seldom be effected in a simple manner. The object of this note is to show that the drag on any straight segment of a body can be found directly from the solution in terms of the velocity variables.

The use of the hodograph method in incompressible flow dates from the time of Helmholtz and Kirchhoff. More recently it has been extensively used in the study of compressible flow, particularly in the transonic region where the usual linearization procedures break down. In incompressible flow Ψ is a harmonic function of u and v, the cartesian components of velocity. It is usually more convenient to work with the polar coordinates q and θ. For compressible flow we introduce a variable τ defined by $\tau = q^2/q_m^2$ where q_m is the maximum velocity attainable by the gas. Ψ now satisfies a second order linear partial differential equation in τ and θ and the solution of this obtained by separating the variables is of the form $\psi_n(\tau)\sin(n\theta+\epsilon_n)$. $\psi_n(\tau)$ is a certain hypergeometric function multiplied by a power of τ. The details of this procedure and the main properties of $\psi_n(\tau)$ are to be found in Modern Developments in Fluid Dynamics (1953). For our purposes we regard $\psi_n(\tau)\sin(n\theta+\epsilon_n)$ as the compressible analogue of the harmonic function $q^n\sin(n\theta+\epsilon_n)$ which is the solution appropriate to incompressible flow.

We are concerned with a class of problems in which an obstacle is placed in a stream which is uniform at infinity with velocity q_0. θ is

---

† Communicated by the Author. This research has been sponsored in part by the Research and Development Command, U.S. Air Force under contract AF 61 (514)—1170, through the European Office A.R.D.C.

measured from the direction of this uniform stream. The obstacle is such that its profile consists of segments along which either the magnitude or the direction of the velocity vector is constant. This may appear to be a rather severe restriction but in fact it is only for obstacles of this type that the boundary value problem can be exactly formulated and hence solved in the hodograph plane. We consider the drag on a straight segment inclined at an angle α to the free stream. For incompressible flow the velocities at the two ends will be denoted by q_1 and q_2. The stream function will be of the form

$$\Psi=\sum a_n q^n \sin(n\theta+\epsilon_n).$$

If p and ρ are respectively the pressure and the density, then the excess pressure over the pressure at infinity p_0 is given by Bernoulli's theorem in the form

$$p-p_0=\tfrac{1}{2}\rho q_0^2-\tfrac{1}{2}\rho q^2.$$

The total drag in the direction of the main stream is

$$\sin\alpha\int p\,ds=L\sin\alpha(p_0+\tfrac{1}{2}\rho q_0^2)-\tfrac{1}{2}\rho\sin\alpha\int q^2\,ds,$$

where the integration is taken along the body contour and L is the total length. Now on the boundary Ψ is a constant which we can take to be zero and $q=d\phi/ds$ where ϕ is the velocity potential. Hence

$$\int q^2\,ds=\int q\,d\phi=\int_{q_1}^{q_2} q\frac{\partial\phi}{\partial q}\,dq.$$

Corresponding to $\Psi=q^n\sin(n\theta+\epsilon_n)$ we have $\phi=-q^n\cos(n\theta+\epsilon_n)$. It follows that the total drag is given by the expression

$$L\sin\alpha(p_0+\tfrac{1}{2}\rho q_0^2)+\sum\frac{na_n\rho\sin\alpha\cos(n\alpha+\epsilon_n)}{2(n+1)}(q_2^{n+1}-q_1^{n+1}).$$

In this formula $\cos(n\alpha+\epsilon_n)=\pm 1$ since $\sin(n\alpha+\epsilon_n)=0$.

For a similar straight profile in compressible flow we denote by τ_1 and τ_2 the values of τ at the two ends. The appropriate form of Bernoulli's equation is now

$$p=p'(1-\tau)^{\beta+1}$$

where p' is the stagnation pressure, $\beta=1/(\gamma-1)$ and γ is the adiabatic index of the gas. The velocity potential ϕ corresponding to a solution $\Psi=\psi_n(\tau)\sin(n\theta+\epsilon_n)$ is

$$\phi=-\frac{2\tau}{n}(1-\tau)^{-\beta}\psi_n'(\tau)\cos(n\theta+\epsilon_n)$$

where the dash denotes differentiation with respect to τ. The contribution to the total drag arising from this term is found to be

$$\frac{p'n\sin\alpha\cos(n\alpha+\epsilon_n)}{2q_m}\int_{\tau_1}^{\tau_2}\frac{(2\beta+1)\tau-1}{\tau^{3/2}}\psi_n(\tau)\,d\tau.$$

It is rather surprising that the integral in this term can be evaluated explicitly. This is achieved by substituting for $\psi_n(\tau)$ in the original partial differential equation and integrating by parts. Corresponding to the solution

$$\Psi = \sum a_n \psi_n(\tau) \sin (n\theta + \epsilon_n)$$

which is to vanish on $\theta = \alpha$ we find, after a certain amount of algebra, that the total component of the drag in the direction of the main stream is

$$\frac{p' n a_n \sin \alpha \cos (n\alpha + \epsilon_n)}{q_m(1-n^2)} [2\tau^{1/2}\psi_n'(\tau)(1-\tau) + \tau^{-1/2}\psi_n(\tau)\{1+(2\beta+1)\tau\}]_{\tau_1}^{\tau_2}.$$

The summation can be over any sequence of positive numbers n which does not include the value $n=1$. This restriction is of no significance as it can be shown that the presence of a term corresponding to $n=1$ in the solution requires the fluid to be at rest at infinity. Such a term cannot therefore arise in problems of flow past a body such as we are considering.

A similar result may be shown to hold for Tricomi's equation which is an approximation to the full hodograph equation and valid for small perturbations about a uniform flow at a Mach number of one.

REFERENCE

Modern Developments in Fluid Dynamics : High Speed Flow, 1953, Volume 1 (Oxford : Clarendon Press).

The Protons Emitted from Iron-54 and Iron-56 on Bombardment with 13·5 MeV Neutrons†

By P. V. MARCH and W. T. MORTON
Department of Natural Philosophy, University of Glasgow

[Received November 20, 1957]

ABSTRACT

Energy spectra and angular distributions of protons emitted from the isotopes ^{54}Fe and ^{56}Fe on bombardment with neutrons with an energy of 13·5 MeV have been studied using photographic emulsions. The angular distributions of protons with energy greater than 7 MeV show a marked forward peak suggesting the occurrence of direct interaction.

§ 1. INTRODUCTION

STUDIES of the inelastic scattering of protons with energies in the region 10–30 MeV (Gugelot 1954, Eisberg and Igo 1954, and Cohen 1957) have indicated the occurrence of interaction processes other than the immediate formation of a compound nucleus. Brown *et al.* (1957), found evidence that direct interaction also occurs in (n, p) reactions at 13·2 MeV. To obtain more information about the direct interaction mechanism, similar studies of (n, p) reactions were undertaken by the present authors with improved energy resolution.

The isotopes ^{54}Fe and ^{56}Fe were chosen for investigation because the effects of the Coulomb barrier should be similar, whereas the (n, p) cross sections should differ considerably in magnitude due to the differences in the Q values for the (n, p) reaction. The relative contributions to proton emission of compound nucleus formation and of the direct interaction might be expected to be different for each isotope (e.g. Brown and Muirhead 1957).

§ 2. EXPERIMENTAL PROCEDURE

2.1. *Exposure and Examination of the Photographic Plates*

The separated isotopes consisted of layers 1 cm^2 in area and 7 mg/cm^2 in thickness electroplated on to gold foils. The ^{56}Fe separated isotope contained 99·9% ^{56}Fe, while the ^{54}Fe separated isotope contained 67% ^{54}Fe and 32% ^{56}Fe. The separated isotopes were placed in contact with the surface of an Ilford C2, 4 in. × 1 in. × 400 μ, nuclear research emulsion and covered by a gold strip of size 4 in. × 1 in. × 400 μ. The gold, which has a very small (n, p) cross section, was used to shield the surface of the emulsion from external sources of protons.

Six emulsions were exposed simultaneously mounted hexagonally around the neutron source using the geometrical arrangement described by Brown *et al.* (loc. cit.). Two of the emulsions were in contact with

---

† Communicated by Professor P. I. Dee, F.R.S.

^{54}Fe targets, two with ^{56}Fe, and two were exposed without an iron isotope between the emulsion surface and the gold strip.

The neutrons, produced by the T(d, n)^{4}He reaction, were incident on the isotopes at an angle of 30° ±2° to the emulsion surface and had an energy of 13·5±0·1 MeV.

The emulsions were scanned using ×50 oil immersion objectives and ×10 eyepieces for tracks entering the surface of the emulsion. All singly charged tracks were assumed to be protons. (Deuteron emission was expected to be small as a result of unfavourable Q values.) Only tracks whose angle of dip in the emulsion was between 10° and 45° were accepted for measurement. These limits were taken to minimize the possible energy loss in the isotope layer and to ensure that the majority of the high energy protons stopped within the emulsion. Hence, protons making angles greater than 140° with the direction of the incident neutrons were not accepted.

The range, angle of dip and the angle in the plane of the emulsion with respect to the direction of the incident neutrons were measured for every track accepted. The energies of the protons were obtained using the range energy tables of Rotblat (1951).

2.2. *Subtraction of Background*

The majority of the background protons are due to the interaction of neutrons with the emulsion nuclei within a distance of 1–2 microns from the emulsion surface. The tracks produced by these protons cannot be optically resolved from those protons entering from outside the emulsion. The only other source of background is the gold shield.

Table 1

Isotope	Number of protons observed	Background	Number of protons from isotope
^{54}Fe	1823	321	1502
^{56}Fe	2479	1257	1222

The emulsions covered directly by the gold strips were used as control plates; the distributions in angle and energy of the protons observed in these plates were subtracted directly from those found in equal areas of the emulsions in contact with the separated isotopes.

This procedure neglects the effect on the range of the protons from the gold strips of their passage through the isotope layer. However, since these protons comprise only about 20% of the total background and the energy loss in the isotope layer is small for many of the events, this procedure is considered justified.

The total number of protons observed entering the emulsion surface for each isotope and the background subtractions are given in table 1.

2.3. *Correction for Energy Loss*

The protons originating within the separated isotopes lose energy in their passage through the isotope layer to the emulsion surface. Allowance was made for this loss by adding to the observed energy of each proton the energy it would have lost in traversing half the thickness of the isotope layer, taking account of its observed angle of dip with respect to the emulsion surface. Thus, a proton having a dip of 30° and having a range in the emulsion corresponding to an energy of 4 MeV would be considered to have an initial energy of $4\cdot3\pm0\cdot3$ MeV.

2.4. *Determination of the Neutron Flux*

The neutron flux was obtained by scanning a known volume of emulsion for protons resulting from the collision of the incident neutrons with the hydrogen present in the emulsion. These recoil protons, which produce the majority of the tracks found within the emulsion, are easily identified by applying the relationship,

$$Ep=(13\cdot5\pm0\cdot1)\cos^2\theta$$

where Ep is the energy of the recoil proton and θ is the spatial angle between the direction of the recoil proton and the incident neutron.

§ 3. RESULTS

The total cross section for the emission of protons from each isotope was obtained by extrapolating the angular distribution to 180°. The values obtained were 600 ± 60 mb for ^{54}Fe and 95 ± 20 mb for ^{56}Fe.

The angular distributions of the protons emitted from ^{54}Fe and ^{56}Fe for three different ranges of proton energy are shown in figs. 1 and 2.

The energy spectra of the protons emitted from ^{54}Fe and ^{56}Fe are shown in figs. 3 and 4. The three distributions given in each figure cover the angular ranges 0°–60°, 60°–90°, and 90°–140°.

The solid line curves in figs. 3 and 4 are the proton distributions expected for the (n, p) reaction on the basis of the statistical theory of Weisskopf and Ewing (1940). In these calculations the Coulomb barrier penetrabilities given by Blatt and Weisskopf (1952) for a nuclear radius of $1\cdot3\times10^{-13}\,A^{1/3}$ cm were used together with the formula given by Lang and Le Couteur (1954) for the density of nuclear levels as a function of excitation energy. The calculated energy distribution for ^{56}Fe was normalized to the observed distribution for the angular range 90°–140°. The curves shown for the other two angular ranges were obtained by assuming that the angular distribution of protons due to this process is isotropic. For ^{54}Fe the Coulomb barrier should be almost identical, but the number of protons emitted with low energy is considerably greater than for ^{56}Fe; this is presumably due to the (n, np) reaction (see § 4). Thus for ^{54}Fe the calculated (n, p) distribution was normalized to the observed distribution for proton energies greater than 4 MeV in the angular range 90°–140°. The broken line was drawn through the observed distribution for protons with energies below 4 MeV in this angular range.

Fig. 1

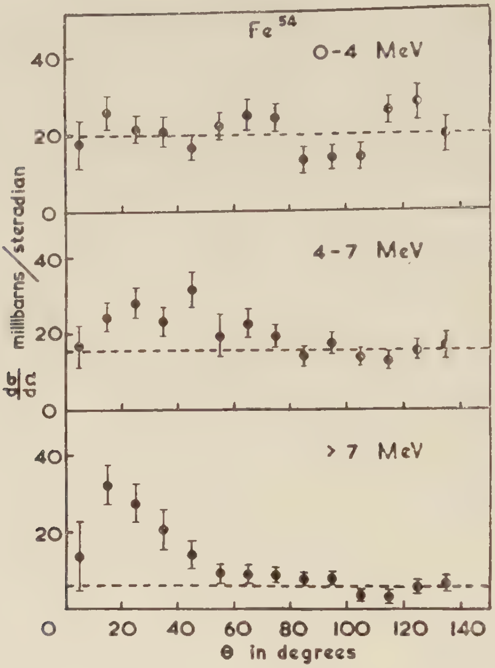

Angular distributions of the protons emitted from ^{54}Fe.

Fig. 2

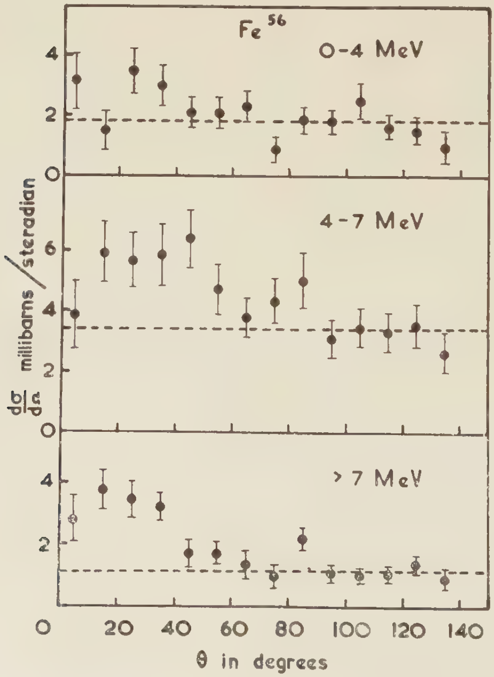

Angular distributions of the protons emitted from ^{56}Fe.

Fig. 3

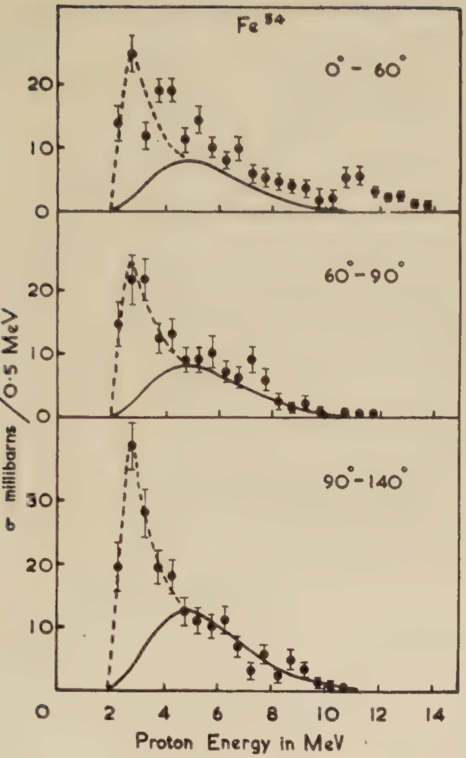

Energy spectra of the protons emitted from ^{54}Fe.

Fig. 4

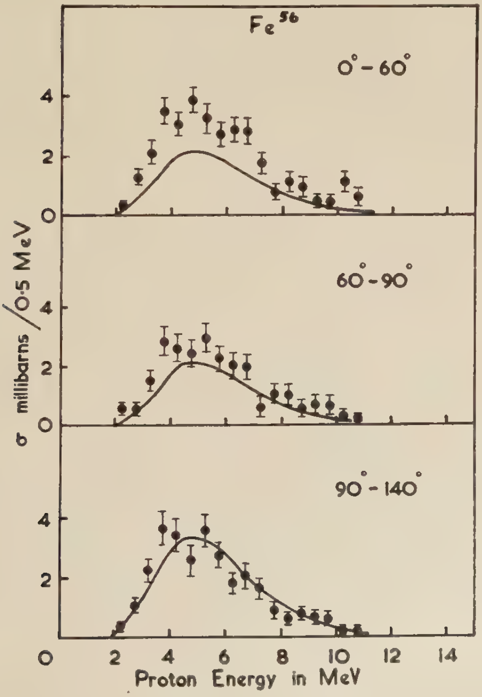

Energy spectra of the protons emitted from ^{56}Fe.

The curves drawn on the other two angular intervals were obtained by assuming that protons emitted by these processes are emitted isotropically.

§ 4. DISCUSSION

The angular distributions of the protons emitted from both ^{54}Fe and ^{56}Fe are approximately flat at angles greater than 90° for all energy intervals. To illustrate any departure from isotropy at forward angles, the dashed line was drawn through the mean of the experimental points at backward angles. The protons emitted from both isotopes with energies less than 4 MEV are approximately isotropic. For proton energies between 4 and 7 MEV there is a tendency for the distribution to peak at forward angles and for proton energies greater than 7 MEV there is a marked peak at angles below 60° for both isotopes.

The preferential emission of protons in the forward direction at high energies cannot be explained by the statistical theory for the decay of the compound nucleus but would be expected if protons were emitted as an immediate result of the collision of the incident neutron with a proton of the nucleus.

The large number of protons with energies below 4 MEV emitted by ^{54}Fe is probably due to the (n, np) reaction which is favoured relative to the (n, 2n) reaction due to the differences in Q values for the two reactions as shown in table 2.

Table 2

Isotope	Q value in MEV			Maximum energy of emitted proton	
	(n, p)	(n, np)	(n, 2n)	(n, np)	(n, p)
^{54}Fe	+0·34	− 9·2	−13·8	4·3	13·9
^{56}Fe	−2·93	−10·2	−11·2	3·3	10·6

Thus in ^{54}Fe the (n, 2n) reaction cannot occur when the energy of the incident neutron is 13·5 MEV, while the (n, np) reaction is possible for proton energies from 0 to 4·3 MEV and so has only to compete with the (n, nγ) reaction.

For ^{56}Fe the (n, np) reaction is only favoured over the energy range 0–1·0 MEV where proton emission is prevented by the Coulomb barrier.

Figures 1 and 2 show that protons emitted from ^{54}Fe with energy below 4 MEV have an isotropic angular distribution which is consistent with an (n, np) reaction involving the decay of a compound nucleus. The good fit of the higher energy protons to the calculated energy spectrum for the angular range 90°–140° for both isotopes suggests that these protons also result from the decay of a compound nucleus.

For both ^{54}Fe and ^{56}Fe there are more high energy protons at forward angles than would be expected from compound nucleus decay. These protons are probably due to a direct interaction process. Their energy spectrum is approximately flat from 4 MeV to the maximum energy allowed by the Q value for the (n, p) process. The statistical accuracy of the results are such that the presence or absence of structure in the energy spectrum, similar to that found by Gugelot (1954) and Cohen (1957) in the inelastic scattering of protons, cannot be confirmed.

If the isotropic part of the angular distributions are assumed to be due to compound nucleus processes and the forward peaking to a direct interaction, we get the cross sections for these processes given in table 3.

Table 3

Isotope	Cross section in millibarns				
	Compound nucleus (n, p)	Compound nucleus (n, np)	Direct interaction	Total	Allan total
^{54}Fe	306	224	70	600 ± 60	680
^{56}Fe	75	0	20	95 ± 20	190

The direct interaction cross section obtained in this way does not include any isotropic component and so may be an underestimate.

The reaction denoted (n, p) in this table includes both the reactions (n, pγ) and (n, pn). The reaction (n, pn) does not suffer as a result of competition with the (n, 2n) reaction, and is possible for proton energies in the range 0–4·3 MeV for ^{54}Fe and 0–3·3 MeV for ^{56}Fe. In these energy intervals it will dominate over the reaction (n, pγ) but at higher energies the protons arise entirely from (n, pγ) reactions. Hence a comparison of the cross section for proton emission above these energies with the (n, pγ) cross sections determined by activation method can be made. Paul and Clark (1953) obtained a value of 97 ± 12 mb and Forbes (1952) a value of 124 ± 12 mb for the reaction (n, pγ) in ^{56}Fe at 14 MeV. The present results give a value of 93 ± 20 mb for the (n, pγ) reaction at 13·5 MeV.

Allan (1957) has measured the energy spectrum of protons emitted from ^{54}Fe and ^{56}Fe at an angle of $34° \pm 20°$ to the incident neutron direction. The total cross section he obtained is shown in the final column of table 3. Allan obtained these figures by assuming an isotropic angular distribution, and thus probably over-estimated these cross sections by about 30%.

Austern *et al.* (1953) suggested that proton emission was enhanced by interactions at the nuclear surface. The shape of the angular distribution was characterized by the allowed values of orbital angular momentum with which the neutron can be captured by the nucleus. This theory does not, however, give absolute cross sections.

Brown and Muirhead (loc. cit.) consider a model which assumes that nucleon–nucleon interactions can occur throughout the nuclear volume and eject protons directly. They calculate the cross section for the (n, p) direct interaction at 14 MeV to be 55 mb for ^{54}Fe and 30 mb for ^{56}Fe. These values are in reasonable agreement with those obtained here. Their energy spectra and angular distributions, while showing the main tendencies of the present results, are not in detailed agreement.

The surface interaction calculations of Elton and Gomes (1957) are also in qualitative agreement with our results.

The present results do not determine the details of the direct interaction process sufficiently well to make significant comparisons with these theories.

Fig. 5

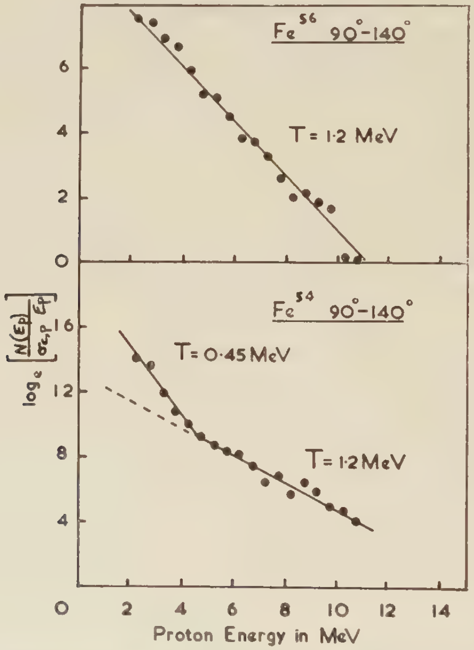

Proton spectra of ^{54}Fe and ^{56}Fe corrected for Coulomb barrier penetrabilities.

Recently Brown and De Dominicis (1957) have formulated the problem of inelastic scattering of nucleons by nuclei in terms of nuclear dispersion theory. They show that expressions for the contribution of both the 'direct interaction' and of the 'compound nucleus' to the inelastic scattering may be obtained by this method.

In fig. 5

$$\log_e \left(\frac{N(Ep)}{\sigma_{c,p} Ep}\right)$$

is plotted against Ep, where $N(Ep)$ is the number of protons observed with an energy Ep in the angular range 90°–140°, and $\sigma_{c,p}$ is the cross section for the formation of a compound nucleus as given by Blatt and Weisskopf (loc. cit.) for a nucleus of radius $1{\cdot}3\times10^{-13}\,A^{1/3}$ cm. The experimental points are consistent with a straight line for ^{56}Fe and two straight lines for ^{54}Fe. On such a plot a straight line indicates that the density of nuclear levels varies as $\exp(E)$ where E is the excitation energy of the residual nucleus, and its slope is equal to $1/T$ where T is the nuclear temperature at the average excitation energy. The figure illustrates the occurrence of the (n, np) reaction in ^{54}Fe at energies below 4 MeV and shows that a temperature of 1·2 MeV gives the best fit for the (n, p) reaction in both isotopes.

§ 5. CONCLUSIONS

The major contribution to the (n, p) reaction at 13·5 MeV in both ^{54}Fe and ^{56}Fe is that made by the decay of the compound nucleus. In both isotopes considerable direct interaction effects have been observed. The protons resulting from direct interactions are emitted preferentially at forward angles and have an approximately flat energy spectrum.

ACKNOWLEDGMENTS

The authors with to thank Professor P. I. Dee for his interest and encouragement ; they also wish to express their thanks to Dr. G. Brown who contributed to the work on ^{56}Fe, and Dr. H. Muirhead for their help and advice, Dr. A. M. Ward for his help during the exposures at the H.T. set, and Miss E. Rose for help with the microscope work. They also wish to thank A.E.R.E., Harwell, for providing separated isotopes. One of us (W. T. M.) would also like to express his gratitude to the Department of Scientific and Industrial Research for a maintenance grant.

REFERENCES

ALLAN, D. L., 1957, *Proc. phys. Soc. Lond.*, A, **70,** 195.
AUSTERN, N., BUTLER, S. T., and MCMANUS, H., 1953, *Phys. Rev.*, **92,** 351.
BLATT, J. M., and WEISSKOPF, V. F., 1952, *Theoretical Nuclear Physics* (New York : Wiley).
BROWN, G. E., and DE DOMINICIS, C. T., 1957, *Proc. phys. Soc. Lond.*, A, **70,** 686.
BROWN, G., MORRISON, G. C., MUIRHEAD, H., and MORTON, W. T., 1957, *Phil. Mag.*, **2,** 785.
BROWN, G., and MUIRHEAD; H., 1957, *Phil. Mag.*, **2,** 473
COHEN, B. L., 1957, *Phys. Rev.*, **105,** 1549.
EISBERG, R. M., and IGO, G., 1954, *Phys. Rev.*, **93,** 1039.
ELTON, L. R. B., and GOMES, L. G., 1957, *Phys. Rev.*, **105,** 1027.
FORBES, S. G., 1952, *Phys. Rev.*, **88,** 1309.
GUGELOT, P. C., 1954, *Phys. Rev.*, **93,** 425.
LANG, J. M. B., and LE COUTEUR, K. J., 1954, *Proc. phys. Soc. Lond.*, A, **67,** 856.
PAUL, E. B., and CLARKE, R. L., 1953, *Canad. J. Phys.*, **31,** 267.
ROTBLAT, J., 1951, *Nature, Lond.*, **167,** 550.
WEISSKOPF, V. F., and EWING, D. H., 1940, *Phys. Rev.*, **57,** 472.

Boundary Layer Growth on a Spinning Body: Accelerated Motion†

By Y. D. WADHWA
Department of Applied Mathematics,
Indian Institute of Technology, Khargpur, India

[Received October 31, 1957]

ABSTRACT

The motion in the boundary layer when a body of revolution is started to move along its axis of symmetry and simultaneously to rotate about it with a velocity varying as the *n*th power of time, is investigated. The corresponding problem for an impulsive start was tackled by Illingworth. It is found that the separation is delayed by acceleration. Also, the time that elapses before separation first takes place is lessened by increasing the velocity of spin.

§ 1. INTRODUCTION

THE aim of the researches on unsteady boundary layers has been to determine the time that elapses after the start when separation first takes place. The method of Goldstein and Rosenhead (1936) has proved quite satisfactory to this end, and describes the early stages of the development of the boundary layer almost accurately. The method has been extended by Illingworth (1954) to consider the motion due to an impulsively started spinning body of revolution. Squire (1954) has discussed the growth of three-dimensional boundary layers on the same lines—again a case of impulsive start. Wundt (1955) has studied the early stages of the boundary layer growth on yawed cylinders when the potential velocity varies as the *n*th power of time. The case of impulsive start can be obtained as a special case. It is worthwhile considering the Illingworth's problem, viz., the motion due to a spinning body, the translatory and rotatory motions being acquired from rest by an acceleration varying as some power of time. The aim is to show that it takes more time for separation to occur in the accelerated case than in the case of impulsive start. The extension of the present analysis to Squire's paper is straightforward.

§ 2. EQUATIONS OF MOTION

As in Illingworth (1954) we choose the independent variables x, y, and t such that t denotes the time from the start of the motion, x measures the distance from the nose of the body along any meridian curve, and y is the distance along the normal to this curve. This means that the frame of reference moves forward with the body but does not rotate with it. If u, v, w, are the velocity components in the directions of x, y and the transverse direction respectively and $r(x)$ is the radius of the body at the station x, the equations of motion are

---

† Communicated by the Author.

$$\frac{\partial}{\partial x}(ru)+\frac{\partial}{\partial y}(rv)=0, \qquad (1)$$

$$\frac{\partial u}{\partial t}+u\frac{\partial u}{\partial x}+v\frac{\partial u}{\partial y}-\frac{w^2}{r}\frac{dr}{dx}=\frac{\partial U}{\partial t}+U\frac{\partial U}{\partial x}+\nu\frac{\partial^2 u}{\partial y^2}, \qquad (2)$$

$$\frac{\partial w}{\partial t}+u\frac{\partial w}{\partial x}+v\frac{\partial w}{\partial y}+\frac{uw}{r}\frac{dr}{dx}=\nu\frac{\partial^2 w}{\partial y^2}, \qquad (3)$$

where $U(x, t)$ is the velocity of the main stream. It is supposed that the body and the fluid are at rest at $t\leqslant 0$. At $t=0$, the body is given a translatory velocity and a rotatory velocity varying as t^n so that the boundary conditions to be satisfied are

$$u=v=w=0 \quad \text{for} \quad t\leqslant 0 \text{ and for all } y\,; \qquad (4)$$

$$\left.\begin{array}{ll} u=v=0, \quad w=\Omega r t^n & \text{at } y=0 \\ \left.\begin{array}{l} u=U(x,t)=P(x)\,.\,t^n \\ w=0 \end{array}\right\} & \text{at } y=\infty \end{array}\right\} \text{for } t\geqslant 0. \qquad (5)$$

We use the Stokes' stream function ψ such that

$$u=\frac{1}{r}\frac{\partial\psi}{\partial y}, \qquad v=-\frac{1}{r}\frac{\partial\psi}{\partial x}, \qquad (6)$$

and choose

$$\eta=y/2\sqrt{(\nu t)}, \qquad (7)$$

$$\psi=2\sqrt{(\nu t)}\sum_{\lambda=0}^{\infty} t^{n+\lambda(n+1)}\,\Psi_{n,\lambda}(x,\eta), \qquad (9)$$

$$w=\sum_{\lambda=0}^{\infty} t^{n+\lambda(n+1)}\,\Phi_{n,\lambda}(x,\eta). \qquad (9)$$

Substituting in equations (2) and (3), equating coefficients of like powers of t, and rearranging we obtain linear partial differential equations to determine $\Psi_{n,\lambda}$ and $\Phi_{n,\lambda}$. These can be reduced to linear ordinary differential equations if we choose

$$\left.\begin{aligned}
\Psi_{n,0}(x,\eta)&=r\,Pf_1(\eta),\\
\Psi_{n,1}(x,\eta)&=r\left[P\frac{dP}{dx}f_{21}(\eta)+\frac{P^2}{r}\frac{dr}{dx}f_{22}(\eta)+r\Omega^2\frac{dr}{dx}f_{23}(\eta)\right],\\
\Psi_{n,2}(x,\eta)&=r\left[P^2\frac{d^2P}{dx^2}f_{31}(\eta)+P\left(\frac{dP}{dx}\right)^2 f_{32}(\eta)+\frac{P^2}{r}\frac{dP}{dx}\frac{dr}{dx}f_{33}(\eta)\right.\\
&\quad+\frac{P^3}{r}\frac{d^2r}{dx^2}f_{34}(\eta)+\frac{P^3}{r^2}\left(\frac{dr}{dx}\right)^2 f_{35}(\eta)+\Omega^2 r\frac{dP}{dx}\frac{dr}{dx}f_{36}(\eta)\\
&\quad\left.+\Omega^2 Pr\frac{d^2r}{dx^2}f_{37}(\eta)+\Omega^2 P\left(\frac{dr}{dx}\right)^2 f_{38}(\eta)\right],
\end{aligned}\right\} \qquad (10)$$

$$\left.\begin{aligned}
&\Phi_{n,0}(x,\eta)=r\Omega g_1(\eta),\\
&\Phi_{n,1}(x,\eta)=\Omega\left[r\frac{dP}{dx}g_{21}(\eta)+P\frac{dr}{dx}g_{22}(\eta)\right],\\
&\Phi_{n,2}(x,\eta)=\Omega\left[rP\frac{d^2P}{dx^2}g_{31}(\eta)+r\left(\frac{dP}{dx}\right)^2 g_{32}(\eta)+P\frac{dP}{dx}\frac{dr}{dx}g_{33}(\eta)\right.\\
&\qquad\qquad+P^2\frac{d^2r}{dx^2}g_{34}(\eta)+\frac{P^2}{r}\left(\frac{dr}{dx}\right)^2 g_{35}(\eta)+\Omega^2r^2\frac{d^2r}{dx^2}\,{}_{36}g(\eta)\\
&\qquad\qquad\left.+\Omega^2r\left(\frac{dr}{dx}\right)^2 g_{37}(\eta)\right].
\end{aligned}\right\} \qquad (11)$$

If the differentiations with respect to η be denoted by dashes the resulting equations become

$$f_1'''+2\eta f_1''-4nf_1'=-4n, \quad . \quad . \quad . \quad . \quad . \quad . \quad (12\,a)$$

$$f_{2i}'''+2\eta f_{2i}''-4(2n+1)f_{2i}'=4s_{2i}, \quad . \quad . \quad . \quad . \quad . \quad . \quad (12\,b)$$

$$f_{3i}'''+2\eta f_{3i}''-4(3n+2)f_{3i}'=4s_{3i}, \quad . \quad . \quad . \quad . \quad . \quad . \quad (12\,c)$$

$$g_1''+2\eta g_1'-4ng_1=0, \quad . \quad . \quad . \quad . \quad . \quad . \quad (13\,a)$$

$$g_{2i}''+2\eta g_{2i}'-4(2n+1)g_{2i}=4t_{2i}, \quad . \quad . \quad . \quad . \quad . \quad . \quad (13\,b)$$

$$g_{3i}''+2\eta g_{3i}'-4(3n+2)g_{3i}=4t_{3i}, \quad . \quad . \quad . \quad . \quad . \quad . \quad (13\,c)$$

where

$$\left.\begin{array}{ll}
s_{21}=f_1'^2-f_1f_1''-1, & t_{21}=-f_1g_1',\\
s_{22}=-f_1f_1'' & t_{22}=2f_1'g_1-f_1g_1',\\
s_{23}=-g_1^{\,2} & t_{31}=f_1'g_{21}-f_{21}g_1',\\
s_{31}=f_1'f_{21}'-f_1''f_{21}, & t_{32}=-f_1g_{21}'-f_{21}g_1',\\
s_{32}=2f_1'f_{21}'-f_1f_{21}''-f_1''f_{21}, & t_{33}=2f_1'g_{21}+2f_{21}'g_1+f_1'g_{22}-f_{21}g_1'\\
s_{33}=3f_1'f_{22}'-f_1f_{22}''-f_1f_{21}''-f_1''f_{21} & \qquad -f_1g_{21}'-f_1g_{22}'-2f_{22}g_1',\\
\qquad -2f_1''f_{22}, & t_{34}=f_1'g_{22}-f_{22}g_1',\\
s_{34}=f_1'f_{22}'-f_1''f_{22}, & t_{35}=2f_{22}'g_1+f_1'g_{22}-f_1g_{22}',\\
s_{35}=-f_1'f_{22}'-f_1f_{22}'', & t_{36}=-f_{23}g_1',\\
s_{36}=f_1'f_{23}'-f_1f_{23}''-2g_1g_{21}, & t_{37}=2f_{23}'g_1-f_{23}g_1'.\\
s_{37}=f_1'f_{23}'-f_1''f_{23}, & \\
s_{38}=f_1'f_{23}''-f_1f_{23}''-2f_1''f_{23}-2g_1g_{22}. &
\end{array}\right\}$$

$$. \quad . \quad . \quad (14)$$

§ 3. Solutions of the Equations

Equations (12) and (13) can be written in the form

$$f''+2\eta f'-4mf=F(\eta). \quad . \quad . \quad . \quad . \quad . \quad . \quad . \quad (15)$$

The two particular integrals of (15) are

$$p=\sum_{r=0}^{m}A_{2r}\eta^{2r},$$

$$q=pE+\sum_{r=0}^{m-1}B_{2r+1}\,\eta^{2r+1}\,.\,E', \quad . \quad . \quad . \quad . \quad . \quad . \quad (16)$$

where $E = \operatorname{erf} \eta = 2\alpha \int_0^{\eta} \exp(-\xi^2)\, d\xi$, and $\alpha = 1/\sqrt{\pi}$

$$A_{2r+2} = \frac{2(m-r)}{(r+1)(2r+1)} A_{2r},$$

$$B_{2r+1} = \frac{2(m+r)B_{2r-1} - 2rA_{2r}}{r(2r+1)}, \quad B_{2m+1} = 0.$$

Hence the complete solution of (15) is

$$f = Ap + Bq + p \int \frac{qF}{p'q - pq'}\, d\eta + q \int \frac{pF}{pq' - p'q}\, d\eta, \quad . \quad . \quad (17)$$

where A and B are arbitrary constants to be determined from the boundary conditions

$$\left.\begin{aligned} &f_1(\eta) = f_1'(\eta) = f_{ij}(\eta) = f_{ij}'(\eta) = 0, \\ &g_1(\eta) = 1, \qquad g_{ij}(\eta) = 0. \end{aligned}\right\} \text{ at } \eta = 0, \quad . \quad . \quad . \quad (18)$$

$$\left.\begin{aligned} &f_1'(\eta) = 1, \qquad f_{ij}(\eta) = 0, \\ &g_1(\eta) = g_{ij}(\eta) = 0. \end{aligned}\right\} \text{ at } \eta = \infty. \quad . \quad . \quad (19)$$

However, the values of the functions at the wall and hence the skin friction and the separation point cannot be obtained in a general form. We therefore consider the particular case of uniformly accelerated motion ($n=1$). The case of an impulsive start can also be obtained by putting $n=0$.

§ 4. UNIFORMLY ACCELERATED MOTION

For the case of uniformly accelerated motion $n=1$. The solutions of eqns. (12 *a*) and (13 *a*) satisfying the conditions (18) and (19) for this particular case can be obtained as

$$f_1 = \eta(1 + \tfrac{2}{3}\eta^2)E + \tfrac{2}{3}\alpha(1+\eta^2)\exp(-\eta^2) - \tfrac{2}{3}(\alpha + \eta^3), \quad . \quad . \quad (20)$$

$$g_1 = -(1 + 2\eta^2)E - 2\eta\alpha \exp(-\eta^2) + 1 + 2\eta^2. \quad . \quad . \quad . \quad . \quad (21)$$

With these values of f_1 and g_1, the values of s_{2i} and t_{2i} can be determined. The solutions of eqns (12 *b*) and (13 *b*) for this case ($n=1$) become

$$\begin{aligned} f_{21}' = {} & E^2\left(-\frac{1}{4} + \frac{1}{2}\eta^2 + \frac{1}{3}\eta^4 + \frac{2}{9}\eta^6\right) + E\left[\frac{1}{4} - \frac{16}{15}\alpha\eta + \frac{3}{2}\eta^2 + \eta^4 - \frac{2}{9}\eta^6\right. \\ & \left. - \frac{8\alpha^2}{675}(15 + 90\eta^2 + 60\eta^4 + 8\eta^6) + \left(\frac{4}{3}\eta + \frac{4}{9}\eta^3 + \frac{4}{9}\eta^5\right)\alpha \exp(-\eta^2)\right] \\ & + \left[\alpha^2 \exp(-2\eta^2)\left(\frac{8}{9} + \frac{1}{9}\eta^2 + \frac{2}{9}\eta^4\right) + \alpha \exp(-\eta^2)\left\{-\frac{16}{15}\alpha + \frac{1}{2}\eta\right.\right. \\ & \left. + \frac{10}{9}\eta^3 - \frac{2}{9}\eta^5 - \frac{16\alpha^2}{675} + (33\eta + 28\eta^3 + 4\eta^5)\right\} + \frac{16}{15}\alpha\eta - 2\eta^2 - \frac{4}{3}\eta^4 \\ & + \frac{8\alpha^2}{675}(15 + 90\eta^2 + 60\eta^4 + 8\eta^6), \quad . \quad . \quad . \quad . \quad . \quad . \quad (22) \end{aligned}$$

$$
\begin{aligned}
f_{22}' = {} & E^2\biggl(-\frac{1}{4}-\frac{3}{2}\eta^2-\frac{7}{3}\eta^4-\frac{2}{3}\eta^6\biggr)+E\biggl[\alpha\exp(-\eta^2)\biggl(-\frac{4}{3}\eta-4\eta^3\\
& -\frac{4}{3}\eta^5\biggr)+\frac{1}{4}-\frac{16}{15}\alpha\eta+\frac{3}{2}\eta^2+\frac{7}{3}\eta^4+\frac{46}{45}\eta^6-\frac{16\alpha^2}{225}(15+90\eta^2+60\eta^4\\
& +8\eta^6)\biggr]+\biggl[\alpha^2\exp(-2\eta^2)\biggl(-\frac{5}{3}\eta^2-\frac{2}{3}\eta^4\biggr)+\alpha\exp(-\eta^2)\biggl\{-\frac{16}{15}\alpha\\
& +\frac{23}{30}\eta+\frac{82}{45}\eta^3+\frac{46}{45}\eta^5-\frac{32\alpha^2}{225}(33\eta+28\eta^3+4\eta^5)\biggr\}+\frac{16}{15}\alpha\eta-\frac{16}{45}\eta^6\\
& +\frac{16\alpha^2}{225}(15+90\eta^2+60\eta^4+8\eta^6)\biggr], \qquad (23)
\end{aligned}
$$

$$
\begin{aligned}
f_{23}' = {} & E^2\biggl(-2\eta^2-\frac{8}{3}\eta^4-\frac{8}{9}\eta^6\biggr)+E\biggl[\alpha\exp(-\eta^2)\biggl(-\frac{8}{3}\eta-\frac{40}{9}\eta^3-\frac{16}{9}\eta^5\biggr)\\
& +4\eta^2+\frac{16}{3}\eta^4+\frac{16}{9}\eta^6-\frac{8\alpha^2}{135}(15+90\eta^2+60\eta^4+8\eta^6)\biggr]\\
& +\biggl[\alpha^2\exp(-2\eta^2)\biggl(-\frac{8}{9}-\frac{16}{9}\eta^2-\frac{8}{9}\eta^4\biggr)+\alpha\exp(-\eta^2)\biggl\{\frac{8}{3}\eta+\frac{40}{9}\eta^3\\
& +\frac{16}{9}\eta^5-\frac{16\alpha^2}{135}(33\eta+28\eta^3+4\eta^5)\biggr\}+\biggl\{-2\eta^2-\frac{8}{3}\eta^4-\frac{8}{9}\eta^6+\frac{8\alpha^2}{135}\\
& \times(15+90\eta^2+60\eta^4+8\eta^6)\biggr\}\biggr]. \qquad (24)
\end{aligned}
$$

$$
\begin{aligned}
g_{21} = {} & E^2\biggl(\frac{1}{4}+\frac{3}{2}\eta^2+\frac{7}{3}\eta^4+\frac{2}{3}\eta^6\biggr)+E\biggl[\alpha\exp(-\eta^2)\biggl(\frac{4}{3}\eta+4\eta^3+\frac{4}{3}\eta^5\biggr)\\
& -\frac{1}{4}+\frac{16}{15}\alpha\eta-\frac{3}{2}\eta^2-\frac{7}{3}\eta^4-\frac{46}{45}\eta^6+\frac{16\alpha^2}{225}(15+90\eta^2+60\eta^4+8\eta^6)\biggr]\\
& +\biggl[\alpha^2\exp(-2\eta^2)\biggl(\frac{5}{3}\eta^2+\frac{2}{3}\eta^4\biggr)+\alpha\exp(-\eta^2)\biggl\{\frac{16}{15}\alpha-\frac{23}{30}\eta\\
& -\frac{82}{45}\eta^3-\frac{46}{45}\eta^5+\frac{32\alpha^2}{225}(33\eta+28\eta^3+4\eta^5)\biggr\}-\frac{16}{15}\alpha\eta+\frac{16}{45}\eta^6\\
& -\frac{16}{225}\alpha^2(15+90\eta^2+60\eta^4+8\eta^6)\biggr], \qquad (25)
\end{aligned}
$$

$$
\begin{aligned}
g_{22} = {} & E^2\biggl(\frac{1}{4}-\frac{5}{2}\eta^2-3\eta^4-\frac{10}{9}\eta^6\biggr)+E\biggl[\alpha\exp(-\eta^2)\biggl(-4\eta-\frac{44}{9}\eta^3\\
& -\frac{20}{9}\eta^5\biggr)-\frac{1}{4}+\frac{16}{15}\alpha\eta+\frac{5}{2}\eta^2+\frac{13}{3}\eta^4+2\eta^6-\frac{32\alpha^2}{675}(15+90\eta^2\\
& +60\eta^4+8\eta^6)\biggr]+\biggl[\alpha^2\exp(-2\eta^2)\biggl(-\frac{16}{9}-\frac{17}{9}\eta^2-\frac{10}{9}\eta^4\biggr)\\
& +\alpha\exp(-\eta^2)\biggl\{\frac{16}{15}\alpha+\frac{13}{6}\eta+\frac{10}{3}\eta^3+2\eta^5-\frac{64\alpha^2}{675}(33\eta+28\eta^3+4\eta^5)\biggr\}\\
& -\frac{16}{15}\alpha\eta-\frac{4}{3}\eta^4-\frac{8}{9}\eta^6+\frac{32\alpha^2}{675}+(15+90\eta^2+60\eta^4+8\eta^6)\biggr]. \qquad (26)
\end{aligned}
$$

The functions s_3, and t_3, can now be determined, and eqns. (12 c) and (13 c) can then be solved. But because of the cumbersome algebra that sets in, the solution is given only upto the second term.

The formulae for the skin friction, then, take the form

$$\tau_x=\mu\left(\frac{\partial u}{\partial y}\right)_{y=0}=2P(x)\alpha\sqrt{(\mu\rho t)}\left[1+t^2\left\{0\cdot42613\,\frac{dP}{dx}+0\cdot04008\,\frac{P}{r}\frac{dr}{dx}+0\cdot21396\Omega^2\,\frac{r}{P}\frac{dr}{dx}\right\}+\dots\right], \quad (27)$$

$$\tau_z=-\mu\left(\frac{\partial w}{\partial y}\right)_{y=0}=2\Omega x r\sqrt{(\mu\rho t)}\left[1+t^2\left\{0\cdot04008\,\frac{dP}{dx}+0\cdot21217\,\frac{P}{r}\frac{dr}{dx}\right\}+\dots\right]. \quad (28)$$

§ 5. SEPARATION POINT FOR A SPHERE

We can now apply the results to bodies of given shape. In the case of a sphere we have

$$U(x,t)=t\,.\,P(x)=t\,.\,\tfrac{3}{2}A\sin(x/a),$$
$$r(x)=a\sin(x/a), \quad (29)$$

where A is the uniform acceleration with which the fluid moves relative to the sphere, and a is the radius of the sphere. Defining a non-dimensional time $\xi=At^2/2a$ and $\beta=a^2\Omega^2/A^2$ we have

$$\tau_x=1\cdot69257\sqrt{(\mu\rho t)}\,.\,A\sin(x/a)\,[1+\xi(1\cdot39863+0\cdot28528\beta)\cos(x/a)+\dots] \quad (30)$$

$$\tau_z=1\cdot12838\Omega\sqrt{(\mu\rho t)}\,.\,a\sin(x/a)\,[1+0\cdot75675\xi+\dots]. \quad (31)$$

Hence the separation first occurs at $x=a\pi$, i.e. at the rear stagnation point, and the value of ξ is given by

$$1-\xi\,(1\cdot39863+0\cdot28528\beta)=0. \quad (32)$$

Since ξ denotes the distance through which the liquid particles at infinity have moved in time t, it can be compared with ξ_1 obtained by Illingworth.

β	ξ	ξ_1
0	0·71499	0·423
0·1	0·70069	0·415
1	0·59386	0·315
10	0·23521	0·139

Thus the table shows that $\xi>\xi_1$, i.e., the liquid particles at infinity have gone much farther off in the case of accelerated start than in the case of impulsive start when separation first takes place. Also, as in the case of impulsive start, ξ decreases as β increases showing that the separation occurs sooner the greater the velocity of spin.

REFERENCES

GOLDSTEIN, S., and ROSENHEAD, L., 1936, *Proc. Camb. phil. Soc.*, **32**, 392.
ILLINGWORTH, C. R., 1954, *Phil. Mag.*, **45**, 1.
SQUIRE, L. C., 1954, *Phil. Mag.*, **45**, 1272.
WUNDT, VON H., 1955, *Ingen.-Arch.*, **23**, 212.

The Ultimate Distribution of Impurity in the Zone-Melting Process†

By L. W. Davies
Division of Radiophysics, C.S.I.R.O., Sydney, Australia

[Received November 27, 1957]

In the zone-melting process of Pfann (1952), molten zones of constant length are caused to pass along a solid ingot of material, which it is desired to refine with respect to impurities whose distribution coefficients k between solid and liquid differ from unity. The coefficient k is defined as the ratio of impurity concentration in the solid to that in the liquid from which the solid is freezing. It is of interest to determine analytically the ultimate distribution of a given impurity in the ingot after the passage of an infinite number of molten zones.

We make the usual assumptions of perfect mixing in the liquid and negligible diffusion of impurity in the solid; the value of the distribution coefficient k is assumed independent of concentration. Since the ultimate distribution $y(x)$ is unaffected by the passage of a further molten zone, we may write down the equation (Pfann 1952)

$$y(x)=k\int_x^{x+1} y(\xi)\,d\xi, \qquad (1)$$

where the distance x is measured in units of the zone length, and the zone moves in the direction Ox.

Let the ingot be N zones in length, where N need not be integral. In the last zone-length of the ingot to solidify, i.e. for $N-1\leqslant x\leqslant N$, the length of the molten zone decreases progressively to zero; accordingly for the last zone eqn. (1) is replaced by

$$y(x)=\frac{k}{N-x}\int_x^{N} y(\xi)\,d\xi, \qquad (2)$$

of which the solution is

$$y(x)\equiv y_{01}(x)=y_1(N-x)^{k-1},\ N-1\leqslant x\leqslant N, \qquad (3)$$

where the constant y_1 is the impurity concentration at $x=N-1$.

The distribution (3) is a boundary condition which has to be taken into account in the solution of (1). For example, the ultimate distribution $y_{12}(x)$ in the range $N-2\leqslant x\leqslant N-1$ is given by

$$y_{12}(x)=k\int_x^{N-1} y_{12}(\xi)\,d\xi+k\int_{N-1}^{x+1} y_{01}(\xi)\,d\xi. \qquad (4)$$

From this equation we derive

$$(D+k)y_{12}(x)=ky_{01}(x+1) \qquad (5)$$

---

† Communicated by the Author.

of which the solution is

$$y_{12}(x)=A_{12}\exp(-kx)+k\exp(-kx)\int\exp(kx)\,y_{01}(x+1)\,dx.$$

With the aid of eqn. (3), integration successively by parts yields

$$y_{12}(x)=A_{12}\exp(-kx)-y_1(N-1-x)^kM\{1,\,1+k,\,k(N-1-x)\},\qquad N-2\leqslant x\leqslant N-1 \quad . \quad . \quad . \quad . \quad (6)$$

where

$$M(\alpha,\beta,z)=1+\frac{\alpha}{1\,.\,\beta}z+\frac{\alpha(\alpha+1)}{2\,!\,\beta(\beta+1)}z^2+\ldots$$

is a confluent hypergeometric function, and the constant

$$A_{12}=y_1\exp\{k(N-1)\}. \quad . \quad . \quad . \quad . \quad . \quad . \quad . \quad (7)$$

By a derivation in succession of the distributions y_{01}, y_{12}, $y_{23}\ldots$ in the 1, 2, 3, ... zones from the end of the ingot, we find for the distribution in the range $N-(r+1)\leqslant x\leqslant N-r$,

$$\left.\begin{aligned}y_{r,\,r+1}(x)&=A_{r,\,r+1}\exp(-kx)+k\exp(-kx)\int\exp(kx)\,y_{r-1,\,r}(x+1)\,dx\\&=A_{r,\,r+1}\exp(-kx)+A_{r-1,\,r}\,kx\exp\{-k(x+1)\}+\ldots\\&\quad\ldots+A_{12}\frac{k^{r-1}}{(r-1)!}(x+r-2)^{r-1}\exp\{-k(x+r-1)\}\\&\quad+k^ry_1\exp(-kx)\int\ldots\int\exp(kx)(N-r-x)^{k-1}\,d^rx,\end{aligned}\right\}\quad(8)$$

where the constants

$$\begin{aligned}A_{r,\,r+1}=y_r\exp\{k(N-r)\}-\Big[&A_{r-1,\,r}\,k(N-r)\exp(-k)\\&+A_{r-2,\,r-1}\frac{k^2}{2!}(N-r+1)^2\exp(-2k)+\ldots\\&+A_{12}\frac{k^{r-1}}{(r-1)\,!}(N-2)^{r-1}\exp\{-(r-1)\}k\Big]. \quad . \quad . \quad . \quad (9)\end{aligned}$$

and y_r is the value of $y(x)$ at $x=N-r$. Term by term integration yields the result

$$\begin{aligned}\int\ldots\int\exp(kx)(N-r-x)^{k-1}\,d^sx&=\frac{(-1)^s\exp(kx)}{k(k+1)\ldots(k+s-1)}\\&\quad\times(N-r-x)^{k+r-1}\,M\{s,\,s+k,\,k(N-r-x)\}\quad(10)\end{aligned}$$

and this together with eqns. (8) and (9) gives the desired analytical expression for the ultimate distribution :

$$\left.\begin{aligned}y_{r,\,r+1}(x)=\exp\{k(\chi-r)\}\Big[&y_r-k(\chi-r)y_{r-1}+\frac{k^2}{2!}(\chi-r)^2y_{r-2}-\ldots\\&+\frac{(-k)^{r-1}}{(r-1)\,!}(\chi-r)^{r-1}y_1\Big]\\&+\frac{(-k)^ry_1}{k(k+1)\ldots(k+r-1)}(\chi-r)^{k+r-1}M\{r,\,r+k,\,k(\chi-r)\}\\&\qquad 0\leqslant(\chi-r)\leqslant1\qquad r=1,\,2,\,\ldots\,\nu\end{aligned}\right\}\quad(11)$$

where we have put

$$\chi=N-x \quad . \quad . \quad . \quad . \quad . \quad . \quad . \quad . \quad . \quad . \quad (12)$$

and ν is the integer such that $0<(N-\nu)\leqslant 1$. It is readily seen that the ultimate distribution has a functional form which is independent of the length N of the ingot.

In the figure is shown the distribution (11) for the last four zones of an ingot, where the value $k=0{\cdot}1$ has been chosen. This is in good agreement with the ultimate distribution calculated by Burris *et al.* (1955), who used a numerical method of solution of the ingegral equation.

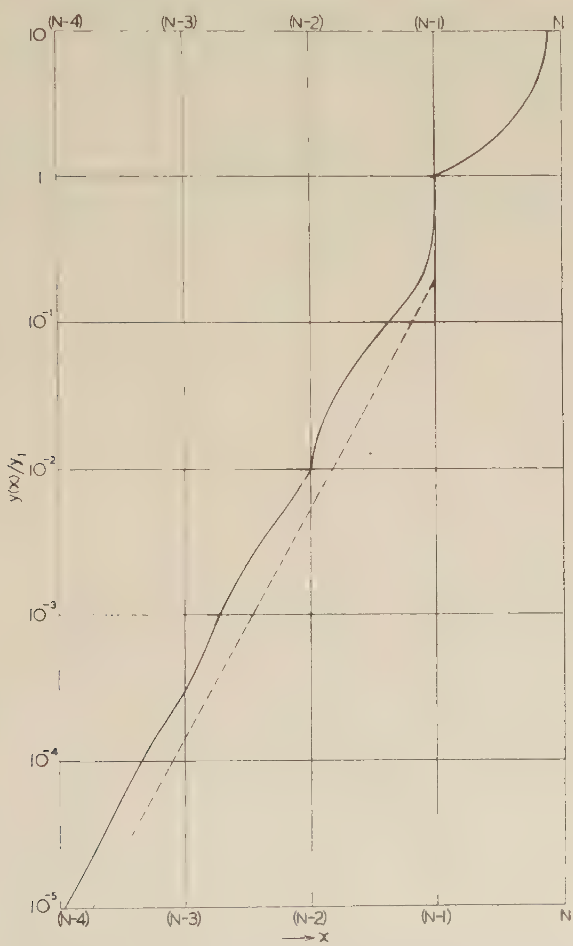

The ultimate distribution of a zone-melted impurity, for which $k=0{\cdot}1$.
(————) according to eqn. (11).
(— — —) Pfann's solution.

By neglecting the effect on the ultimate distribution of the distribution in the last zone, Pfann (1952) wrote down as solution of eqn. (1)

$$y(x)=A \exp (\lambda x), \qquad (13)$$

where A is a constant, and λ is the non-zero root of the transcendental equation

$$\lambda=k\,(\exp\lambda-1). \qquad (14)$$

This distribution is also shown in the figure, with arbitrary constant A. The ultimate distribution (11) appears to approach Pfann's solution as one moves further from the last zone: however, the author has been unable to demonstrate this analytically.

Note added in proof.—The author is grateful to the referee for drawing to his attention a paper by I. Braun (1957, *Brit. J. appl. Phys.*, **8**, 457) on the ultimate distribution in the zone melting process, published after the above was written.

REFERENCES

BURRIS, L., STOCKMAN, C. H., and DILLON, I. G., 1955, *J. Metals, N.Y.*, **7**, 1017.
PFANN, W. G., 1952, *J. Metals, N.Y.*, **4**, 151.

The Positron Decay of the Ground State of Aluminium-26[†]

By P. S. Fisher[‡] and D. W. Hadley[§]
Department of Physics, University of Birmingham

and G. Speers
The Radiochemical Centre, Amersham

[Received November 19, 1957]

Abstract

An investigation has been made of the long-lived ground state of ^{26}Al. The gamma ray spectrum has been determined with a scintillation spectrometer, and the half-life calculated both by comparing the ratio of the masses of ^{26}Al and ^{27}Al in the source and by comparison of reaction cross sections, the value obtained being $0{\cdot}8\times10^6$ years ($\pm30\%$).

The positron spectrum, measured using an overcompression cloud chamber, is consistent with that expected for a unique second forbidden transition, thus helping to confirm that the ground state of ^{26}Al is a $5+$ level, decaying to a $2+$ excited level in ^{26}Mg.

An Appendix describes the radio-chemical separation procedure for extraction of the active aluminium from the magnesium targets.

§ 1. Introduction

Aluminium-26 is one of the odd–odd nuclei of mass number $4n+2$ in which states of isotopic spin $T=0$ and $T=1$ are expected to lie close together, one forming the ground state. The indentification of these states depends on accurate determinations of Q-values for nuclear reactions and on a study of the cascade transitions in (p, γ) capture reactions. Superallowed beta decay is expected between one or both of these two states and the $J=0$, $T=0$ state ground of the even–even isobars.

In the case of mass 26, arguments such as these (summarized by Kluyver *et al.* 1954 and by Kavanagh *et al.* 1955) suggest a decay scheme whose main features are shown in fig. 1. The two odd nucleons in ^{26}Al are expected to be in the $d_{5/2}$ shell and could couple to give, among others, states with $(J, T)=(0, 1)$ and $(5, 0)$ of which the first would be the analogue of the 0^+ ground state of ^{26}Mg. The 6·7 sec positron decay, first observed by Frisch (1934), is assumed to take place from a $T=1$ state identified in the (p, γ) reaction at 230 kev excitation, the ground state decaying much more slowly to excited states of the stable isobar ^{26}Mg. The ground state decay was first reported by Simanton *et al.* (1954), who detected positrons of energy about 1 mev and gamma radiation of energy about 1·8 mev, the half-life being estimated as about 10^6 years.

[†] Communicated by Professor W. E. Burcham.

[‡] Now at Palmer Physical Laboratory, Princeton, New Jersey, U.S.A.

[§] Now at Nuclear Physics Research Laboratory, The University, Liverpool.

Handley and Lyon (1955) observed the spectrum of gamma radiation from ^{26}Al and Laubitz (1955) obtained evidence from the positron spectrum for the unique second forbidden nature of the ground state transition shown in fig. 1. The present work was undertaken with the object (*a*) of confirming the lifetime observed by Simanton *et al.* and (*b*) of further establishing the energy spectrum of the positron decay. Since the work was finished the results of an extensive investigation of the lifetime have been published by Rightmire *et al.* (1957) who established also a 16% *K*-capture branch in the decay. Reports of decay scheme studies have also appeared from Ferguson (1957) and Johnson and Moffat (1957).

Fig. 1

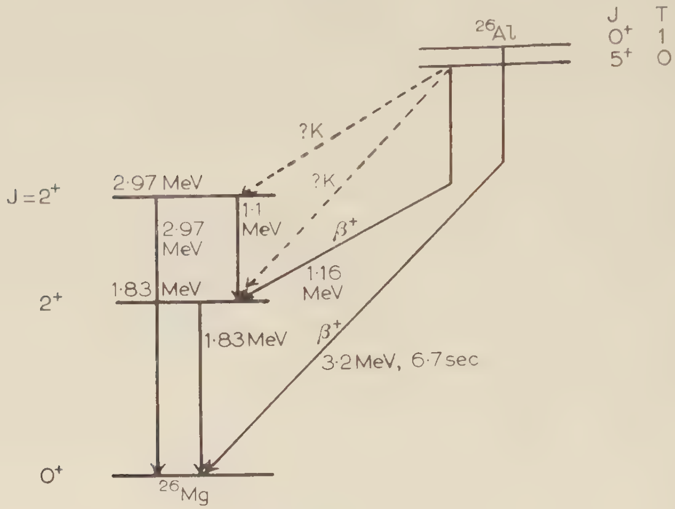

Decay scheme of ^{26}Al.

§ 2. Preparation of the ^{26}Al Source and Estimate of Half-Life

Magnesium targets were bombarded by a 15 MeV deuteron beam in the Nuffield cyclotron of the University of Birmingham. ^{26}Al was produced by the reactions ^{25}Mg (d, n) and ^{26}Mg (d, 2n) and at the same time ^{22}Na was formed by the reaction ^{24}Mg (d, α). Both ^{22}Na and ^{26}Al were extracted at the Radiochemical Centre, Amersham, the procedure for the ^{26}Al being described in the Appendix to this paper. The ^{26}Al source was placed close to a sodium iodide scintillation spectrometer and the gamma-ray spectrum was recorded, the main features, shown in fig. 2, agreeing with those found by Handley and Lyon. The half-life of the ^{26}Al was estimated by calculating the efficiency of the scintillating crystal and by comparing the total gamma disintegration rate with the disintegration rate of the ^{22}Na made in the same bombardment. In another experiment the ^{26}Al activity was compared with the yield of ^{34}Cl obtained by deuteron bombardment of a sulphur target. Estimates of lifetime made by these methods depend on the assumption of equal cross sections for the reactions compared. The results obtained varied between 1·3 and $4{\cdot}6\times10^6$ years and were clearly inferior to those of Rightmire *et al.* (1957) who quote, as the mean of many observations, a half-life of $1{\cdot}1\pm0{\cdot}1\times10^6$ years.

Fig. 2

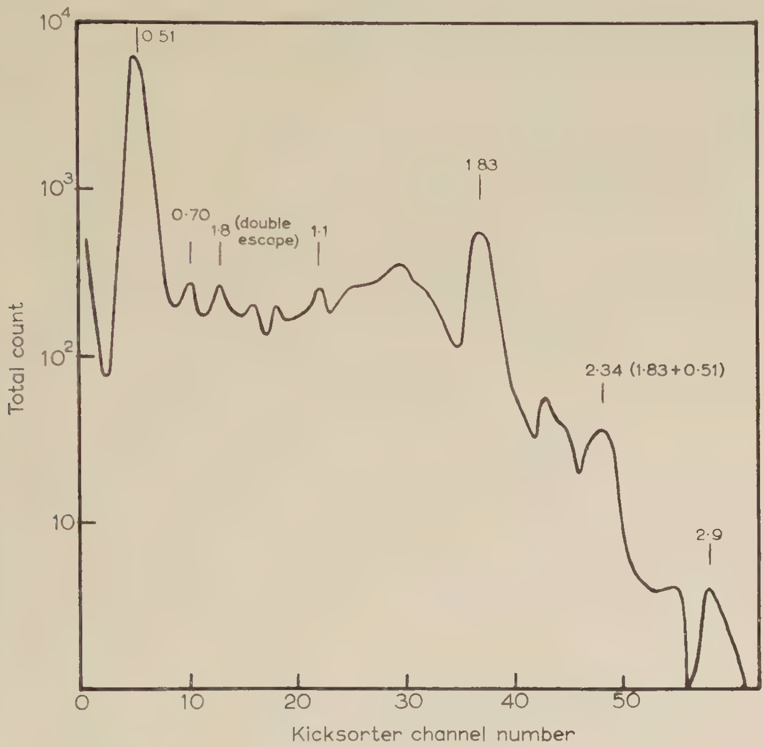

Gamma-ray spectrum of ^{26}Al. Energies marked are in MeV.

In order to avoid the necessity for making assumptions about the reaction cross sections a source of ^{26}Al containing a known weight of ^{27}Al carrier was analysed in a solid-source mass spectrometer. The ratio ^{26}Al/^{27}Al was found to be $2{\cdot}45\pm0{\cdot}37\times10^{-5}$. From the gamma disintegration rate observed with the scintillation spectrometer the half-life was found to be $T_{1/2}=0{\cdot}8\pm0{\cdot}2\times10^6$ years. This value, although less accurate, agrees with the results of Rightmire *et al.*, and confirms that no large error arises from the assumptions made in the ^{22}Na/^{26}Al comparison.

§ 3. THE POSITRON SPECTRUM

The activity of the best available source was too low for the positron emission to be studied with a normal type of magnetic spectrometer and it was decided to use a 9 in. overcompression cloud chamber (Walker *et al.* 1956) fitted with a magnetic field of 500 gauss and filled with

Fig. 3

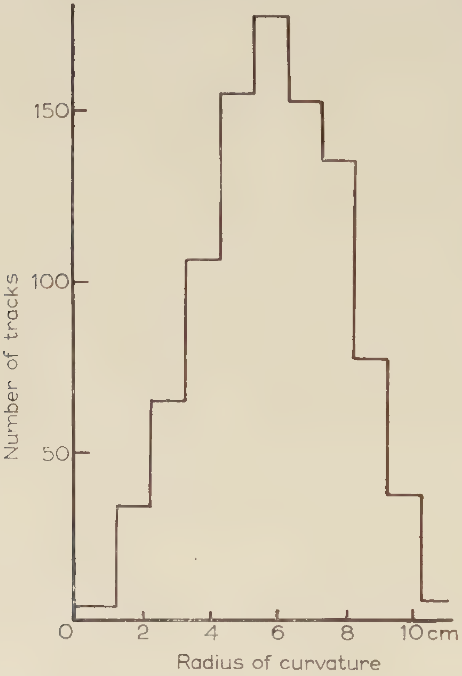

Momentum distribution of positrons from ^{26}Al.

Fig. 4

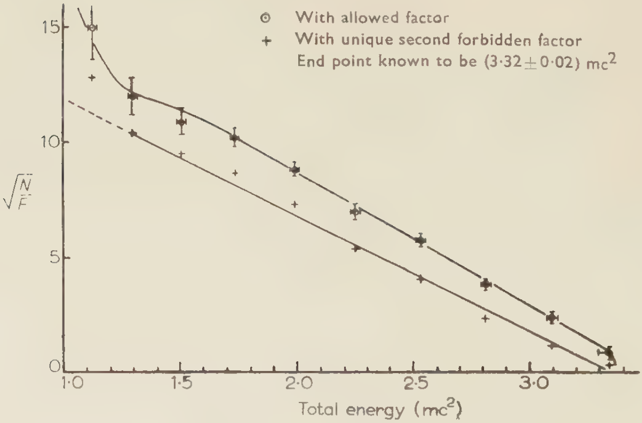

Kurie plot for ^{26}Al.

hydrogen at atmospheric pressure. A suitable mounting for the source was made by spreading the active aluminium oxide as evenly as possible over a 5 micron aluminium foil, to which it was affixed by zapon.

To check that the overcompression chamber was a suitable apparatus for such measurements, a source of ^{22}Na, which is known to yield a Kurie plot of allowed shape, was mounted similarly to the aluminium and its positron spectrum investigated. Compton electrons arising from the accompanying gamma rays could be distinguished by their charge from the emitted positrons. No account was taken of the small number of positrons arising from pair production in the source, but this should not be a serious error, for such positrons would be of low energy, and would appear in that part of the spectrum already distorted due to source thickness. Within the statistical deviations, the Kurie plot was found to be linear from 150 kev to the end point of 540 kev, provided that only tracks lying within 25° of the horizontal were accepted for measurement, thus demonstrating that the overcompression chamber was suitable for investigating the activity of weak beta-emitters.

With the ^{26}Al source in position it was found difficult to maintain satisfactory operation of the chamber, owing to the presence of an impurity which contaminated the filling gas. This meant that many of the expansions were of poor quality, and if tracks observed on all photographs had been measured there would have been an excess of low energy positrons, because the lower the energy the greater the ionization and hence the greater the probability of seeing the track. A certain minimum quality of acceptance had thus to be defined, and in spite of this being largely a subjective criterion, two observers with independent criteria obtained similar positron distributions within statistical errors, although in one case 50% more tracks were measured. There was rarely more than one measurable track per expansion, and less than 1000 suitable tracks were obtained from 4000 photographs.

The positron distribution obtained is shown in fig. 3. The allowed Kurie plot (fig. 4), although not departing greatly from linearity, yields a maximum positron energy well in excess of the value of 1·16 (±0·02) Mev known from the reaction data. After application of the unique second forbidden shape factors (Konopinski 1955) the best straight line through the experimental points does yield the correct end point, although the statistics are not sufficiently good to establish this type of transition with certainty. Taken together with the evidence of other workers, the experiment supports the decay scheme given in fig. 1.

ACKNOWLEDGMENTS

We wish to thank Professor W. E. Burcham for advice during this experiment. Thanks are due also to Miss S. Chesters for assisting in the determination of the gamma-ray spectrum and to Mr. K. C. Sachdev for helping in running the cloud chamber and rescanning the films. We are grateful to Dr. G. H. Palmer, of the Atomic Energy Research Establishment, Harwell, for analysing the aluminium sample in a solid source mass spectrometer.

One of us (P. S. F.) is indebted to the Department of Scientific and Industrial Research for the award of a Research grant, and the other (D. W. H.) to the Fentham Trust and the University of Birmingham for support.

REFERENCES

FERGUSON, J. M., 1957, *Bull. Amer. phys. Soc.*, **2,** **395.**

FRISCH, O. R., 1934, *Nature, Lond.*, **133,** 721.

HANDLEY, T. H., and LYON, W. S., 1955, *Phys. Rev.*, **99,** 755.

JOHNSON, R. G., and MOFFAT, R. D., 1957, *Bull. Amer. phys. Soc.*, **2,** 230.

KAVANAGH, R. W., MILLS, W. R., and SHERR, R., 1955, *Phys. Rev.*, **97,** 248.

KLUYVER, J. C., VAN DER LEUN, C., and ENDT, P. M., 1954, *Physica*, **20,** 1287, 1299.

KONOPINSKI, E. J., 1955, in *Beta and Gamma-Ray Spectroscopy*, edited by Kai Siegbahn (Amsterdam: North Holland Publishing Co.).

LAUBITZ, M. J., 1955, *Proc. phys. Soc. Lond.* A, **68,** 1033.

RIGHTMIRE, R. A., KOHMAN, T. P., and ALLEN, A. J., 1957, *Inter. J. appl. Radiation Isotopes*, **2,** 274.

SIMANTON, J. R., RIGHTMIRE, R. A., LONG, A. L., KOHMAN, T. P., 1954, *Phys. Rev.*, **96,** 1711.

WALKER, J., TAGLIAFERRI, G., BOWER, J. C., and HADLEY, D. W., 1956, *J. sci. Instrum.*, **33,** 113.

APPENDIX

Extraction of ^{26}Al *from Residues from Deuteron Bombarded Magnesium Targets*

The starting material was residues remaining after ^{22}Na had been extracted from deuteron bombarded magnesium. For extraction of the ^{22}Na the active surface had been dissolved off in acetic acid, and from this acetic acid solution the ^{22}Na (together with added carrier sodium) was precipitated by addition of excess uranyl acetate and ethanol. The residue therefore contained large quantities of magnesium, some uranium and its decay products, and traces of ^{22}Na.

1. The bulk of the ^{22}Na remaining together with the bulk of the uranium was precipitated by addition of the correct quantity of sodium chloride solution.

2. To the supernatant was added aluminium chloride solution ($\equiv$ 15 mg Al) and ferric chloride solution ($\equiv$ 100 mg Fe). The solution was evaporated to remove the bulk of the ethanol.

3. Ammonia and ammonium chloride solution was added in presence of tannic acid. The precipitate contained the aluminium and iron,

together with a trace of uranium. The precipitate was washed, dried and ignited at 1000°c.

4. The residue was fused with potassium bisulphate, dissolved in water, and a second tannin precipitation carried out. The precipitate was washed, dried, and ignited at 1000°c.

5. The residue was fused with potassium bisulphate, the pH adjusted to approximately 4 by addition of sodium hydroxide solution. The iron was precipitated as hydroxide, leaving the aluminium in solution. This ferric hydroxide precipitate served to ' scavenge ' radioactive impurities, especially uranium decay products, from solution.

6. The pH of the solution was adjusted to approximately 4, a tannin precipitation carried out, the precipitate dried and ignited at 1000°c.

7. The residue was fused with postassium bisulphate, and dissolved in water. A trace of uranium was still present in the solution. To the solution was added methyl orange indicator, followed by ammonium hydroxide solution, drop by drop, until the indicator turned yellow. The precipitate was centrifuged off, digested with ammonium carbonate solution (to remove uranium) and washed with water.

8. At this stage the only activities detected with a gamma-ray spectrometer were ^{26}Al, and, rather surprisingly ^{22}Na. The precipitate was dissolved in dilute nitric acid, sodium chloride ' hold-back carrier ' added, and aluminium hydroxide precipitated by addition of 10% hexamine solution.

9. The precipitate was washed with sodium chloride solution, taken up in nitric acid and the hexamine precipitation in presence of sodium ' hold-back carrier ' repeated.

10. The precipitate was taken up in a small volume of sodium hydroxide solution, a trace of solid residue was centrifuged off, dilute sodium chloride solution added, and aluminium hydroxide precipitated by addition of ammonium chloride.

11. The precipitate was washed and dissolved in the smallest volume of dilute nitric acid. Examination of the solution with a gamma-ray spectrometer showed that the 1·28 MEV peak of ^{22}Na was now absent. Ammonia was then added to the solution to precipitate aluminium hydroxide.

When held at red heat on a platinum foil for several minutes the aluminium hydroxide decomposed to aluminium oxide, which formed a source suitable for use in the cloud chamber.

The Remanent Magnetism of Some Lavas in the Deccan Traps†

By E. R. DEUTSCH
Department of Physics, Imperial College of Science and Technology

and C. RADAKRISHNAMURTY and P. W. SAHASRABUDHE
Tata Institute of Fundamental Research, Bombay

[Received September 1, 1957 and in revised form December 9, 1957]

ABSTRACT

The magnetizations of over 400 basalt specimens from the Deccan Traps have been found to be aligned in general along a NNW-SSE to NW-SE axis dipping towards the south. The results are consistent with the supposition that India has drifted northwards through over 50° of latitude and rotated 25° anticlockwise within the last 70 million years. In all three localities, the poles corresponding to the upper rocks are nearer the present geographical poles than those from the lower flows. The discrepancy may represent a northward drift of India during the formation of the Deccan Traps, but there are other possible explanations and further data are necessary to elucidate the problem.

§ 1. INTRODUCTION

AN earlier survey of the Deccan Traps (Clegg *et al.* 1956) was undertaken by the Physics Department of Imperial College in the winter of 1954–55 to initiate a project of palaeomagnetic research in India. Some 450 basalt specimens from two areas, Khandala and Linga (fig. 1, (1) and (2)), were examined at that time and shown to possess on the whole consistent remanent magnetizations whose direction is almost perpendicular to that of the present earth's field. The mean declination and dip for the two localities were N 155° E and 53° downwards respectively. This result is in good agreement with that found independently by Irving (1956), and is most plausibly interpreted on the assumption that at the time when the rocks were laid down, during the late Cretaceous or early Eocene periods, India occupied a position considerably to the south of the equator, and that it has since drifted northwards and rotated in an anticlockwise direction. The ancient positions of the North and South poles corresponding to this direction of magnetization differed strikingly from those obtained by other workers for British, North American and Icelandic rocks of the same period, and this suggested that at least part of the postulated movement of India may have been in relation to other continents.

The present investigation has been carried out with the aim of extending the previous work to other areas in the Deccan Traps. This is of considerable importance, since the formation covers a large area in Western

---

† Communicated by Dr. J. A. Clegg.

India (about 200 000 square miles), and attains a thickness of several thousand feet in some places, and it is highly probable that rocks from different areas may differ considerably in age. Moreover, by extending the survey, it was possible to compare magnetic results obtained from rocks of various petrological types, for in a number of localities in the Deccan Traps acid volcanic rocks occur in addition to the much more prevalent plateau basalts. One of the best known of such localities is

Fig. 1

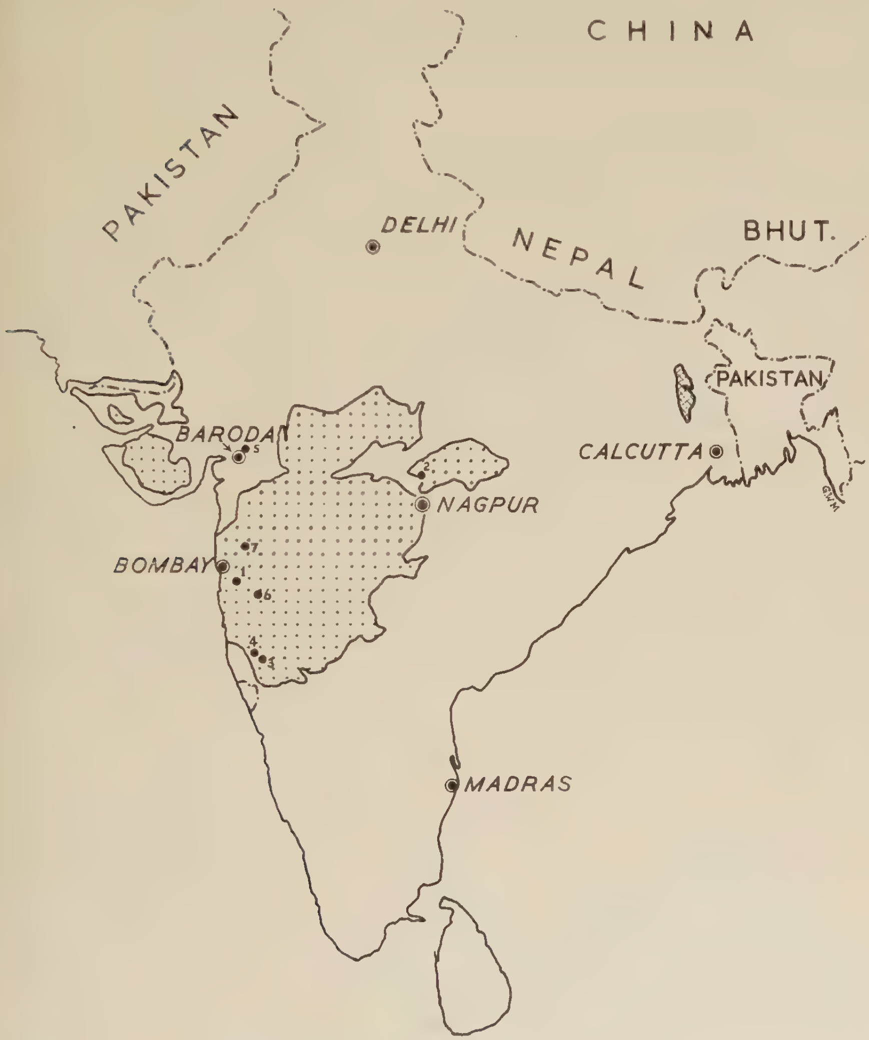

Palaeomagnetic Surveys (Deccan Traps).

(1) Khandala area.
(2) Linga area.
(3) Nipani area.
(4) Amba area.
(5) Pavagadh area.
(6) Kambatki area.
(7) Igatpuri Ghats.

Mt. Pavagadh (fig. 1 (5)), a prominent hill northeast of the city of Baroda in the north of Bombay Province where basic as well as acid lavas were collected. In the south of Bombay Province, 400 miles from Mt. Pavagadh, two other localities were sampled in detail: the Nipani area (3), near the small town of that name on the Kolhapur Belgaum highway, and the Amba area (4), constituting a hill of the Western Ghats about 50 miles northwest of Nipani on the Kolhapur–Ratnagiri highway. Apart from the three major surveys, two small test collections involving a small number of samples were made from two hills, the Kambatki (6) and Igatpuri (7) Ghats, situated between the two southern areas and Mt. Pavagadh. A preliminary and less complete account of measurements on rocks from Nipani, Amba, and Mt. Pavagadh has been given previously by Clegg *et al.* (1957).

§ 2. COLLECTION AND MEASUREMENT

Between October 1955 and November 1956, we undertook a number of field trips to the localities concerned and collected altogether 157 blocks of rock. At the collecting sites, these were marked with reference to the horizontal plane and to magnetic north, and the majority were taken to Bombay, where a palaeomagnetic laboratory suitable for the investigation of weakly magnetized geological specimens had been set up at the Tata Institute. Some of the rocks were shipped to Imperial College, London, for study. In each laboratory cylinders were cut from the blocks and the direction and intensity of their remanent magnetization were measured by means of a simplified adaptation of the astatic magnetometer described by Blackett (1952). In this, the standard procedure used by Clegg *et al.* (1954) was followed. In the present paper, the word 'specimen' will be used to denote each cylinder cut from a block, and the word 'sample' to denote a block. Altogether 480 specimens were measured, or an average of roughly three specimens to a sample. The results for the three areas are described separately below.

§ 3. THE NIPANI AREA

The Deccan Trap flows in this region are exposed mainly on a number of low hills and in quarries. The present collection was made from two series of outcrops of basaltic lava, one occurring on the prominent escarpment lying three miles south of Nipani, and the other in two quarries on the plain ten miles north of Nipani. Samples were taken on the escarpment from five sites representing at least three distinct flows and a vertical column of nearly 200 feet. The single flow exposed in the quarries was 650 feet below the highest flow sampled on the escarpment, but since the two localities were about 13 miles apart, a regional northward tilt of the flows by about $\frac{1}{2}°$ would suffice to place the quarry flow above the escarpment flows on the stratigraphic column. Despite the remarkable horizontality of the flows characteristic of most of the Deccan Traps (Wadia

Table 1. Summary of Investigations

1 Area and section	2 Mean latitude (North)	3 Mean longitude (East)	4 Elevations (above mean sea level) (ft.)	5 Total No. of sites visited	6 Total No. of specimens measured	7 Mean intensity of magnetization ($\times 10^{-3}$ c.g.s.)	8 Mean declination (East of true North)	9 Mean dip[1] (positive downwards)	10 Radius of 50% circle of confidence[2]
Nipani, *Lower*	16° 32′	74° 19′	1850	2	44[3]	1·87	168°	+60°	1·9°
,, *Upper*	16° 21′	74° 24′	2325–2500	5	74[3]	1·96	338°	−32°	2·1°
Amba, *Lower*	17° 00′	73° 46′	500–1800	5	109[4] (17)[5]	3·49 (1·81)[5]	144° (159°)[5]	+60° (−75°)[5]	2·0° (4·5°)[5]
,, *Upper*	16° 59′	73° 47′	2050–2075	3	54	3·13	335°	−26°	3·3°
Pavagadh *Lower* (basic)[6]	22° 28′	71° 34′	1125–2425	8	69	2·22	351°	−16°	3·5°
,, (acid tuffs)	22° 28′	71° 33′	2490–2600	2	15	0·29	355°	+17°	3·4°
,, (rhyolites)[7]	22° 28′	71° 33′	2625–2725	2	69	0·59			

[1] Measured relative to a horizontal plane.

[2] Fisher's method (1953).

[3] Four specimens had inverted dips and are here omitted.

[4] Specimens with downward dips only.

[5] Specimens with anomalous upward dips.

[6] Chiefly basalt.

[7] Much of this group was randomly magnetized, so that a significant mean direction could not be computed.

1953), such a possibility cannot be completely ruled out. However, for the purpose of this paper, the quarries will be referred to as ‘ lower Nipani ’, and the escarpment as ‘ upper Nipani ’.

The results are shown in table 1 and the directions of magnetization of individual specimens are plotted in fig. 2. Specimens cut from one sample in each of the lower and upper sections showed scattered directions of magnetization, and these have been omitted. It is evident from fig. 2

Fig. 2

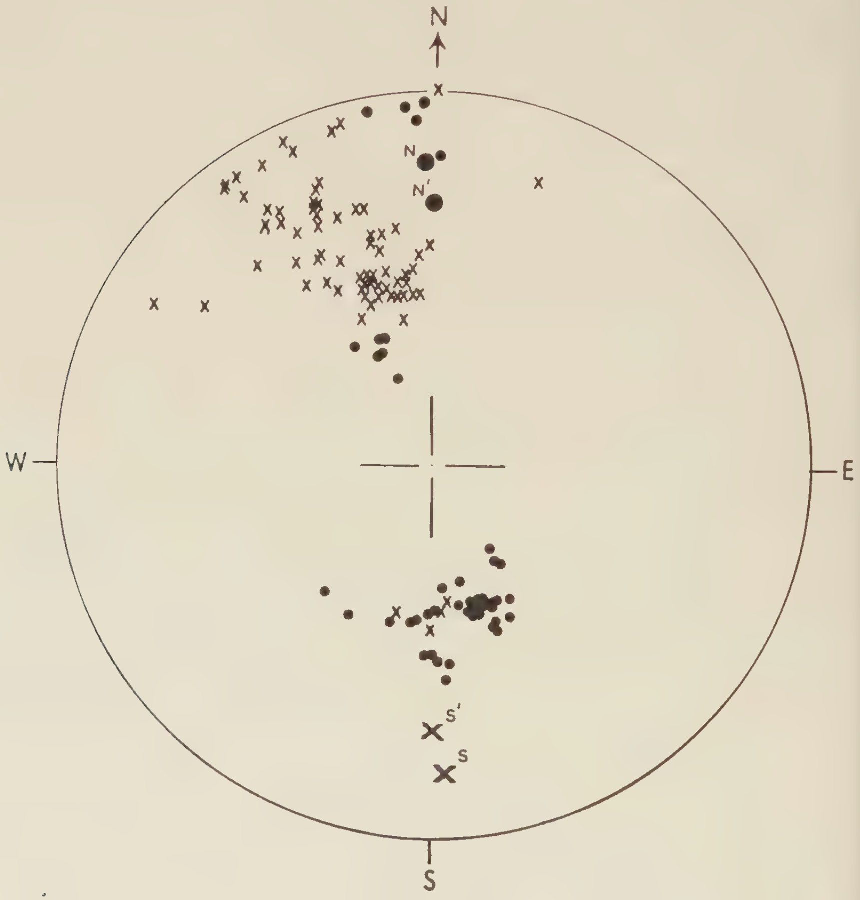

Nipani Area.
All Flows.
Directions of North-seeking Polarizations :
X Up ● Down
Directions corresponding to :
Present Poles :
● N X S
Dipoles :
● N^1 X S^1

that the magnetic directions are grouped into two main classes, the lower Nipani specimens generally having SSE declinations with rather steep downward dips, while most of the upper Nipani specimens have NNW declinations with shallower upward dips.

§ 4. THE AMBA AREA

A vertical sequence of at least 1600 feet of basaltic lava flows is partly exposed on the steep side of the Amba Ghat, which lies on the western edge of the Deccan plateau just above the coastal plain. In the topography of the Western Ghats this hill occupies a place corresponding to the

Fig. 3

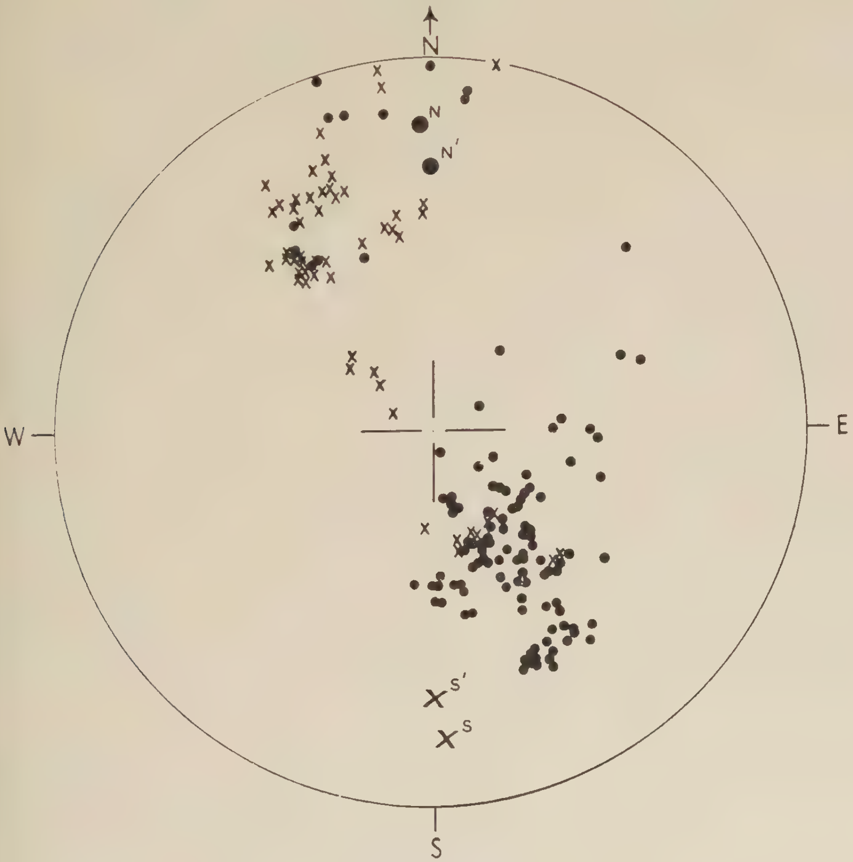

Amba Area.

Directions of North-seeking Polarizations :

X Up ● Down

Directions corresponding to :

Present Poles :

●N X S

Dipoles :—

●N1 X S1

Bhor Ghat at Khandala, 130 miles to the north, mentioned previously by Clegg *et al.* (1956). Eight sites representing five or more distinct flows were sampled and again the polarizations fell into two major groups (fig. 3 and table 1), with most of the directions aligned approximately along a NNW–SSE axis dipping downwards towards the south, similar to the preferential direction at Nipani. A sub-division into ' upper ' and ' lower ' Amba areas was made to distinguish the three highest sites, which were magnetized towards the NNW with an upward dip, from the five lower sites where the great majority of the samples had polarizations directed towards the SSE, but with rather steeper downward dips. As found in the Nipani area, a few of the lower Amba specimens yielded consistently odd results, with generally SSE declinations as expected, but also steep upward, instead of downward dips. Since 17 specimens from two samples and two different flows were here involved, values for their mean direction have been listed separately in table 1.

§ 5. The Pavagadh Area

Mount Pavagadh is separated from the main body of the Deccan Traps by a distance of about 30 miles. It rises abruptly from the plains of Gajerat to a height of 2811 feet above sea level. The main mass of the hill, up to a height of about 2400 feet, consists of numerous nearly horizontally bedded flows of porphorytic as well as non-porphorytic basalt and olivine dolerite, together with some basic tuffs. Above this level the extensive Mauliya plateau is covered with green rhyolitic tuffs, and is capped with a large mass of rhyolite which rises steeply from the plateau to the summit. These acid rocks were first identified by Fermor (1906) who suggested that they might be interbedded with basic lavas, but Mathur and Dubey (1934) have since shown them to be younger than the basic lavas, and it is now believed that both the rhyolitic tuffs and the overlying rhyolites belong to an acid cycle of igneous activity which may have taken place considerably later than that which produced the basic rocks below. In the present account (see table 1) the lower basic rocks will be referred to as the ' Lower Pavagadh ' and the upper acid tuffs and rhyolites will be termed ' Upper Pavagadh '.

Eight flows of largely basic composition were investigated in the lower Pavagadh area. The magnetic directions (fig. 4) were predominantly N to NNW declinations with shallow upward dips. Fifteen specimens from eight samples of acid tuffs of the upper Pavagadh area were also examined. Their magnetizations were found to be directed nearly towards the north, as in the basic rocks, and the dips were again shallow, but slightly downwards. The data for the tuffs are plotted as open circles in fig. 5. The mean direction of magnetization is 5° west of north with shallow downward dip.

Directions for 69 specimens cut from 14 samples of rhyolite are also plotted on the same diagram. The results show too much scatter to permit the computation of a significant mean direction of magnetization. Different specimens of rhyolite, even from samples collected at points not far apart, gave in some cases results which completely disagreed with one another, and they reacted quite differently to simple tests for their stability. The close spacing of the cluster of dots on the lower left side of fig. 5 would alone suggest that the 16 specimens concerned have stable magnetizations, particularly in view of the large angles which these make with the geomagnetic field. To test this, a number of the specimens were subjected

Fig. 4

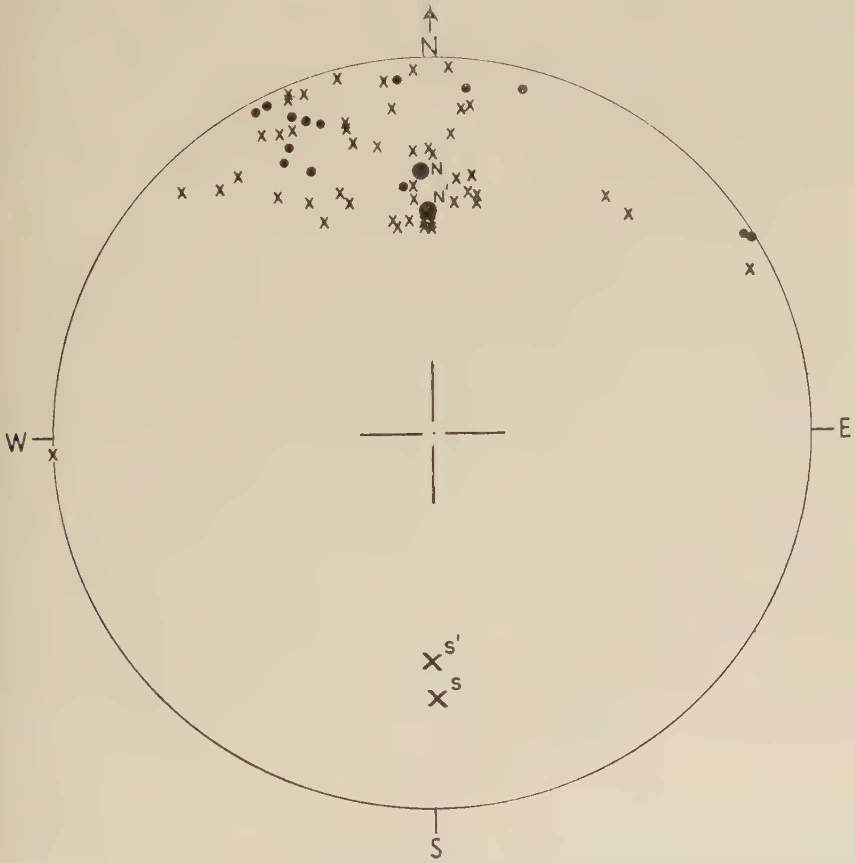

Pavagadh Area.
Flows 1–8.
Directions of North-seeking Polarizations :
X Up ● Down
Directions corresponding to :
Present Poles :
● N X S
Dipoles :
● N^1 X S^1

to a.c. demagnetizing fields of 200 oersteds r.m.s.; this had no effect on their remanent polarizations. At the other extreme, when some of the specimens from samples showing much scatter were placed for periods varying from a few hours to a few weeks with their magnetization axes at

Fig. 5

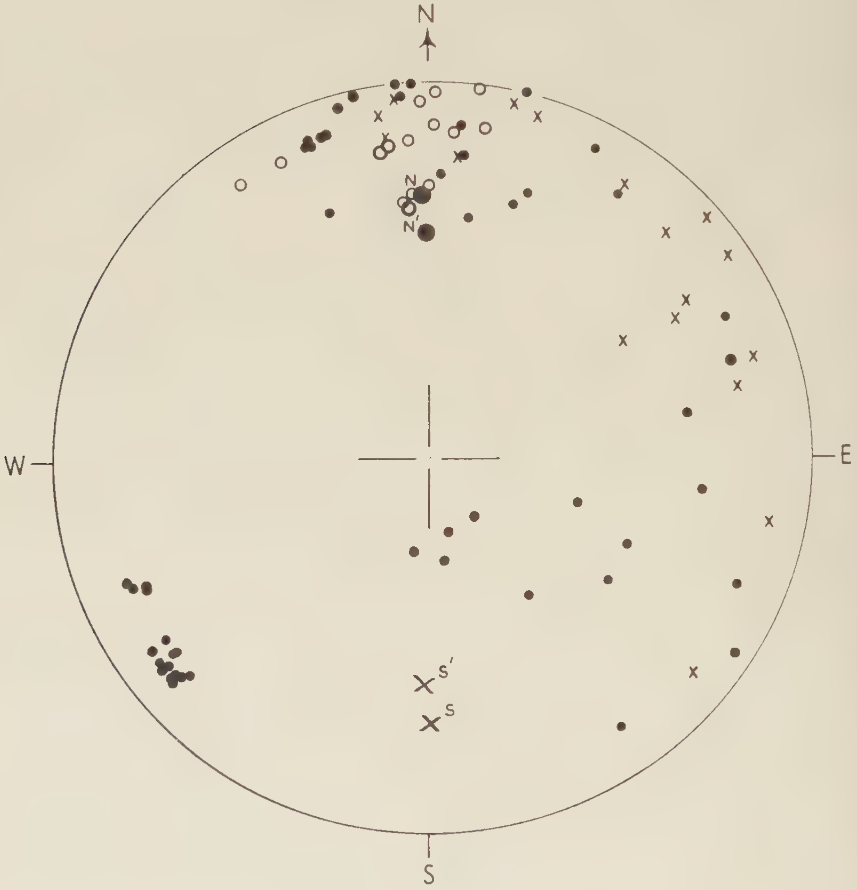

Pavagadh Area.
All acid rocks (Tuff and Rhyolite).
Directions of North-seeking Polarizations :
X Up (Rhyolites). ● Down (Rhyolites)
○ Down (Tuffs)

Directions corresponding to :
Present Poles :
●^{N} X^{S}
Dipoles :
●$^{N^1}$ X$^{S^1}$

right angles to the earth's field, and re-measured, this axis was usually found to have been pulled towards the magnetic meridian, in some cases through a complete right angle.

§ 6. TEST COLLECTIONS

Four samples each from two flows of the Kambatki Ghat south of Poona, and from four flows of the Igatpuri Ghat northeast of Bombay, were examined. The lower Kambatki flow gave a mean declination of 176° and a mean dip of +60°, whilst the corresponding values for the three upper Igatpuri flows were 161° and +51°. These results are similar to those obtained for the Khandala, Linga, lower Nipani and lower Amba areas, but not enough samples have been examined to justify any further conclusions. The upper flow at the Kambatki Ghat and the lowest flow at the Igatpuri Ghat had respectively NE and NW declinations with steep downward dips, perhaps due to partial instability.

§ 7. DISCUSSION OF RESULTS

The complete results for the Nipani, Amba, and Pavagadh areas are summarized in table 1. The general direction of magnetization is along a NW–SE to NNW–SSE axis dipping towards the south. This is in broad agreement with the earlier results of Irving (1956) and Clegg *et al.* (1956), and supports the supposition that India has moved northwards across the Equator relative to the earth's geographical axis, and rotated in an anticlockwise direction, since the rocks were laid down. In the Nipani and Amba areas the lower flows have reverse (southeasterly) magnetizations with rather steep downward dips, while the uppermost flows are normally magnetized and the dips are significantly less. In the Pavagadh area there is also a significant difference between the lower basic rocks and the acid tuffs above, both having normal polarizations and shallow dips, but whereas the dips of the lower flows are upwards, those of the overlying tuffs are downwards. No significant mean direction could be computed for the rhyolities overlying the tuffs.

7.1. *The Directions of the Magnetic Axes and Ancient Pole Positions*

Since the period of time over which the rocks from each individual site were extruded is likely to have been large in comparison with the period of secular variation, it is reasonable to suppose that the magnetic directions shown in table 1 correspond to those of a central magnetic dipole coaxial with the earth's rotational axis. In column 4 of table 2 the values of the ancient latitude λ of the various sites have been computed on this assumption, from the mean dip θ, using the formula

$$\tan \lambda = \tfrac{1}{2} \tan \theta.$$

Table 2

1 Area and section	2 Mean declination (East of true North)	3 Mean magnetic dip	4 Ancient latitude of site	5 Ancient pole position		6 Ancient latitude of Bombay	7 Ancient magnetic dip at Bombay	8 Sense of magnetization
				Latitude	Longitude			
Linga *complete*	164°	+48° down	29° S	37° N	83° W	31° S	+50° down	Reversed
Khandala *complete*	147°	+50° ,,	39° S	25° N	79° W	39° S	+58° ,,	,,
Nipani *lower*	168°	+60° ,,	41° S	35° N	95° W	39° S	+58° ,,	,,
Amba *lower*	144°	+60° ,,	41° S	27° N	76° W	39° S	+58° ,,	,,
Nipani *upper*	338°	−32° up	17° S	52° N	70° W	14° S	−27° up	Normal
Amba *upper*	335°	−26° ,,	14° S	52° N	64° W	12° S	−23° ,,	,,
Pavagadh *lower*†	351°	−16° ,,	8° S	58° N	91° W	12° S	−23° ,,	,,
Pavagadh *upper*‡	335°	+17° down	9° N	75° N	89° W	5° N	+10° down	,,

† Mainly basalt. ‡ Acid tuffs only.

The 'reversely' and 'normally' magnetized series of flows have been grouped together for comparison. Column 5 of table 2 shows the ancient positions of the North geographical pole calculated from the values of λ, and from the mean declinations. These pole positions are compared with those obtained previously by Clegg *et al.* (1956). The few anomalous results from the various sites (e.g. the 17 specimens from the lower Amba area showing upward dips) have been omitted from this table.

The discrepancies between the values of λ shown in column 4 arise partially because the various sites are separated by distances of several hundreds of miles, and a better comparison is obtained by referring all the results to a single locality. For this purpose Bombay (present latitude 19° N) has been chosen, and columns 6 and 7 of table 2 show the ancient latitude and the ancient axial dipole field dip at Bombay, corresponding to the pole positions in column 5.

7.2. *Possible Implications of the Results*

From the summarized results set out in table 2 it is apparent that the rocks from the various localities visited fall into three main groups, viz.:

(*a*) Those of the lower Nipani and lower Amba sections, for which the magnetic directions and ancient pole positions correspond reasonably well to those obtained previously for the Linga and Khandala areas by Clegg *et al.* (1956).

(*b*) Those of the upper Nipani and upper Amba sections together with the basic rocks of lower Pavagadh, which are normally magnetized and have markedly shallower upward dips, and for which the corresponding ancient pole positions lie considerably closer to the present geographical pole.

(*c*) The upper rhyolitic tuffs of upper Pavagadh, which are again normally magnetized, but which have a shallow downward dip corresponding to a low northerly latitude.

The mean directions of magnetization for these three groups, obtained from table 2 (directions are referred to Bombay) are

	Mean declination	Mean dip
(*a*)	N 156° E	+56° down
(*b*)	N 341° E	−24° up
(*c*)	N 355° E	+10° down

One obvious possible explanation of these facts is that the three groups of rocks were laid down during different geological epochs, between each of which India moved northward relative to the earth's geographical axis. It may also be that the earth's magnetic field underwent a reversal between the first and second of the epochs. The geological evidence provides some support for this view. Thus in the Amba Area there is a section 200–300 feet thick between the uppermost 'reversed' and lower 'normal' flows in which no exposures were found, so that the upper and lower sections probably differ considerably from one another in age. Again in the Nipani area a horizontal gap of 13 miles, containing four outcrops, separates the two localities, so that a strong possibility exists that the missing section represents a relatively long time interval, although it is not definitely established that the 'upper' Nipani rocks are indeed younger than those of the 'lower' Nipani area. The unusual sequence on Mt. Pavagadh is of particular interest. The lower basic rocks may well belong to the uppermost flows of the Deccan Traps, and it is probable that a considerable time elapsed between the last basalt outpouring and the beginning of the acid cycle responsible for the overlying rhyolitic tuffs. Mathur and Dubey (1934) quote results of radioactive age determinations of basalt and rhyolite specimens from Mt. Pavagadh, made by the helium method. Although helium dating seldom yields precise results they estimate from their data that the age of the basalt is early Eocene, in conformity with the remainder of the Deccan Traps, while that of the rhyolite is Miocene. If we assume the position of India at the end of the Cretaceous period to be that originally postulated by Clegg *et al.* (1956) and by Irving (1956), and the drift to have proceeded at a more

Fig. 6

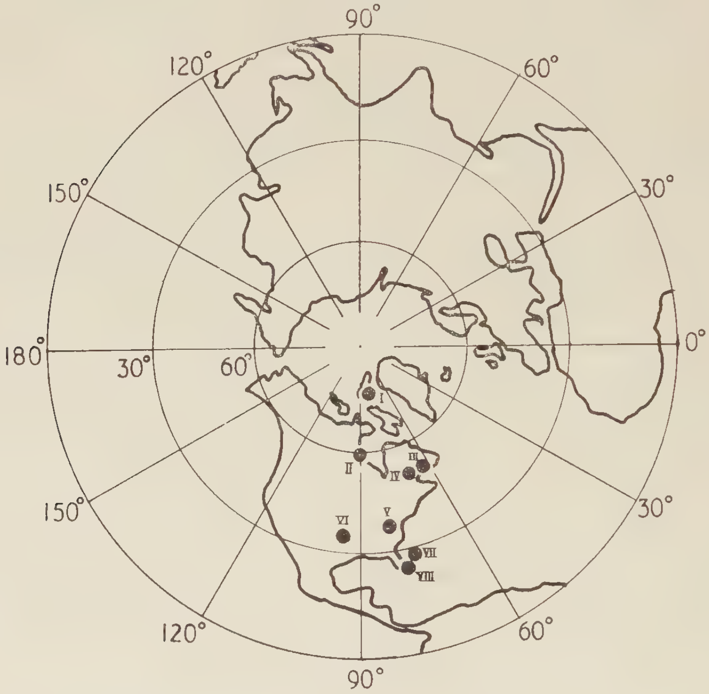

I. Pavagadh (Upper)
II. Pavagadh (Lower)
III. Amba (Upper)
IV. Nipani (Upper)
V. Linga
VI. Nipani (Lower)
VII. Amba (Lower)
VIII. Khandala

or less constant rate up to the present time, the area under investigation should have crossed the equator during the early Miocene. The observed mean dip of the tuffs would tend to support this supposition.

On the other hand, it is by no means certain, on the basis of the evidence so far available, that this variation of magnetic dip with depth can be taken as positive evidence of a continuous northward movement of India. One major difficulty in the interpretation of the results arises from the uncertainty in the relative dating of the basic rocks from the various sites. For the total depth of the Deccan Traps, particularly towards their eastern edge, is known to exceed 10 000 feet in places (Wadia 1953), and as it was only possible to sample a small fraction of this range at any of the sites visited, it seems improbable on primae faciae considerations that the rocks of either of the two categories (*a*) and (*b*) above are from corresponding parts of the stratigraphical column.

There are obviously other possible physical causes which may have given rise to the difference in inclination between the categories (*a*), (*b*) and (*c*). It may, for instance, be due to some physical phenomenon associated with different depths of burial, such as the magnetostriction effect suggested by Graham (1957). Alternatively it may result from partial magnetic instability, and the consequent pulling of the magnetic directions towards that of the present earth's field. For rocks which are magnetized normally this latter effect would tend to reduce the magnetic dip, while for those magnetized reversely it would tend to increase the dip. In this connection it is worth noting that the rocks of category (*a*) which have the steepest dips, are reversely magnetized, while those of categories (*b*) and (*c*), with shallower dips, are all normal.

Work is continuing in an attempt to find exposures of intermediate sections in the areas sampled so far, and the survey is also being extended to include a detailed study of vertical sequences in other parts of the Deccan Traps.

ACKNOWLEDGMENTS

We wish to express our gratitude to Professor P. M. S. Blackett, at whose instigation this project was undertaken, and to Dr. J. A. Clegg, under whose general direction it has been carried out, for their continued help and interest. Also at the Physics Department of Imperial College, London, special thanks are due to Mr. G. W. Massé for his aid in cutting many of the specimens and in preparing the diagrams.

We are indebted to numerous colleagues at the Tata Institute of Fundamental Research, Bombay, and especially to Professor B. Peters for his support and encouragement of this research, and to Dr. D. Y. Phadke, who took part in the first of two rock collecting trips to the southern part of Bombay Province. We have received valuable aid from many members of the staffs of the Geological Survey of India; in particular, Mr. M. Hazra and Mr. Y. S. Sahasrabudhe of the Bombay Office have given much helpful advice.

Dr. D. H. Griffiths of the Department of Geology, University of Birmingham, has repeatedly assisted us with useful suggestions and information.

Finally, we are indebted to the Department of Scientific and Industrial Research for the award of a grant to finance the survey.

REFERENCES

BLACKETT, P. M. S., 1952, *Phil. Trans. roy. Soc.* A, **897,** 309.
CLEGG, J. A., ALMOND, M., and STUBBS, P. H. S., 1954, *Phil. Mag.*, **45,** 583.
CLEGG, J. A., DEUTSCH, E. R., EVERITT, C. W. F., and STUBBS, P. H. S., 1957, *Advanc. Phys.*, **6,** 219.
CLEGG, J. A., DEUTSCH, E. R., and GRIFFITHS, D. H., 1956, *Phil Mag.*, **1,** 419.
FERMOR, L. L., 1906, *Records, Geol. Survey of India,* **34,** 148.
FISHER, R. A., 1953, *Proc. roy. Soc.* A, **217,** 295.
GRAHAM, J. W., 1957, *Advanc. Phys.*, **6,** 362.
IRVING, E., 1956, *Geofis. Pura e applic.* (*Milan*), **33,** 23.
MATHUR, K. K., DUBEY, V. S., 1934, *Proc. Ind. Sci. Congr.*, 21st Sess. (*Abstracts*), 348.
WADIA, D. N., 1953, *Geology of India* (London : Macmillan & Co.), 3rd edition.

The Electronic Structure of the Metals of the First Transition Period†

By W. M. LOMER and W. MARSHALL
Atomic Energy Research Establishment, Harwell, Berks.

[Received October 31, 1957]

ABSTRACT

Three distinct lines of experimental work now point towards a new conception of the electronic structure of the transition metals. Recent x-ray work has shown that in Fe and Cr the valence electrons are not as well localized near the atoms as had been supposed, while in Co, Ni and Cu the compact 3d-shell is nearly complete. Saturation magnetic moments of Ni rich alloys show that Ti and V act as though they had respectively four and five electrons to contribute to the conduction band of Ni. Neutron diffraction evidence shows that pure Ti and V have no magnetic moments, ordered or disordered, and that in Ni–Cr alloys the Cr atom carries a moment not much different from Ni, though each added atom removes nearly 5 μ_B from the saturation moment. We therefore suggest that elements of atomic number less than Fe have few 3d electrons and many conduction electrons, while for those above iron this is reversed. It appears as though this conclusion can be maintained almost independently of crystal structure or composition of alloy. On this basis the variation of saturation magnetic moment of all the binary ferromagnetic alloys can be explained.

§ 1. INTRODUCTION

THE electronic structure of the first long period elements has been discussed for many years (see e.g. Hume-Rothery and Coles 1954). In particular the ferromagnetic elements have been of interest, and there has been much debate about the most suitable model for their description. Recently the technique of neutron diffraction has allowed us to learn a great deal more about the spatial distribution of magnetic moment in both pure metals and alloys. In addition, a recent x-ray study by Weiss (1957) has shown that the spatial distribution of electron density is very different in the metals Cr and Fe from what it is in the free atoms of these elements. In this paper we outline a scheme of metallic valences which is directly suggested by the new experimental results and which appears to correlate a wide range of observations with a minimum of assumptions. In § 2 we outline the experimental results, and in § 3 state the main assumptions and implications of the model proposed. § 4 is devoted to a discussion of the pure metals from vanadium to zinc. § 5 handles the binary magnetic alloys. § 6 includes some speculations on the interrelation of electronic structure and crystal structure.

---

† Communicated by the Authors.

§ 2. EXPERIMENTAL RESULTS

2.1. *X-ray Electron Counts*

Weiss (1957) reports the results of careful determination of the crystal form factors for the pure metals Cr, Fe, Co, Ni, Cu. He separates the electron density into three parts: the compact argon core containing 18 electrons, the electrons whose radial density distribution resembles atomic 3d functions, and those roughly uniformly distributed over the crystal. The contribution of the argon core can be accurately calculated, and Weiss discusses the residual scattering power, which is to be interpreted as arising only from the d-like electron density. He measures the decrease in integrated intensity of reflection from certain planes as the scattering angle is increased. This decrease is interpreted as due to the primary extinction, and is consistent with the d-like radial distribution. The absolute intensity extrapolated to zero scattering angle leads to the following numbers of electrons in d-like orbitals:

Cr, 0·2; Fe, 2·3; Co, 8·4; Ni, 9·5; Cu, 10.

The accuracy is quoted to be ±0·3 electron. The remaining valence electrons are concluded to be in conduction states, with a roughly uniform density distribution. The number of conduction electrons are therefore about: Cr, 5·8; Fe, 5·7; Co, 0·6; Ni, 0·5; Cu, 1. While the experiment says little about the actual distribution of these electrons, they certainly *do not show a marked density peak in the same position as that of the atomic 3d functions.* For convenience we shall denote these states as 4c states, indicating that they are conduction band states built up mainly from 4s and 4p atomic states (but in fact containing some admixture of all higher states).

2.2. *Neutron Diffraction*

It is found (Shull and Wilkinson 1955) that the neutron diffraction from ferromagnetic crystals is consistent with a distribution of electron spin corresponding to 3d functions around each atom. The total electron spin so measured is consistent with the observed saturation magnetic moment, so that we may conclude that the magnetic electrons are 3d-like in electron density: for Fe, Co and Ni there are about 2, $1\frac{1}{2}$, $\frac{1}{2}$ respectively.

Above the Curie point (Wilkinson and Shull 1956, Lowde 1956) spin disorder scattering is found. Although the mean magnetic moment is zero, it appears that every atom carries the same spin as in the magnetized state, but now randomly oriented except for a certain amount of short range order (Elliott and Marshall 1957). To describe such a system, in which the spin on each atom is well-defined, the Van Vleck (1953) model seems appropriate.

In ferromagnetic alloys, neutron observations demonstrate that in general terms each atom tends to carry approximately the moment appropriate to it in the pure metal (Shull and Wilkinson 1955). Each alloy system really merits detailed discussion (§ 5).

2.3. *Magnetic Measurements*

The course of the saturation ferromagnetic moment in many alloy systems has been studied. The results are summarized by (e.g. Bozorth 1951), but in many instances it is necessary to consult the original papers for detail. Many of the alloys follow the Slater–Pauling curve (fig. 1), but many do not. The strongest deviations from this curve, in the **Ni**–Cr, **Ni**–V, and **Co**–Cr series of alloys, will receive a ready explanation on the proposed scheme.

Fig. 1

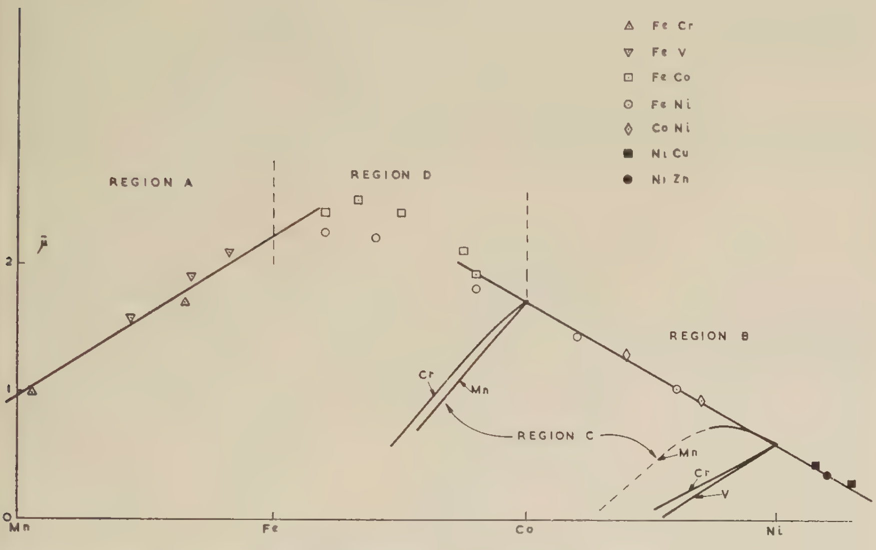

Slater–Pauling curve of mean saturation magnetic moment per atom in binary alloy systems plotted against number of electrons per atom (after Bozorth).

§ 3. THE PROPOSED SCHEME OF STRUCTURES

The proposed scheme is based on the separation of the electronic states into 3d-like states and conduction states, the number of electrons in the 3d-like states for the pure metals being just as found by Weiss. It is by no means easy to determine theoretically what a full self-consistent field solution for any particular metal would be like, and information on free atoms is of little direct use. Our picture is that as the nuclear charge is increased and electrons are added to the argon core from potassium right through to chromium, there are practically no 3d-like electrons; they are all ‘conduction electrons’ with spatial density distribution quite unlike that of the atomic 3d-states. At chromium the d-levels begin to fill. At cobalt there is a sudden change to a configuration with a high number of d-like electrons and few conduction electrons. This type of structure of course persists through copper, zinc and gallium with their intact $(3d)^{10}$ filled shells. We make no attempt at the moment to give this picture theoretical backing. Note that the main determining feature of the metal which fixes the number of d electrons is the nuclear charge of the atom; the crystal structure we would choose to regard as a consequence of the electronic structure, playing only a minor role in determining just what that electronic structure is to be.

Now let us take a brief look at the expectations for alloys. Here we use the model suggested by Friedel (1954), which reconciles the localization of electron charge near positively charged impurities with the original ideas of Hume-Rothery *et al.* (1934) and Jones (1934) of adding electrons to a nearly rigid conduction electron band structure. This is to be considered along with the existence of an equilibrium between the conduction and d state occupations. In alloying elements of similar electronic structure, i.e. high d-like elements amongst themselves or low d-like elements amongst themselves we expect only smooth variations of macroscopic quantities such as the mean magnetic moment—although, as we shall see in § 5, we do not expect this variation to be of the same type in the two cases. But now let us examine the case of a high d element dissolved in a low d one, e.g. Ni in Fe. The conduction electrons cannot be localized very effectively in most metals, so that a nickel atom substituted into an iron lattice must find considerable 4c electron density overlapping onto it. The only reasonable recourse open to restore approximate electrical neutrality in the cell occupied by the nickel atom is for it to delocalize some of its d-like electrons, by promoting them into the conduction band of the alloy. Thus the high d elements may lose some d electrons when dissolved in low d elements.

The remaining case to consider is that of a low d element, say V, dissolved in a high d element, say Ni. The five 4c electrons of the vanadium may be regarded as added to the nickel conduction band. They therefore disturb the equilibrium between conduction and d-like levels, with consequent changes in magnetic properties. Friedel's description in terms of the V atom removing localized states from the conduction band is preferable to the more naïve concept of adding conduction electrons to the conduction band, and then allowing them to overspill into the high-density states provided by the d band. Whichever language we use, the essence of our suggestion is that V is five times as effective as Cu in increasing the occupation of d states in Ni.

Let us then summarize our hypotheses.

(1) The valence electrons may be divided into two classes—conduction electrons distributed over the metal, and d electrons concentrated near each atom.

(2) The magnetic properties are due essentially to the spin moment of d electrons only.

(3) The interactions between magnetic moments of near-neighbour atoms in a crystal are unknown even as to sign; minor component moments may be parallel or antiparallel to a ferromagnetic solvent moment.

(4) For some metals, the number of d electrons is an integer, while for others two different configurations may be in dynamic equilibrium with the conduction band (Mott and Stevens 1957).

(5) In alloys of whose components have roughly the same conduction electron density, each atom retains approximately the d electron configuration characteristic of the pure metal.

(6) In alloys where the conduction electron densities of the pure metals are very different, the number of d electrons on the minor component may change to decrease this difference. Mn and Fe in high-d solvents become high-d atoms ; Ni and Co in low d solvents lose one or two d electrons (starred columns in table 1).

(7) In alloys whose major component has equilibrium between conduction and d states, each addition of a conduction electron by alloying causes the occupation of one d state.

§ 4. THE PURE METALS

Cu. The electronic structure of metallic copper can scarcely be questioned. We concur with the usual assignment $(3d)^{10}$ $(4s)^1$.

Ni. The structure of nickel lies between $(3d)^{10}$ and $(3d)^9$ $(4s)^1$. The precise description adopted depends on the view we take of spatial correlations of d-like and conduction electrons. If all correlation is neglected we would arrive at the simplest form of ' collective electron ' treatment in terms of ordinary d and s bands. However, we prefer to believe that the number of $(3d)^8$ ions is very low—i.e. that two 3d holes are seldom found on the same atom. We therefore think of the d electrons in terms of the Van Vleck model, in which the proportions of $(3d)^{10}$ and $(3d)^9$ configurations are in dynamic equilibrium, and in which $(3d)^8$ configurations do not occur†. Above the Curie point the spin orientation of the $(3d)^9$ configurations shows no long range order, and so gives rise to diffuse spin disorder neutron scattering. For pure nickel the proportion of $(3d)^9$ is about 60% and $(3d)^{10}$ about 40% so that the mean spin moment per atom is $0{\cdot}6\,\mu_B$, as observed. It may be that in fact the proportion of $(3d)^9$ is somewhat lower than 60%, for there will be some contribution to the observed moment both from imperfectly quenched orbital magnetic moment, and from partial spin alignment of the conduction electrons.

We regard the 4s electrons (0·6 per atom) as uncorrelated with the d electron holes, and so use a simple band of conduction states.

Co. The discussion for cobalt is essentially similar ; the two configurations involved now are $(3d)^9$ and $(3d)^8$ (4s) carrying spin moments of one and two Bohr magnetons respectively. Neglecting orbital and conduction electron contributions to the saturation magnetization the value $\bar{\mu}=1\cdot7\,\mu_B$ for Co indicates 70% $(3d)^8$ and 30% $(3d)^9$.

---

† The actual proportion of $(3d)^8$ states in pure nickel is not known. It simplifies our discussion of saturation magnetization to suppose it is low. It is hoped to discuss the value of the Curie temperature using this supposition in a later paper. The general picture of the alloying behaviour of saturation moments is not, however, sensitive to the supposition.

Fe. The iron atom we believe may exist in two distinct states; a high-d state analogous to Ni and Co (occurring in some alloys), or in a low-d state. Body-centred cubic iron we think is the latter, being in the *pure* configuration $(3d)^2$ $(4c)^6$. There is no equilibrium between this and other states, and the d electrons do not contribute to the Fermi surface (Mott and Stevens 1957). The two aligned electron spins contribute an effective magnetic moment of $2\,\mu_B$. Measurements of the gyromagnetic ratio show that the orbital momentum contribution is about $0\cdot1\,\mu_B$. The remainder of the observed saturation moment, $2\cdot22\,\mu_B$/atom, may be contributed by conduction electron polarization. Griffith (1956) has suggested that the d orbitals concerned are the E_g orbitals which are split off from the rest by the crystalline field. This assignment will allow us to assume that the orbital magnetic moment is well quenched as is observed.

Mn. Manganese is probably similar to iron. The pure metal may contain both $(3d)^1$ $(4c)^6$ and $(3d)^2$ $(4c)^5$ configurations in dynamic equilibrium, and in some alloys Mn may take up configurations $(3d)^7$ or $(3d)^6$ 4s.

Cr. Chromium appears to be a mixture of $(3d)^1$ $(4c)^5$ and $(4c)^6$ configurations. The antiferromagnetic structure (Shull and Wilkinson 1953) is attributed to the spin of the former configuration.

V. Vanadium is probably pure $(4c)^5$ configurations, for Shull finds no magnetic scattering (Shull and Wilkinson 1953).

Ti. Titanium is probably pure $(4c)^4$ on the same reasoning.

§ 5. THE FERROMAGNETIC BINARY ALLOY SYSTEMS

In this section we apply the ideas of the preceding sections to the saturation magnetization curves of binary alloys, and to the moment carried on the atoms of each constituent; results of experiments are available for saturation moments of most systems, but only a few neutron diffraction results are available to apportion the total moment between constituents. For each dilute alloy we shall try to assign an electronic configuration to both matrix and solute. It is satisfactory that treating each alloy on its own merits in this empirical way leads to a consistent and plausible scheme of structures, summarized in table 1.

Ideally, we want the results for very dilute alloys, so that we may neglect interaction between solute atoms. These results are of course the most difficult to get. Only in exceptional cases, where a linear extrapolation of results at moderate concentration back to zero concentration is acceptable, can the variation of mean moment be given to better than $\pm0\cdot2\,\mu_B$ per solute atom. In systems with limited primary solubility ranges (notably **Fe** Mn, **Co** Fe, **Fe** Ni, **Co** Al) the uncertainty is considerably greater.

It is also true that it is not possible to assign an accurate magnetic moment to an atom of a given electronic structure; to a first approximation we may suppose that the 3d electrons always produce a state of maximum possible spin, and that this is the whole observed magnetic moment. But in fact terms of the order of 0·1 or 0·2 μ_B per atom may arise from incompletely quenched orbital motion and from spin polarization of the conduction band electrons. We cannot therefore expect perfect agreement with experiment; discrepancies of up to 0·2 or 0·3 μ_B between assignment and observation are not immediately relevant.

Table 1

	Ti	V	Cr	Mn	Mn*	Fe	Fe*
c	4	5	5 ↔ 6	5 ↔ 6	0	6	1 ↔ 0
d	0	0	1 ↔ 0	2 ↔ 1	7	2	7 ↔ 8
μ	0	0	1 ↔ 0	2 ↔ 1	3	2	3 ↔ 2

← low d elements →

	Co	Co*	Ni	Ni*	Cu	Zr
c	1 ↔ 0	3 ↔ 2	1 ↔ 0	3 ↔ 2	1	2
d	8 ↔ 9	6 ↔ 7	9 ↔ 10	7 ↔ 8	10	10
μ	2 ↔ 1	4 ↔ 3	1 ↔ 0	3 ↔ 2	0	0

← high d elements →

The number of conduction electrons *c*, number of d electrons *d*, and atomic magnetic moment μ for atoms of the first transition period. The starred columns refer to the behaviour of the element in solutes of the opposite type configuration. Where no starred column is given the behaviour is the same in both high and low-d solvents. Equilibrium between structures is indicated by horizontal arrows.

The Slater–Pauling curve of average saturation magnetic moment of the transition metal alloys provides an invaluable general background to our discussion. The curve is shown in fig. 1 which plots the known behaviour of many alloys against their effective electron configuration. The alloys of adjacent metals define the course of the main curve. Roughly speaking we see that alloys of low d elements with iron form branch A of the curve, while alloys of high d elements with other high d elements form branch B. The maximum of the curve, part C, is formed from alloys of iron with high d elements. Alloys of low d elements other than iron with the high d elements, cobalt and nickel, give the curves D showing very strong deviations from the main curves. We shall now discuss these four types of alloys A, B, C and D in turn. A summary of this discussion is given in table 2.

Table 2. Variation of saturation magnetic moment in Bohr magnetons per atom of Fe, Co, and Ni with alloy content

Solute / Solvent	Al	Si	Sc	Ti	V	Cr
Fe (*a*)	$(3c)^3$ −2·2	$(3c)^4$ −2·2	$(4c)^3$ −2·2	$(4c)^4$ −2·2	$(4c)^5$ −2·2	$-(3d)^1(4c)^5$ −3·2 $(4c)^6$ −2·2
(*b*)	−2·3	−2·2	—	—	−2·2	−2·9
Co (*a*)	$(3c)^3$ −4·0	$(3c)^4$ 5·0	$(4c)^3$ −4·0	$(4c)^4$ −5·0	$(4c)^5$ −6·0	$+(3d)^1(4c)^5$ −5·0 $(4c)^6$ −7·0
(*b*)	−2·4?	−5·3	—	—	—	−6·4
Ni (*a*)	$(3c)^3$ −3·0	$(3c)^4$ −4·0	$(4c)^3$ −3·0	$(4c)^4$ −4·0	$(4c)^5$ −5·0	$+(3d)^1(4c)^5$ −4·0 $(4c)^6$ −6·0
(*b*)	−3·0	−3·4 −4·3	—	−3·8	−5·2	−4·5

Table 2 (*cont.*)

Solute / Solvent	Mn	Fe	Co	Ni	Cu	Zn
Fe (*a*)	0 $\pm(3d)^2(4c)^5$ -4 $\pm(3d)^1(4c)^6$ -1 -3	$(3d)^2(4c)^6$	$(3d)^6(4c)^3$ $1{\cdot}8+\delta_6$ $(3d)^7(4c)^2$ $0{\cdot}8+\delta_7$ $(3d)^8(4c)^1$ $-0{\cdot}2$	$(3d)^7(4c)^3$ $0{\cdot}8+\delta_7$ $(3d)^8(4c)^2$ $-0{\cdot}2$	$(3d)^{10}4c$ $-2{\cdot}2$	$(3d)^{10}(4c)^2$ $-2{\cdot}2$
(*b*)	~−0·2?	2·22	1·2	0·6?	—	−2·0
Co (*a*)	$-(3d)^7$ $-4-\delta_7$	$(3d)^7 4c$ $1+\delta_7$ $(3d)^8$ 1	$(3d)^8 4c$ 2 $(3d)^9$ 1	$(3d)^9$ 4c −1 $(3d)^{10}$ −1	$(3d)^{10}4c$ −2	$(3d)^{10}4c^2$ −3·0
(*b*)	−4·5	+1·1	(f.c.c. 1·751) 1·715	−0·95	—	—
Ni (*a*)	$+(3d)^7$ +3	$(3d)^7 4c$ $2+\delta_7$ $(3d)^8$ 2	$(3d)^8 4c$ 1 $(3d)^9$ 1	$(3d)^9$ 4c 1 $(3d)^{10}$ 0	$(3d)^{10}4c$ −1	$(3d)^{10}(4c)^1$ −2·0
(*b*)	~+3	2·2	1·2	0·604	−1	−2·0

Row (*a*) indicates the suggested electronic configuration (the prefix ± indicating ferro- or antiferro-magnetic coupling) and the corresponding predicted change in moment per added atom. Where two configurations are in equilibrium both are indicated. The orbital contributions to $(d)^8$ and $(d)^9$ have been neglected; they are about 0·1 μ_B. Row (*b*) gives the observed values.

5.1. *Type A Alloys*

These are alloys of low-d elements, Al, Si, Ti, V, Cr and Mn with Fe, and should behave according to hypothesis (5), § 3. Because Fe is in a pure $(3d)^2(4c)^6$ configuration in which the magnetic electrons do not contribute to the Fermi surface, replacing an iron atom by any element does not affect the magnetic properties of the other iron atoms. The mean magnetic moment will decrease by $2{\cdot}2\,\mu_B$ for each magnetically inert atom added. Cr and Mn contribute their own 3d spin moments, either antiparallel or parallel to the iron 3d spins, giving correspondingly more or less rapid decreases of saturation moment. Let us consider the alloys one by one.

Fe Al. The initial slope of the moment-concentration curve is observed to be $-2{\cdot}3$ (Fallot 1936), in good agreement with the expected $-2{\cdot}2$. At 18% Al superlattice lines appear and the moment falls more rapidly.

Fe Si. The initial slope is $-2{\cdot}2$ (Fallot 1936). The moment falls more rapidly beyond 7% Si, where superlattice lines appear.

Fe Sc, **Fe** Ti, have not been studied ; we expect a slope of $-2{\cdot}2$.

Fe–V. Experimentally (Fallot 1936) the slope is observed to be $-2{\cdot}2$, as expected ; this holds up to 30% V at which there is a phase change.

Fe–Cr. Cr is a mixture of $(4c)^6$ and $(4c)^5(3d)^1$ configurations. When Cr is added to iron, if the proportion of $(4c)^5(3d)^1$ atoms is x, the mean moment will vary by $-2{\cdot}2-x$ if the Cr spin is antiparallel to the iron, or $-2{\cdot}2+x$ if the Cr spin is parallel to the iron spin. The experiments of Shull and Wilkinson (1955) show that the moment on Cr differs from that on Fe by $\pm 3\,\mu_B$ in these alloys. We accept the solution that the Cr moment is about $-1\,\mu_B$, i.e., antiparallel to the iron moment. (The second solution $\bar{\mu}_{Cr}=5$ would require five d-like electrons, which does not fit our general scheme. In addition it implies a rapid variation of the moment on iron atoms, which is not seen in other systems.) The initial rate of decrease of saturation moment estimated from Fallot's (1936) curves is $-2{\cdot}9$. This suggests the Cr atoms enter 70% as $(4c)^5(3d)^1$, and 30% as $(4c)^6$. This would not be inconsistent with extrapolation of Shull's results (see fig. 2 (*a*)).

At higher concentration of Cr, the experiments show the mean slope to be about $-2{\cdot}2$ (the value quoted by Stoner 1947). The change in slope may be due to an antiferromagnetic coupling between neighbouring chromium atoms. If this coupling is more important than that between chromium and iron atoms, we would suppose that by the time a concentration of about 40% Cr is reached the net moment on Cr atoms will be zero, so that the mean slope over a wide concentration range corresponds to dilution of the iron, as observed. Shull and Wilkinson, however, shows a small positive moment on Cr atoms at 45%. It would be interesting to have confirmation of this, and to know if, say at 60% Cr the moment is still larger, for we would expect it to remain essentially zero. At still larger concentrations of Cr the antiferromagnetic structure of pure Cr must develop, and dissolved iron will be unaligned, so the mean moment on iron atoms must fall in Cr-rich alloys, as observed.

Fig. 2

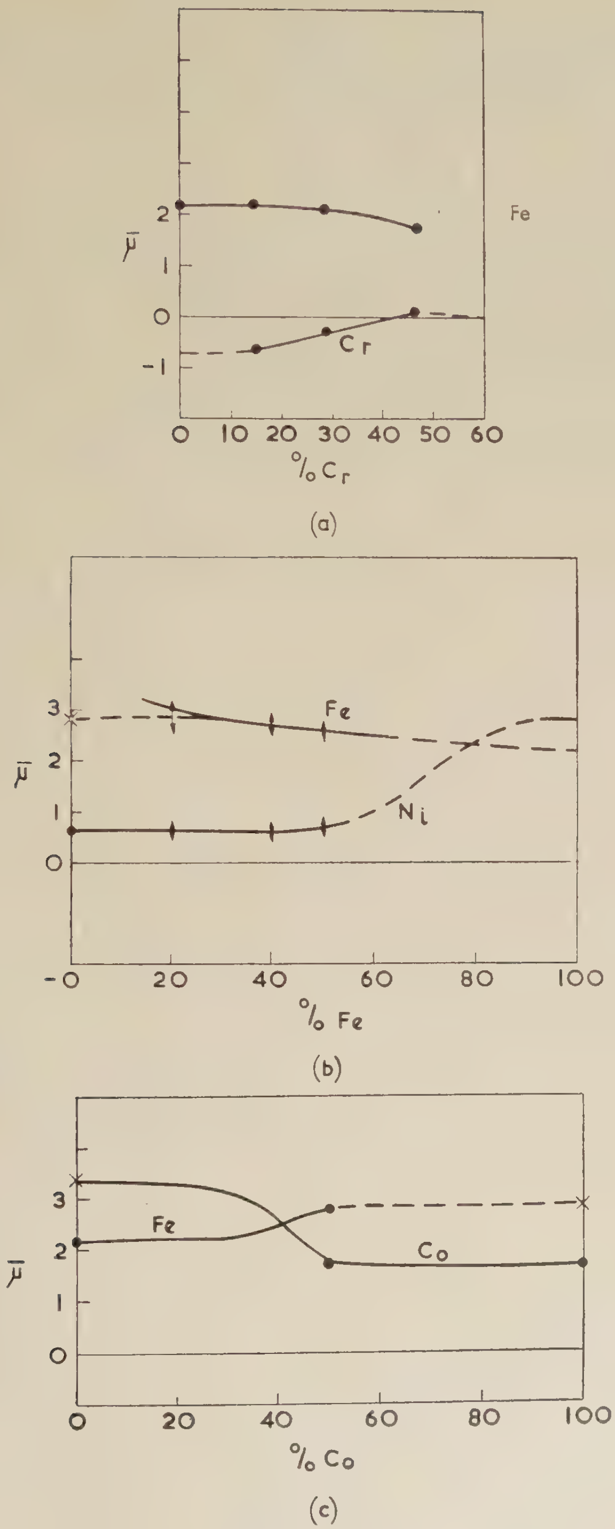

Atomic moments in alloys as observed by neutron diffraction.

• observed points. — — — predicted extrapolation.

(*a*) Fe–Cr system. (*b*) Ni–Fe system. (*c*) Fe–Co system.

Fe–Mn. Mn we expect to enter Fe as a mixture of $(3d)^1(4c)^6$ and $(3d)^2(4c)^5$ configurations. If the relative proportions are $(1-x)$ to x, the small concentration results would be

$$\mu_{\mathrm{Mn}}=\pm(1+x)$$
$$d\bar{\mu}/dc=-2{\cdot}2\pm(1+x).$$

Sadron's (1932) experimental results are completely at variance with this. He quotes $d\bar{\mu}/dc=-2{\cdot}0$ at zero concentration. However, the solubility of Mn is only 3·5 atm % in α-iron, so that it is difficult to obtain accurate enough results on solutions of accurately determined concentration. A new measurement for this system would be very welcome ; if Sadron's result is confirmed it will be difficult to fit smoothly into our scheme, though it is possible that Mn enters iron as $(4c)^7$. This would be surprising in view of the very well established result that magnetically active d electrons are present round Cr atoms dissolved in iron.

5.2. *Type B Alloys*

These are alloys of Ni and Co with other high d elements and hypothesis (5) is to be combined with hypothesis (7). The mean moment of Ni and Co atoms in these alloys is controlled by the equilibrium between the number of conduction electrons and the number of d holes. As indicated in § 2 the perturbation of the conduction band on adding alloying elements is equivalent to adding electrons to a rigid conduction band. But if these conduction states are in equilibrium with a set of d states with a high density of states, the net effect is the removal of a corresponding number of d-holes. This argument is independent of the use of conventional band or a Van Vleck description of the d-states, though they differ in their description of the distribution of spin moment in the alloys.

Ni–Cu. Cu enters as $(3d)^{10}$ 4c, that is, carrying 0·4 more conduction electron than pure Ni giving a corresponding decrease in total Ni moment of 0·4 μ_{B}. The inert $(3d)^{10}$ replaces the mean Ni configuration of moment 0·6 μ_{B}, and the total change is therefore -1 μ_{B} for each added copper atom, just as observed (Marian 1937). On this model $\bar{\mu}_{\mathrm{Cu}}=0$, $\bar{\mu}_{\mathrm{Ni}}=(0{\cdot}6-c)/(1-c)$; on the simplest band theory $\bar{\mu}_{\mathrm{Cu}}=\bar{\mu}_{\mathrm{Ni}}=(0{\cdot}6-c)$.

Ni–Zn. Zn will be twice as effective as Cu in reducing the moment and so $d\bar{\mu}/dc$ should be -2. Experimentally it is observed to be $-2{\cdot}1$ (Marian 1937).

Co–Cu. In this case the Cu replaces on average the configuration $(3d)^{8{\cdot}3}(4s)^{0{\cdot}7}$, i.e., a moment of 1·7 μ_{B} is lost on average, and a further 0·3 μ_{B} is lost from the localization of a further 0·3 conduction electrons around Cu. Hence $d\bar{\mu}/dc=-2{\cdot}0$. There are no experimental results to compare to the prediction.

Co–Zn. Here we expect $d\bar{\mu}/dc=-3{\cdot}0$ but no experimental results seem to be available.

Ni–Co. Both pure metals are ferromagnets with approximately the same number of conduction electrons per atom. We therefore expect an almost linear variation of the mean moment with Co concentration from the initial value of 0·604 to the final value 1·714. This is experimentally observed; there is a slight change of slope at the f.c.c. → h.c.p. phase change. (Weiss and Forrer 1929).

5.3. *Type C Alloys*

These are alloys of Co and Ni with low 3d elements and show the greatest deviation from the Slater–Pauling curve. It has been suggested that the very rapid fall in the mean moment with increasing concentration of the low 3d element is due to large moments coupled antiparallel to the cobalt or nickel moments. But Shull and Wilkinson's results on **Co**–Cr show that this is certainly not the case in this alloy but that the fall is due to the decrease in the mean Co moment on alloying. It therefore seems likely that in none of these alloys is there a large antiparallel moment on the low 3d element. A natural explanation is that the large number of conduction electrons which these elements have enter the conduction band of the metal, disturbing the equilibrium between the various 3d configurations in nickel or cobalt and so suppressing the mean moment rapidly, according to hypothesis (7).

Ni–Al. We expect $d\bar{\mu}/dc$ to be about $-3{\cdot}0$. Experimentally (Marian 1937) it is observed to be $-3{\cdot}0 \pm 0{\cdot}2$.

Ni–Si. Here we expect $d\bar{\mu}/dc$ to be $-4{\cdot}0$. Marian (1937) has found experimentally a value $-3{\cdot}4$.

Ni–Ti. We suppose that titanium enters in the configuration $(4c)^4$ so we expect about $d\bar{\mu}/dc = -4$. Experimentally the value is $-3{\cdot}8$ (Marian 1937).

Ni–V. Vanadium has the configuration $(4c)^5$ so we expect approximately $d\bar{\mu}/dc = -5$. Experimentally the value is $-5{\cdot}2$ (Marian 1937).

Ni–Cr. Cr enters Ni as a mixture of $3d^1(4c)^5$ and $(4c)^6$. Experimentally (Marian 1937) $d\bar{\mu}/dc = -4{\cdot}5$, which is fitted if the weights of these configurations are respectively 75% to 25%, with the spin on Cr atoms parallel to the Ni spins, giving $\bar{\mu}_{\mathrm{Cr}} = 0{\cdot}75$, $\bar{\mu}_{\mathrm{Ni}} = 0{\cdot}6 – 4{\cdot}65c$, $d\bar{\mu}/dc = -4{\cdot}5$.

Co–Al. Here we expect $d\bar{\mu}/dc$ to be about $-4{\cdot}0$. Experimentally Farcas (1937) has found a value of $-2{\cdot}4$. This is a difficult alloy to work with as only 1% of Al is soluble in Co at 300°c so this experimental result may be open to some doubt.

Co–Si. We expect a value for $d\bar{\mu}/dc$ about $-5{\cdot}0$. Experimentally Sadron (1932) observed about $-5{\cdot}3$.

Co–Ti. We expect a value of about $-5{\cdot}0$ but this alloy has not been examined experimentally yet.

Co–V. We expect a value of about $-6{\cdot}0$ but no experimental results are available.

Co–Cr. Cr enters Co as a mixture of $3d^1(4c)^5$ and $(4c)^6$; to fit the experimental results (Farcas 1937) the probability of $(3d)^1\,(4c)^5$ is 0·3 and of $(4c)^6$ is 0·7 to give, for small concentrations, $\bar{\mu}_{\mathrm{Cr}} = 0{\cdot}3$, $\bar{\mu}_{\mathrm{Co}} = 1{\cdot}7 – 5c$ and $d\bar{\mu}/dc = -6{\cdot}4$.

5.4. *Type D Alloys*

These are the alloys which form the maximum of the Slater–Pauling curve and the explanation of their properties rests on hypothesis (6). It is convenient to treat not only Fe–Co and Fe–Ni here, but to take all Fe and Mn alloys with high-d metals. There are two main ideas in this discussion. First, as described in § 3, high-d elements Ni and Co may be expected to lose one or two 3d electrons when they are dissolved in iron, in order to compensate the charge-overlap effect. The second assumption is that Fe and Mn are finely balanced between low-d and high-d so that when they dissolve in a high-d solvent the inverse of the previous effect causes them to gain not one or two d electrons, but to switch right over to a high-d configuration with less than one conduction electron.

An unsatisfactory feature of the discussion of these alloys stems from our inability to predict the extent of quenching of orbital moment. A static cubic crystalline field quenches the orbital moment of $(d)^9$ and $(d)^8$ configurations, and the observed gyromagnetic ratios for Ni and Co confirm the smallness of orbital contribution for these configurations. But such static fields do not quench the orbital moment in $(d)^6$ and $(d)^7$ configurations, and we have no direct experimental information on the matter. It seems doubtful that we should really expect a large orbital contribution ; as a working hypothesis, we suppose that the spin moment is the major contribution for these configurations also.

Fe–Co. Pure cobalt is a mixture of $(3d)^8$ and $(3d)^9$ configurations. The charge-overlap effect promotes some of these d electrons into the conduction band when Co is dissolved in iron ; it may enter iron as either a mixture of $(3d)^6$ and $(3d)^7$, or $(3d)^7$ and $(3d)^8$. It is impossible to decide between these on the basis of the experiment, because we do not know how well the orbital momentum is quenched in the $(d)^6$ and $(d)^7$ configurations. The spin moment of $(3d)^7$ alone would give $\mu_{\mathrm{Co}}=3$ and $d\bar{\mu}/dc=0{\cdot}8$. The experimental value (Weiss and Forrer 1929) of $d\bar{\mu}/dc$ is 1·2. If the orbital contribution of $(d)^7$ is greater than 0·4 there must be some admixture of $(d)^8$ configuration ; if it is less than 0·4 there is some admixture of $(d)^6$.

Now consider cobalt-rich alloys. We suppose that small concentrations of iron dissolve in a high-d state, some mixture of $(3d)^7$ and $(3d)^8$ or possibly $(3d)^6$ and $(3d)^7$. It is again impossible to assign weights to the mixture, for the orbital contributions are unknown. However, it is reasonable to say as this is now an alloy of type B, we expect **Co** Fe to form an extension of leg B of the Slater–Pauling curve. If the mixture of $(d)^7$ and $(d)^8$ is considered, with weight x and $1-x$ respectively, and moments $3+\delta_7$ and $2+\delta_8$ respectively, we get

$$\mu_{\mathrm{Co}}=1{\cdot}7+c(0{\cdot}7-x)$$

$$\bar{\mu}_{\mathrm{Fe}}=2+\delta_8+x(1+\delta_7-\delta_8)$$

$$d\bar{\mu}/dc=1+\delta_8+x(\delta_7-\delta_8).$$

Here c is the concentration of Fe atoms and the formulae are correct only to first order in c. Experimentally $d\bar{\mu}/dc$ is observed to be 1·1 so we can get agreement even with small values of δ_7. (The observation is extremely uncertain in the hexagonal cobalt phase—the slope quoted is for f.c.c. phase (Weiss and Forrer 1929).

Because we suppose that in iron rich alloys Fe behaves as a low-3d element but in cobalt rich alloys Fe behaves as a high-3d element it is clear that at some composition range a change over from one type to the other must occur. One possibility is that the change over occurs at the transition between the body-centred and face-centred cubic phases, i.e. at a concentration of about 75% Co. However, we believe it to be more probable that the change over occurs at the maximum of the moment concentration curve, i.e. at about 40% Co, as indicated in fig. 2 (*c*). (Shull and Wilkinson has found that in ordered Fe–Co the Fe moment is $2\cdot8\,\mu_B$. If at this concentration iron were still behaving as a low 3d element and only the Eg orbitals are available then the maximum value for μ_{Fe} would be about 2·2.)

Fe–Ni. The discussion of this alloy is similar to that of Fe–Co. Pure nickel is a mixture of the configurations $(3d)^9$ and $(3d)^{10}$. Because of the change overlap effect in iron rich alloys it will have less 3d electrons and we suppose therefore that it goes in as a mixture of the configurations $(3d)^7$ and $(3d)^8$. If the probability of the former configuration is x and of the latter $(1-x)$ then

$$\bar{\mu}_{Ni}=2+\delta_8+x(1+\delta_7-\delta_8)$$

$$\bar{\mu}_{Fe}=2\cdot2$$

$$d\bar{\mu}/dc=-0\cdot2+\delta_8+x(1+\delta_7-\delta_8).$$

The experimentally observed value of $d\bar{\mu}/dc$ is 0·6 so assuming $\delta_8\sim0\cdot2$ we get $x\sim0\cdot6/0\cdot8+\delta_7$).

For the nickel rich alloys we suppose that iron goes in as a mixture of $(3d)^7$ with probability y, and $(3d)^8$ with probability $(1-y)$. Then

$$\bar{\mu}_{Fe}=2+\delta_8\times y(1+\delta_7-\delta_8)$$

$$\bar{\mu}_{Ni}=0\cdot6+c(0\cdot6-y)$$

$$d\bar{\mu}/dc=2+\delta_8+y(\delta_7-\delta_8).$$

Shull and Wilkinson (1955) results on **Ni**–Fe show that $\bar{\mu}_{Ni}$ is roughly constant so we can set $y\simeq0\cdot6$. Experiments indicate that at zero concentration $\bar{\mu}_{Fe}\simeq3\cdot0$, and $d\bar{\mu}/dc$ is about 2·3 (Peschard 1925).

Neutron diffraction work on iron rich Fe–Ni alloys would provide a clear test of the ideas we have just described. Shull and Wilkinson's experiments have been confined to alloys with less than 50% iron and his results are reproduced in fig. 2 (*b*). The curves we would expect on these ideas have been roughly sketched in also. We expect $\bar{\mu}_{Ni}$ to fall rapidly over the region of concentration where iron changes over from low 3d behaviour to high 3d behaviour. It is difficult to know in this case whether the change over should be associated with the phase transition or the maximum in the magnetic moment curve as these occur at only slightly different concentrations. The sluggish phase transformations would make the experiment a difficult one.

Fe–Cu. This alloy we have included in this section because it is an alloy between Fe and a high 3d element. If the Cu 3d shell remains full, Cu will merely dilute Fe, like a Type A alloy. Unfortunately copper has such a low solubility in iron that it seems unlikely that any experimental results will be obtained on this alloy. Gold, however, does act as a simple diluent (Fallot 1936).

Fe–Zn. Similarly we expect Zn merely to dilute Fe, i.e. $d\bar{\mu}/dc = -2{\cdot}2$. Experimentally the value observed is $-2{\cdot}0$ (Fallot 1936).

Ni–Mn. Manganese is similar to Fe so that for small Mn concentrations we expect Mn to have a high-3d character. Ordered Ni_3 Mn is known to have a mean moment per atom of 1·015 (Kaya and Nakayama 1940) and Shull and Wilkinson (1955) has determined that either

$$\bar{\mu}_{Mn}=+3{\cdot}18(\pm 0{\cdot}25) \text{ and } \bar{\mu}_{Ni}=+0{\cdot}30(\pm 0{\cdot}05)$$

or

$$\bar{\mu}_{Mn}=-1{\cdot}15(\pm 0{\cdot}25) \text{ and } \bar{\mu}_{Ni}=1{\cdot}73(\pm 0{\cdot}05).$$

The first set of results seem the more plausible ones. From these results Mn goes into Ni in nearly the pure configuration $(3d)^7$ with a moment of about $3\,\mu_B$.

The moment of the disordered alloy at room temperature initially rises with the addition of Mn but then passes through a maximum and falls rapidly to zero at about 25% Mn. This fall is probably partly due to the very rapid fall in the Curie temperature with Mn concentration which makes it very difficult to extrapolate to zero temperature to obtain the mean moment per atom at saturation. It seems natural to suppose that Mn enters the disordered alloy just as it enters the ordered alloy, as $(3d)^7$, giving an initial value of $+3{\cdot}0$ for $d\bar{\mu}/dc$ consistently with Sadron's result. At higher concentrations the probability of Mn–Mn nearest neighbours increases and the Mn–Mn coupling is probably antiferromagnetic. This causes the mean moment and the Curie temperature to drop rapidly until both are zero at about a concentration of about 25%. In the ordered Ni_3Mn alloy there are no nearest neighbour Mn–Mn pairs so the ordered alloy is ferromagnetic. An increase in Mn content quickly reduces the moment to zero at about 40% Mn.

Co–Mn. Mn enters Co as it enters Ni, in the $(3d)^7$ configuration, but this time antiparallel to the Co moments to give a value of $d\bar{\mu}/dc$ equal to about 4·0. Crangle (1957) has found experimentally a value of $-4{\cdot}5$. In view of the theoretical uncertainty connected with the orbital contribution in the $(3d)^7$ configuration we do not think the difference between these results is significant. Crangle also reports a value of $-2{\cdot}0$ for Mn in face-centred cubic cobalt, but this result is derived from a long temperature extrapolation. The reliability of such extrapolation in a system where Brockhouse (1957) has reported complicated antiferromagnetic coupling at low temperature is questionable.

An alternative explanation of the result $d\bar{\mu}/dc = -4{\cdot}5$ in terms of Mn as a low-d solute, analogous to that for **Co**-Cr, would give $\mu_{\mathrm{Mn}} = 1{\cdot}75$, $\mu_{\mathrm{Co}} = 1{\cdot}7 - 4{\cdot}5c$ with Mn in the mean configuration $(3d)^{1{\cdot}75}(4c)^{5{\cdot}25}$. Neutron diffraction would readily distinguish between the suggested explanations.

§ 5. CONCLUSION AND DISCUSSION

It is suggested in this paper that the electron distribution round atoms in a metal is very different from that in a free atom of the same element. In particular we have traced some of the consequences of extrapolating Weiss's results on the number of d electrons in various pure metals. In conformity with his work the elements to the left of iron have been denoted as 'low-d'; those to the right as 'high-d' configurations. The dilute binary alloy systems may be correspondingly grouped into four sets; low-d with low-d, and high-d with high-d, low-d in high-d, and high-d in low-d. The behaviour of the first two sets is simple, each atom retaining its own configuration in the alloy; in the high-d matrix some low-d elements retain their own configuration but Fe and Mn (which are near the dividing line between high-d and low-d) changeover to a high-d configuration. High-d atoms near the dividing line (Ni and Co) in a low-d matrix lose one or two d electrons, the others (Cu and Zn) retain their usual configuration.

To these inferences about the electronic structure of the alloys we have added certain assumptions concerning the magnetic moment in ferromagnetic alloys. These are that the magnetic moment is almost entirely the spin moment of electrons in 3d orbitals; that in iron the 3d electrons are not in equilibrium with the conduction electrons, but that in Co and Ni there is such an equilibrium. This equilibrium in Ni and Co exhibits itself as a suppression of d electron spin moments as conduction electrons are added to the system. Conduction electron density changes do not influence the moment in iron. In Fe, Co and Ni any d electron spins carried by the solute atoms may contribute either ferromagnetically or antiferromagnetically to the total moment.

With these assumptions it has proved possible to get quantitative agreement with experiment for all the neutron diffraction experiments which have been carried out on ferromagnetic alloys, as well as with the 22 of the 24 observed values of dependence of saturation magnetization of ferromagnetic alloys. The two outstanding discrepancies are **Fe**–Mn and **Co** Al; both systems have maximum primary solubility ranges of less than 5%.

A limited degree of success can be reported for alloys involving metals from the later periods; the alloys with the Pt group of metals do not readily fit into the scheme; most other available results do.

The most controversial suggestions are that there is little occupation of d states until we reach Cr, and that there is a major break in electronic structure after iron. This is quite different from the type of model in which a d-band of roughly constant band form is filled steadily from Ti to Cu. We make no theoretical apology for this assignment of structures, though it is clearly necessary to establish by calculation whether our opinion is in fact reasonable. A less extreme suggestion, but still a little surprising, is that the electronic structure is not appreciably affected by crystal structure. It seems to us that the nuclear charge is the main determining variable which, together with boundary conditions appropriate to a metal, fixes the electron distribution round any atom. The arrangement, and to some extent, the chemical nature of its neighbours are of secondary importance. The crystal structure is chosen to be most appropriate to the electronic structure, rather than *vice versa.* The small effect of the chemical nature of the solvent is probably a consequence of the rather small range of electronegativity of Fe, Co, and Ni. It will not be surprising if extension to other solvents requires somewhat greater variability in the structure of solute atoms. As an extreme example of this, there can be no doubt that chromous and chromic, ferrous and ferric ions in paramagnetic salts retain only d electrons.

In adopting this model of the transition elements we lose some of the attractive features of the older d-band scheme. The high resistivity of Co and Ni compared with copper is still retained, and their high electronic specific heats are still given essentially the same explanation in terms of a high density of states in the d-band. But both resistivity and electronic specific heat are high in Fe, where we suppose no d-like high-density of states region of Fermi surface (see Mott and Stevens 1957). Equally the wide variation in these quantities from Ti and V to Cr is puzzling—as it was on the band theory. However, resistivity estimates for polyvalent metals are very difficult, and Jones (1957) has pointed out ambiguities in the interpretation of the linear specific heat term. Detailed work is necessary to establish whether or not any of these difficulties will prove unsurmountable.

It should be pointed out that one serious objection to this model is concerned with the g-value of iron. Experimentally it is known that the spectroscopic splitting factor g is greater than two, i.e. the magneto-mechanical ratio is less than two. The small orbital momentum is aligned parallel to the spin. On our model the d-shell is less than half full and might be expected to lead to the opposite result. However, the d-shell does not now exist in isolation. The conduction electrons undoubtedly carry some spin and some orbital momentum. Lack of detailed knowledge of the conduction band precludes detailed discussion of the interactions between it and the d-shell, which may invalidate the naïve conclusion.

Clearly, a great mass of information on transition metals and their alloys could profitably be re-examined in the light of these proposals. In addition, confirmation and extension of the Weiss ' d electron count ' experiments would be welcome. The Fe Co system should be of particular interest: according to Weiss's scheme, the mean number of d electrons per atom should increase from 2 to 8 or 9 between pure Fe and pure Co, and in our view, this should occur precipitously between 15% and 35% Co. Another type of experiment would concern the introduction of strong disorder scattering of x-rays from the widely different numbers of d electrons on the atoms. For example in **Fe** Co we suggest a difference of five d electrons, a very considerable difference in scattering power. Since the conduction electrons will also be localized to some extent to compensate these large differences, the effect must be looked for at large scattering angles where the form factors for d and s electrons are very different.

Any form of test of these ideas must be welcomed, for though the suggested electronic structures seem at first sight quite unacceptable, Weiss's results and the high degree of success of the present interpretation of magnetic properties are difficult to ignore.

ACKNOWLEDGMENTS

It is a pleasure to acknowledge the stimulus given to this work by a discussion held at Cambridge in June 1957, and in particular the interest taken in its development by Dr. R. J. Weiss and Professor N. F. Mott.

REFERENCES

BOZORTH, R. M., 1951, *Ferromagnetism* (New York: Van Nostrand).
BROCKHOUSE, B. N., 1957, *Atomic Energy of Canada Ltd., Chalk River Prog. Rep.* PR–P–33, p. 52.
CRANGLE, J., 1957, *Phil. Mag.*, **2,** 659.
ELLIOTT, R. J., and MARSHALL, W., 1957, *Rev. mod. Phys.*, to be published.
FALLOT, M., 1936, *Ann. de Phys.*, **6,** 304.
FARCAS, T., 1937, *Ann. de Phys.*, **8,** 146.
FRIEDEL, J., 1954, *Advanc. Phys.*, **3,** 447.
GRIFFITH, J. S., 1956, *J. Inorg. Nucl. Chem.*, **3,** 15.
HUME-ROTHERY, W., MABBOTT, G. W., and CHANNEL-EVANS, M. K., 1934, *Phil. Trans. roy. Soc.*, A, **233,** 1.
HUME-ROTHERY, W., and COLES, B. R., 1954, *Advanc. Phys.*, **3,** 149.
JONES, H., 1934, *Proc. roy. Soc.* A, **144,** 255; 1957, *Ibid.*, **240**, 321.
KAYA, S., and NAKAYAMA, M., 1940, *Proc. phys. Math. Soc.* Japan, **22,** 140.
LOWDE, R. D., 1956, *Proc. roy. Soc.* A, **235,** 305.
MARIAN, V., 1937, *Ann. de Phys.*, **7,** 459.
MOTT, N. F., and STEVENS, K. W., 1957, *Phil. Mag.*, **2,** 1364.
PESCHARD, 1925, *C.R. Acad. Sci.*, **180,** 1837.
SADRON, C., 1932, *Ann. de Phys.*, **17,** 371.
SHULL, C. G., and WILKINSON, M. K., 1953, *Rev. mod. Phys.*, **25,** 100; 1955, *Phys. Rev.*, **97,** 304.
STONER, E. C., 1947, *Rep. Prog. Phys.*, **11,** 43.
VAN VLECK, J. H., 1953, *Rev. mod. Phys.*, **25,** 220.
WEISS, R. J., 1957, *Rev. mod. Phys.*, to be published.
WEISS, P., and FORRER, R., 1929, *Ann. de Phys.*, **12,** 371.
WILKINSON, M. K., and SHULL, C. G., 1956, *Phys. Rev.*, **103,** 516.

CORRESPONDENCE

Parity Conservation in Strong Interactions: The ^{7}Be(n, α)^{4}He Reaction[†]

By R. E. Segel[‡]
Aeronautical Research Laboratory, WADC

J. V. Kane
Brookhaven National Laboratory, Upton, N.Y., U.S.A.

and D. H. Wilkinson[§]
Brookhaven National Laboratory, Upton, N.Y., U.S.A.
and Clarendon Laboratory, Oxford

[Received January 4, 1958]

The abundant evidence for the lack of conservation of parity in weak interactions leads us to ask whether parity is conserved in strong interactions.

The spin of the ^{7}Be nucleus is $\frac{3}{2}$ and the parity odd (Ajzenberg and Lauritsen 1955). Since the centrifugal barrier inhibits thermal neutron interactions with orbital angular momentum greater than zero, the parity of the initial system formed by the absorption of a thermal neutron must be odd. The symmetry and parity operators are identical for identical, spinless particles and so a ^{8}Be state of odd parity cannot break up into two alpha-particles if parity is conserved. The Q-value of the ^{7}Be(n, α)^{4}He reaction is (from the known masses) 18·98 MeV (Ajzenberg and Lauritsen 1955); the disintegration of ^{7}Be by slow neutrons into two 9·5 MeV alpha particles would, therefore, indicate a violation of parity conservation: we have sought it.

A thin ^{7}Be target was made by evaporating down a solution of ^{7}Be in HCl. The target was mounted in the dividing wall of a xenon gas scintillation chamber each half of which was viewed by an RCA 6342 photo-multiplier tube. A 0·02 mil nickel foil served as a light shield between the two halves of the chamber. The chamber contained two retractable ^{231}Pa sources for calibration†. During the run the chamber was calibrated about once every two hours. Drifts were less than 2% per hour.

[†] Work performed under the auspices of the United States Atomic Energy Commission.

[‡] Guest scientist at Brookhaven National Laboratory.

[§] The work was begun while this author was Visiting Physicist at Brookhaven National Laboratory during the summer of 1957.

The chamber was placed with the target above the beam hole at the medical facility of the BNL research reactor. The outputs of the phototubes were amplified and fed into a fast–slow coincidence circuit with the slow channels biased to accept all pulses above 5 Mev. The coincidence circuit output gated a 100 channel analyser, and also a two dimensional display (*X–Y–Z* analyser) (Grodzins 1955). Pictures on the *X–Y–Z* analyser were taken for 15-minute periods.

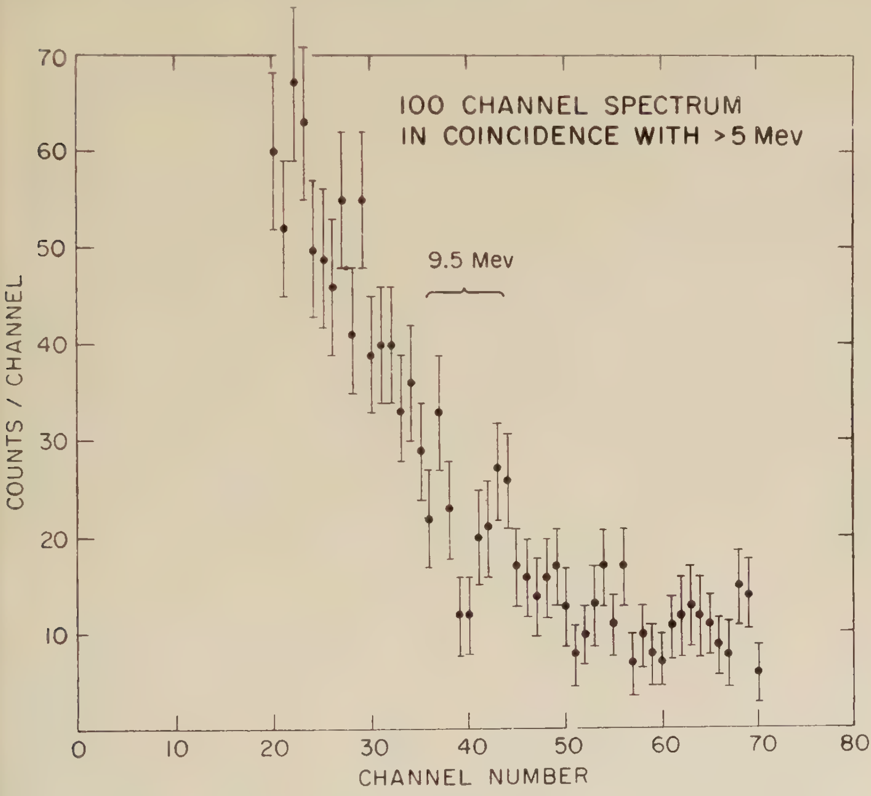

Spectrum observed on 100 channel analyser on one side of xenon gas scintillation chamber in coincidence with all pulses greater than 5 Mev on the other side. Bracket centres on the channel number corresponding to 9·5 Mev alpha particles.

The spectrum as observed on the 100 channel analyser is shown in the figure; the bracket centres on 9·5 Mev. An upper limit of about 100 events leading to a 9·5 Mev alpha group can be set from these data. The large number of big pulses may be due to fission from an as yet undiscovered source.

---

† The authors are indebted to Dr. Elizabeth Baker and Mr. Anthony Fasano for making the target, and to Dr. Brian Pate for preparing the ^{231}Pa sources.

The coordinates of all the events recorded by the X–Y–Z analyser were read and the results are partially summarized in the table.

An upper limit of about 30 9·5–9·5 MeV alpha–alpha coincidence events can be set from these data. From the measured flux (5×10^7 neutrons cm^2/sec), ^{7}Be target strength (4 millicuries or 10^{15} atoms) and running time (7 hours) a corresponding upper limit of 25 millibarns can be set for the (n, α) cross section.

The disintegration of ^{7}Be by slow neutrons has been previously investigated by Hanna (1955) who measured a cross section of 5×10^4 barns for the (n, p) reaction and who gives an upper limit of one barn for the (n, α) cross section.

Total Number of Events Observed in Various Energy Intervals

Energy (MeV)	$Y=5{\cdot}0$–$6{\cdot}8$	6·8–8·6	8·6–10·4	10·4–12·2
$X=6{\cdot}5$–$11{\cdot}5$	85	77	43	33

Following the notation of Lee and Yang (1956), the relative amplitude of the parity non-conserving component of the wave function is designated as $\mathfrak{F}$. A reaction which violates a parity selection rule will have a relative intensity $\mathfrak{F}^2$. So here $\mathfrak{F}^2 \sim \gamma_\alpha^2\,\gamma_p^2$ where the γ^2's represent the reduced widths for the respective reactions. (We are in a region of strongly-overlapping resonances.) The observed width Γ is related to the reduced width by: $\Gamma = 2kP\gamma^2$ where k=wave number, and P=penetration factor which, in both our cases, can be approximated by unity. We therefore find, neglecting fine points:

$$\mathfrak{F}^2 \sim \frac{\Gamma_\alpha}{\Gamma_p} \cdot \frac{k_p}{k_\alpha} \lesssim 1\times10^{-7}.$$

Tanner (1957) puts an upper limit on $\mathfrak{F}^2$ of $\sim 4\times10^{-8}$ by failing to observe a resonant yield in the ground state α group at the 340 kev $J=1+$resonance in the ^{19}F(p, α)^{16}O reaction. Wilkinson (1958) finds an upper limit to $\mathfrak{F}^2$ of $\sim 1\times10^{-7}$ in the ^{4}He(d, γ)^{6}Li reaction, $\mathfrak{F}^2 \lesssim 1\times10^{-7}$ and $\mathfrak{F}^2 \lesssim 3\times10^{-8}$ in the ^{11}B(p, p$'$)^{11*}B and ^{19}F(p, α)^{16*}O reactions respectively. Combining all the results to date, an upper limit of $\mathfrak{F}^2 \lesssim 1\times10^{-7}$ can be set for strong interactions.

We may finally note that our result is not sensitive to whether or not the parity non-conserving forces conserve isotopic spin. This was not true of the earlier ^{19}F(p, α)^{16}O or ^{4}He(d, γ)^{6}Li investigations into parity selection rules.

ACKNOWLEDGMENTS

Grateful acknowledgment is made to the Brookhaven Medical Physics Group for their assistance in the use of the medical facility, and to Dr. Robert Schamberger for several helpful discussions,

REFERENCES

AJZENBERG, F., and LAURITSEN, T., 1955, *Rev. mod. Phys.*, **27,** 77.
GRODZINS, L., 1955, *Rev. sci. Instrum.*, **26,** 1208.
HANNA, R. C., 1955, *Phil. Mag.*, **46,** 381.
LEE, T. D., and YANG, C. N., 1956, *Phys. Rev.*, **104,** 254.
TANNER, N., 1957, *Phys. Rev.*, **107,** 1203.
WILKINSON, D. H., 1958, *Phys. Rev.* (in the press).

On the Fermi Surface of Copper

By F. GARCIA MOLINER
Cavendish Laboratory, Cambridge

[Received August 9, 1957]

PIPPARD (1957) has recently given, on the basis of experimental measurements, a description of the Fermi surface of copper.

It is interesting that these results can be fitted to 1% accuracy with a simple analytical function. The energy E as a function of the components of the electron wave-vector $\mathbf{k}$ must satisfy the correct boundary and symmetry conditions. A Fourier analysis gives terms which are equivalent to taking succesive orders of nearest neighbours in the 'tight-binding' model, as in the interpolation scheme of Slater and Koster (1954).

For a face-centred cubic crystal of lattice constant a, the first two terms must be of the form :

$$E_{\mathbf{k}}=\alpha[(-3+\cos \tfrac{1}{2}ak_1 \cos \tfrac{1}{2}ak_2+\cos \tfrac{1}{2}ak_2 \cos \tfrac{1}{2}ak_3+\cos \tfrac{1}{2}ak_3 \cos \tfrac{1}{2}ak_1) \\ +r(-3+\cos ak_1+\cos ak_2+\cos ak_3)].$$

The shape of the surface E=const. (E_F) is determined by the values of the parameters. We choose $r=0{\cdot}0995$ and $E/\alpha=3{\cdot}6301$, so that the radius vector in the (001) direction is given exactly and the experimental shape of the surface is fitted as closely as possible. This was verified by directly checking 34 experimental points distributed in such a way that, owing to the cubic symmetry, this amounts to studying 162 points in one octant. The maximum error is found to occur at the (110) direction and amounts to 1% of the experimental radius vector. The accuracy improves in going away from this point and the fit is practically perfect over a great deal of the solid angle, in particular in the contact around the (111) direction.

ACKNOWLEDGMENT

I am indebted to Dr. A. B. Pippard, F.R.S., for making his data available and for his interest in this work.

REFERENCES

PIPPARD, A. B., 1957, *Phil. Trans. roy. Soc.*, A, **250,** 325.
SLATER, J. C., and KOSTER, G. F., 1954, *Phys. Rev.*, **94,** 1498.

Electromagnetic Stirring in Zone Refining

By I. Braun†, F. C. Frank, S. Marshall and G. Meyrick
University of Bristol, H. H. Wills Physics Laboratory

[Received November 4, 1957]

The efficiency of the zone refining process can obviously be increased by stirring the molten zone to disperse the impurity rich layer at the solid–liquid interface. Induction heating is sometimes preferred to radiant heat because it produces more convection ; but no marked improvement has been reported. Recently Pfann and Dorsi (1957) have described a method of stirring the melt by passing an electric current through the ingot and impressing a magnetic field across the molten zone. The purpose of this letter is to describe the preliminary results obtained using a rotating magnetic field as the stirring agent, during the purification of aluminium.

The metal, in the form of a rod $\frac{3}{8}$ in. in diameter, 44 cm long and 99·99% pure, was melted in an alumina boat lined with fused alumina powder (which prevented the aluminium sticking to the boat). This, supported inside a transparent quartz tube carried by a trolley, was drawn through a resistance furnace. Round the furnace were mounted three water-cooled copper wire coils at angles of 120° to one another. These were fed with 50 cycle three-phase a.c. adjusted so that each gave approximately the same magnetic field at peak voltage. The resultant rotating field, of roughly 100 oersteds, was sufficient to produce visible stirring in mercury and to spin a large ball bearing. The axis of rotation was perpendicular to the rod axis so that the boundary layer was dispersed by the primary circulation induced in the melt.

During operation the length of the molten zone was maintained roughly constant by varying the power input to the furnace, according to a calibration previously made on a stationary ingot.

In order to test the effect of the stirring, the recrystallization properties of a rod refined with stirring were compared with those of an unstirred ingot. Each rod was given eight horizontal passes in air, at a speed of 2·2 cm per hour ; the aluminium being cleaned in aqua regia initially and after the 3rd, 6th and final passes. In this procedure the impurity rich ends were not cropped. The rods were then cut into a number of pieces, each of which was cold rolled 85%, with intermediate quenching in cold water, and etched in Lacombe's reagent at room temperature. As the specimens were single crystals initially, it was not necessary to polish the surfaces before etching ; but the progress of recrystallization could be detected by treating the material in the rolled condition.

---

† Now at Institute of Technology, Haifa, Israel.

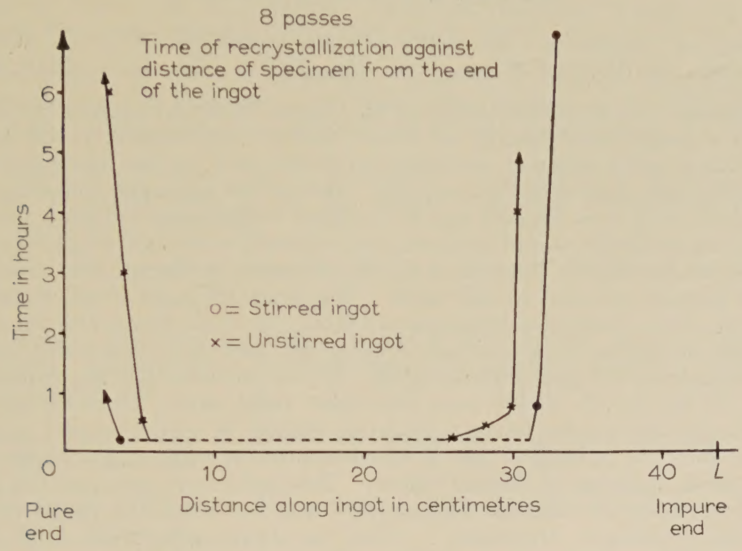

In the figure presented the time taken for complete recrystallization is plotted against the distance of the corresponding specimen from the end of the ingot. For the central portions of both ingots recrystallization was complete beween rolling and first etching (several minutes), but the curves for the ends show a significant increase in the efficiency of segregation of the impurities as a result of stirring.

REFERENCE

PFANN, W. G., and DORSI, D., 1957, *Rev. sci. Instrum.*, **28,** 720.

REVIEWS OF BOOKS

A History of Mechanics. By René Dugas, translated by J. R. Maddox. (London: Routledge & Kegan Paul, Ltd., 1957.) [Pp. 671.] £5 0*s*. 0*d*.

The original French edition (1950) of M. Dugas' book has already established itself as a classic in the history of science, and the publication of this English translation is most welcome, especially as recent work on the history of mechanics is too little known in this country. Before this appeared, the only treatment of the subject in English was Ernst Mach's celebrated volume ; excellent as this is scientifically, and of undiminished interest for its author's philosophical attitude, Mach's history has long been out of date. M. Dugas, it is true, is not entirely beyond criticism on this score. The first 100 pages or so of this book are based on the researches of the great scholar-physicist Pierre Duhem ; but a great deal of further work has been done in the last forty years and Duhem's conclusions have not gone unchallenged. It is a pity also that the illuminating studies of M. Koyré (1939) were not more fully used. Nevertheless, it is extremely gratifying to have a coherent survey of statistics and dynamics down to the time of Galileo that is representative of modern knowledge : this has not been available in English before. This early story occupies 128 pages ; 330 are devoted to classical mechanics ; and the final 178 pages to 'The Principles of Modern Dynamics'. Thus, as seems appropriate, the greater emphasis of this *History* is on the classical theories, but the twentieth century is also treated in considerable detail. Though some continuity in tracing the development of concepts or techniques is lost in a biographical arrangement, M. Dugas' exposition is always clear, and well supported by quotation from the originals. The translation is in general adequate ; the rendering of some proper names (Cues for Cusa ; Erasme for Erasmus ; Huyghens, an erroneous spelling), and the capitalization is not in accord with normal English usage. Apart from a rather unnecessary frequency of misprints the Swiss printers have produced an agreeable volume. It is one which everyone with an interest in the history of science will wish to read, and consult ; and which may well prove to have more than occasional value in the teaching of mechanics.

A. R. H.

BOOK NOTICES

Glass. By G. O. Jones. (London: Methuen & Co. Ltd.; New York: John Wiley & Sons, Inc.) [Pp. vi+119.] Price 8*s*. 6*d*.

Physik im Wandel Meiner Zeit. By Max Born. (Braunschweig: Friedr. Vieweg & Sohn.) [Pp. vii+252.] Price 19.80 DM.

Quantum Mechanics. By P. Mandl. 2nd Edition. (London: Butterworths Scientific Publications.) [Pp. x+267.] Price 35*s*.

Excited States in Chemistry and Biology. By C. Reid. (London: Butterworths Scientific Publications.) [Pp. ix+215.] Price 45*s*.

Electromagnetism and Relativity. By E. G. Cullwick. (London: Longmans, Green & Co. Ltd.) [Pp. xxiii+299.] Price 63*s*.

An Introduction to Probability Theory and its Applications. Volume 1. (2nd Edition.) By W. FELLER. (London : Chapman & Hall.) [Pp. xv+461.] Price 86*s*.

Concepts of Force. By M. JAMMER. (Harvard University Press.) (London : Oxford University Press.) [Pp. viii+269.] Price 45*s*.

The Conservation of Natural Resources. A series of lectures delivered at the Institution of Civil Engineers. (London : The Institution of Civil Engineers.) [Pp. 149.] Price 7*s*. 6*d*. to members and 17*s*. 6*d*. to the public.

Light, Colour and Vision. By Y. LE GRAND. Translated by R. W. G. Hunt, J. W. T. Walsh and F. R. W. Hunt. (London : Chapman & Hall.) [Pp. xiii+512.] Price 63*s*.

Probability and Scientific Inference. By G. S. BROWN. (London : Longmans, Green & Co. Ltd.) [Pp. viii+154.] Price 15*s*.

H. A Lorentz. Impressions of his Life and Work. Edited by G. L. DE HAAS-LORENTZ. (Amsterdam : North-Holland Publishing Company.) [Pp. 172.] Price 10 guilders.

Statistical Theory. By L. HOGBEN. (London : George Allen & Unwin.) [Pp. 510.] Price 45*s*.

Physical Optics. By R. A. HOUSTOUN. (Glasgow : Blackie & Son Limited.) [Pp. 300.] Price 40*s*.

Mathematical Analysis. By T. M. APOSTOL. (Reading, Massachusetts : Addison-Wesley Publishing Co. Inc. ; London : Academic Books Ltd.) [Pp. xii+553.] Price unstated.

Probability, Statistics and Truth. By R. VON MISES. 2nd Revised English Edition prepared by H. Geiringer. (London : George Allen & Unwin.) [Pp. ix+244.] Price 28*s*.

Observation and Interpretation. Proceedings of the Ninth Symposium of the Colston Research Society held in the University of Bristol, April 1st–April 4th) 1957. Edited by S. KORNER in collaboration with M. H. L. PRYCE. (London : Butterworths Scientific Publications.) [Pp. xiv+218.] Price 40*s*.

The Molecular Theory of Solutions. By I. PRIGOGINE. With the collaboration of A. Bellemans and V. Mathot. (Amsterdam : North-Holland Publishing Company.) [Pp. xx+448.] Price 48 guilders.

The Origins of Life. By ALBERT DUCROCQ. Translated by Alec Brown. (London : Elek Books Ltd.) [Pp. xvi+213.] Price 25*s*.

ERRATA

The Surface Energy of Colloidal Metals in Ionic Lattices, by A. B. Scott, 1954, *Phil. Mag.* (7), **45**, 610.

In § 5, the potential energy of two square 36-ion planes, separated by r_0, should be divided by 2 before comparison with the energy of an ion-plane with its image plane, since the separation of the two ion-planes creates twice the crystal surface that is formed when an ion-plane is separated from the metal. The image effect in table 1 should be everywhere doubled and the energy per atom is :

$\sqrt[3]{n}$	KCl	NaCl
3		1·53
4	0·91	0·64
5	0·53	0·47
6	0·42	0·33
7	0·29	0·29
8	0·24	0·23

The observed heat of dissociation then corresponds to a particle of about 42 atoms of K and 20 atoms of Na (page 617).

Page 616, last line, for 294 read 296.

Page 617, first line, for 84 read 80.

Page 618, 18th line, for 0·001 ev read 0·06 ev.

Figure 1, ordinates are in units of $8\,e^2/r_0$.

I am indebted to Professor F. G. Fumi for calling my attention to these errors.

[*The Editors do not hold themselves responsible for the views expressed by their correspondents.*]